

MRI DETECTION OF EARLY-STAGE CEREBRAL  
CORTICAL ABNORMALITIES CAUSED BY FETAL  
EXPOSURE TO ALCOHOL

By

Lindsey A. Leigland

A THESIS/DISSERTATION

Presented to the Department of Behavioral Neuroscience

and the Oregon Health & Science University

School of Medicine

in partial fulfillment of

the requirements for the degree of

Doctor of Philosophy

April 2012

School of Medicine  
Oregon Health & Science University

CERTIFICATE OF APPROVAL

---

This is to certify that the PhD dissertation of

Lindsey A. Leigland

has been approved

---

Christopher Kroenke

---

Anda Cornea

---

Kathleen Grant

---

Charles Meshul

---

Charles Springer

---

Alexander Stevens

## TABLE OF CONTENTS

Table of Contents .....	i
Acknowledgements .....	iv
List of Abbreviations .....	v
List of Equations .....	vii
Chapter 1: General Introduction .....	1
1. Introduction to Fetal Alcohol Spectrum Disorder .....	1
2. Biological Processes During Cortical Development Relevant to Neuroimaging Outcomes .....	2
3. Cerebral Abnormalities in Fetal Alcohol Spectrum Disorder and MRI-Based Strategies for Their Characterization .....	7
4. Summary and Dissertation Goals .....	13
Chapter 2: Early Detection of Fetal Alcohol Spectrum Disorder via Magnetic Resonance Imaging .....	17
1. Introduction .....	17
2. Methods .....	20
3. Results .....	26
4. Discussion .....	31

Chapter 3: A Comparative Analysis of DTI Patterns to Species-Specific Time Courses of Development .....	39
1. A Review of DTI Studies with Reference to Neuroanatomical Development.....	39
2. Methods .....	44
3. Results .....	50
4. Discussion.....	52
Chapter 4. Validation of a Quantitative Model Relating DTI to Cellular Morphology in a Ferret Model of Normal Development .....	54
1. Introduction .....	54
2. Methods .....	59
3. Results .....	68
4. Discussion.....	71
Chapter 5. Characterizing Early Dendritic Development in FASD via DTI: A Histological Comparison .....	75
1. Introduction .....	75
2. Methods .....	79
3. Results .....	86
4. Discussion.....	90
Chapter 6. Summary and Conclusions .....	95
References .....	103

Figure Legends.....125

Figures .....131

## **Acknowledgements**

The following sources provided funding for the research presented:

Oregon Health & Science University Division of Neuroscience, NIH R01 NS070022, NIH P51 RR000163, ABMRF/The Foundation for Alcohol Research, T32 AA007468, The W.M. Keck Foundation, The Medical Research Fund [208], The National Center for Research Resources S10 RR024585

The following people provided help during the performance of the experiments discussed herein:

Erin Taber, Matthew Ford, Aubrey Buckert, Christa Helms, the laboratory of Kathleen Grant (animal experimental procedures), Chris Snelling, the laboratory of John Crabbe (blood ethanol concentration measurements), Barbra Mason, Diana Gordon, Maria Ojeda (histology procedures), Tom Barbara, Jim Pollaro (imaging procedures), Mark Wilcox and the laboratory of Dr. Veronica Alvarez (DiOlistic procedures), Jason Lerch (software and support for isocortical thickness calculations).

I would like to thank all of the people above for their invaluable support in carrying out these experiments.

Additionally, I would like to thank my examination committee (Anda Cornea, Kathleen Grant, Christopher Kroenke, Charles Meshul, Charles Springer and Alexander Stevens) for their support throughout my graduate student career. These are some of the greatest scientists I have had the privilege to know, and their help and feedback has meant a great deal to me.

I would especially like to thank my mentor, Christopher Kroenke, for his unwavering patience and for everything that he has taught me during my time in his laboratory.

I would like to thank Jeri Janowsky for her support both personally and scientifically.

Lastly, I would like to thank my family, Bonnie Leigland, James Leigland, Kirsten Leigland, my husband, Andrew Zimmerman, as well as Rosalind Thomas and the Zimmerman, Brookins and Richart families. Their love, patience and support have carried me throughout the years.

This work is dedicated to William Bracken, Jennings Leigland and John Richart. These individuals have provided unending inspiration for me in all walks of life.

## **List of Abbreviations**

FAS- Fetal Alcohol Syndrome

FASD- Fetal Alcohol Spectrum Disorder

CDC- Centers for Disease Control and Prevention

MRI- Magnetic Resonance Imaging

fMRI- Functional Magnetic Resonance Imaging

MRS- Magnetic Resonance Spectroscopy

DTI- Diffusion Tensor Imaging

FA- Fractional Anisotropy

N- Number of Animals

G- Gestational Day

E- Ethanol-Treated

M/D- Maltose/Dextrin-Treated

C- Untreated or Control

P- Postnatal Day

RF- Radio Frequency

TFCE- Threshold Free Cluster Enhancement

ANOVA- Analysis of Variance

ADC- Apparent Diffusion Coefficient

$\tau_{FA}$ - Exponential Decay Time constant

$t_{event}$  - Event time (End of neurogenesis in cortical layers II/III to eye opening)

$\lambda$ - Eigenvalue of the Diffusion Tensor

O- Eigenvalue of the Fiber Orientation Tensor

NA- Anisotropy of Neuronal Processes

$D_L$ - Water Diffusion Within the Intracellular Compartment Parallel to the Local Axis of the Neuronal Process, or Longitudinal Diffusion

$D_T$ - Water Diffusion Within the Intracellular Compartment Perpendicular to the Local Axis of the Neuronal Process, or Transverse Diffusion

$D_A$ - Intrinsic Diffusion, or  $D_L - D_T$

v- Volume Fraction of Neuronal Processes in DTI Data

D- Dorsal

V- Ventral

Cd- Caudal

R- Rostral

CLS- Coronolateral Sulcus

SS/PSS- Sylvian Sulcus/Presylvian Sulcus

SSS- Suprasylvian Sulcus

Sps- Splenial Sulcus

CS- Cruciate Sulcus

aRF- Anterior Rhinal Fissure

## **List of Equations**

Equation [3.1] – Calculation of Fractional Anisotropy (FA)

Equation [3.2] – Calculation of the Apparent Diffusion Coefficient (ADC)

Equation [3.3] – Conversion of  $A\sigma$  (Rotationally Invariant Measure of Diffusion Anisotropy) to Fractional Anisotropy (FA)

Equation [3.4] – Conversion of Relative Anisotropy (RA) to Fractional Anisotropy (FA)

Equation [3.5] – Cortical Fractional Anisotropy (FA) Decay with Age

Equation [3.6] – Translating Time Model of Neuroanatomical Development

Equation [4.1] – Relationship Between the Diffusion Tensor and the Fiber Orientation Tensor

Equation [4.2] – Transformation Between Surface Models Created From Golgi and Diffusion Tensor Imaging (DTI) Data

## **Chapter 1. General Introduction**

### **1. Introduction to Fetal Alcohol Spectrum Disorder**

Fetal alcohol syndrome (FAS) and the more broad distinction of fetal alcohol spectrum disorder (FASD) are defined by a set of conditions resulting from consumption of alcohol during pregnancy. Maternal ethanol consumption has a variety of effects ranging from altered gene expression (Kaminen-Ahola 2010) to behavioral consequences spanning the lifetime of the offspring (Mihalick 2001, Baer 2003, Arias 2006, Chotro 2007, Youngentob 2007, Chotro 2009). These disorders cause significant mental, physical and financial stress to the individuals and families affected. The Centers for Disease Control and Prevention (CDC) report that the prevalence of FAS is 0.2 – 1.5 per 1000 live births (with FASDs occurring up to 3 times as often as FAS) making these disorders a significant public health concern (CDC 1993, CDC 1995, CDC 1997, CDC 2002). Currently, detection of indicators of FAS and FASD required for diagnosis (facial dysmorphology, growth deficits and central nervous system impairments; [www.cdc.gov](http://www.cdc.gov)) is most easily accomplished years after birth. Studies have reported that the average age of diagnosis of FAS and FASD ranges from 3 to 10 years of age (Streissguth 2004, Elliott 2008). Early diagnosis is extremely important, as this allows for therapeutic intervention at critical time points, potentially reducing the severity of adverse outcomes of these disorders (Streissguth 2004, Olson 2007). However, diagnosis of FASD has been difficult due to the range of associated symptoms, the overlap of symptoms with other developmental disorders, as well as difficulties detecting indicators of FASD in

vivo early in development. While much of the research surrounding FASD is dedicated to discovering improved biomarkers and early detection of biomarkers, diagnosis at early time points in the progression of these disorders is still imperfect.

The research presented here suggests new techniques that may help in early diagnosis of FASD. This research centers on the development of the cerebral cortex, as the period of time, in which neural circuits form, is critical for future behavioral development, and is significantly impacted by prenatal exposure to alcohol.

## **2. Biological Processes During Cortical Development Relevant to Neuroimaging Outcomes**

The cerebral cortex is divided into two major categories based on neuroanatomical criteria, the isocortex and the allocortex. The isocortex is phylogenetically newer than the allocortex, and thus is also commonly referred to as the neocortex. The allocortex has been further subdivided into classifications of the paleocortex (including the olfactory bulb and minor parts of the amygdala) and archicortex (including parts of the hippocampus, the retrosplenial cortex and the entorhinal cortex). Allocortical regions have been suggested to represent cortical contributions to the limbic system, as well as participate in olfactory functions (see Zilles 2004 for review). Allocortical regions comprise a smaller area than the isocortex, and vary in terms of laminar patterns, generally not showing the 6-layered organization typical of the mature isocortex. These

regions do not undergo the same sequence of inside-out cellular production and differentiation throughout development as the isocortex (Sidman 1973, Sidman 1982, Zilles 2004). Additionally, cognitive and behavioral problems are commonly associated with FASD (CDC) that may be associated with developmental abnormalities in the cerebral isocortex. Isocortical areas play roles in sensory processing as well as more executive functions, deficits in which could lead to altered cognition and behavior. Given consistent patterns in neuronal generation and development, as well as potential implications of abnormal isocortical development in the setting of FASD, the development of the isocortex was chosen as a focus for the research presented here.

Both human and animals studies have delineated a series of events that define the formation of the cerebral isocortex. These events include neurogenesis in ventricular and subventricular proliferative zones, neuronal migration to the cortical plate, and neuronal differentiation and synapse formation within the cerebral cortex. Additionally, though the time periods in which these events occur vary greatly among different species, it is commonly accepted that most mammalian species experience the same events along a consistently ordered sequence (Dreher 1988, Robinson 1990, Finlay 1995, Darlington 1999, Clancy 2001). Processes involved in the formation of the isocortex occur along relatively similar schedules with similar physical and chemical cues, making research done in non-human mammals potentially translatable to the human condition. A comparison of critical time-points for isocortical development among different species is shown in Figure 1. This figure was created based on

information from the Department of Health and Human Services as well as from information from Clancy, Darlington and Finlay's model for translating time across species (Clancy 2001). (References for specific events were gathered from Meyer 2000, Ramakers 2005 and Bystron 2008.) It is important to note that these are estimates of relative time periods and important corticogenic events. The beginning of human pregnancy is typically referred to either as the beginning of gestation (referring to the time since last menstruation; often marking the beginning of the first trimester) or the beginning of embryogenesis (or the time since conception; also referred to as post-conceptual age). Time points referring to both of these naming conventions are listed for human development in Figure 1. In most of animal and human research, early development is also referred to in gestational days or post-conceptual days. However, in the context of research, these terms primarily refer to time since conception. Due to the difficulty of obtaining human tissue, and the variability in the definitions of human gestational periods, assessing critical time points through histology during human gestation has classically been difficult. However, close estimates are still useful in translating developmental events among species.

Figure 1

The neural tube closes at approximately embryonic day 27 in humans. At approximately gestational day 33 in humans, neurons migrating from the

ventricular zones form the cortical plate, and neurons begin to proliferate (see Bystron 2008 and Ramakers 2005 for review). Many cells at this point are classified as radial glia, which act as a scaffold for migrating neurons. The proliferation of cells occurs in an “inside-out” manner, wherein newly born cells must migrate through the cortical plate forming the outer layers of the cortex (Rakic 1988, Rakic 1995). As cells arrive at specific areas in the cortex, they form columnar structures. This organization is caused by chemical and physical guidance cues (such as radial glia) that orient the neurons radially, perpendicular to the pial surface, as well as the undifferentiated nature of immature neurons (Rakic 1988, Rakic 1995). Guided by growth cues, neurons migrate to specific places in the cortex, corresponding to their future functionality, and differentiate. The final location and types of cells define the typical, mature 6-layer isocortex (layer VI being furthest away from the pial surface, layer I being closest to the pial surface). At a certain point, suggested to be before gestational week 20, the radial glia have regressed, and those glial cells remaining in the outer layers of the cortex have begun to differentiate (Choi 1978, Sidman 1982). Additionally, approximately relative to the middle of the second trimester in humans, neurons begin to rapidly differentiate (Conel 1939). Generally, this involves the outgrowth of the axon, and subsequent basilar and apical dendrite formation. Further dendritic differentiation involves the lengthening of the primary dendrites, as well as development of secondary branches. It is commonly thought that dendritic branching plays a large part in synapse formation, which in turn determines larger brain circuits. It is known that plasticity in the central nervous system

decreases after critical/sensitive periods which end prior to the completion of myelination with brain WM (Katz 2002, Innocenti 2005, Fields 2008). These critical periods are specific periods of time, during which particular functional systems can be formed. Abnormal development of, or coordination among, multiple neural components (i.e. neurons, dendrites, axons, synapses, sensory afferents) during this time could lead to abnormal maturation and permanent dysfunction. For example, deprivation of visual sensory experience early in brain development has been demonstrated to produce permanent effects on visual system processing (Hubel 1982, Wiesel 1982, Katz 2002). It is important to note that synapses in the developing cerebral cortex have been seen as early as gestational weeks 6 – 7, and that synaptogenesis occurs throughout cortical development, into the first years of postnatal life (see Ramakers 2005 for review). However, synaptogenesis coinciding with dendritic differentiation is thought to be one of the periods when synapses form most rapidly, and this time period also coincides with the critical periods for formation of functional systems. Understanding these patterns is critical to the study of any insult to cortical maturation. Cerebral cortical development was chosen as a focus for the research presented here, as gestational ethanol exposure occurs during this period when critical neuronal systems are formed. Interruptions in the formation of neural circuits are thought to lead to common symptomology associated with FASD. Additionally, specific abnormalities have been shown to be present in the developing cerebral cortex in animals prenatally exposed to ethanol, at a developmental period corresponding to late gestation in humans (as will be

described in the following section). Therefore, identifying these developmental anomalies in vivo could allow for new diagnostic capabilities and therapeutic interventions.

### **3. Cerebral Abnormalities in Fetal Alcohol Spectrum Disorder and MRI-Based Strategies for Their Characterization**

Histological studies have provided evidence of disrupted cortical formation including altered cortical growth cues (Krahe 2009, Lindsley 2011), neuronal generation and proliferation (Miller 1986, Miller 1988, Miller 1990, Miller 1996, Dunty 2001, Miller 2007, Burke 2009), columnar organization (Granato 2006), dendritic morphology (Davies 1981, Hammer 1981, Stoltenburg-Didinger 1983, Fabregues 1985, Hammer 1986, Yanni 2000, Granato 2003, Cui 2010) and cortical plasticity (Backman 1998, Medina 2003, Medina 2008). A specific example of reduced cell number in response to prenatal exposure to ethanol is provided by Dunty and colleagues (Dunty 2001) who employed Nile Blue Sulfate Vital and LysoTracker Red staining techniques, at time points ranging from gestational day 6.5 to 11 in the mouse, to determine that there was increased cell apoptosis and cell death 12 hours after an acute ethanol administration relative to control animals. Additionally, one study used a [<sup>3</sup>H]thymidine stain and autoradiographic techniques to determine that prenatal exposure to ethanol in rats resulted in delayed neuronal generation, altered distribution of neurons, and altered size and orientation of neurons (Miller 1988).

Histological studies have also provided evidence that specific areas of the cortex, such as the somatosensory cortex, may be differentially affected by ethanol exposure (Margret 2005, Granato 2006, Margret 2006, Miller 2007). In a study in macaques, specific gray matter reductions in the parietal cortex of adolescent monkeys that were exposed to ethanol during gestation were found relative to controls (Miller 2007). In studies examining effects of prenatal exposure to alcohol on somatosensory areas in young rats, body and brain masses were lower in the experimental animals relative to controls, and the areas of cortical barrel fields in the somatosensory cortex were lower (Margret 2005, Margret 2006). Additionally, in a study employing immunoreactive calcium binding proteins, the radial distribution of neurons in the primary motor and somatosensory areas of adult rats that were exposed to alcohol during the first postnatal week was disrupted (Granato 2006).

Simplified cerebral cortical neuronal morphology has also been particularly well-documented in analyses utilizing Golgi-staining (Davies 1981, Hammer 1981, Fabregues 1985) and DiOlistic labeling procedures (Cui 2010) in studies modeling FASD. These studies found that dendritic arborization (including dendritic length and number) were reduced in animals exposed to ethanol during gestation and immediately after birth.

It is probable that these abnormalities lead to common symptomology observed in children with FASD. There are a great number of behavioral and cognitive deficits that have been associated with FASD in humans (see Mattson 2011 for review). Additionally, animal studies using a range of ethanol doses

during gestation have shown behavioral and cognitive deficits similar to those seen in humans (see Driscoll 1990, Schneider 2011 for review). However, detecting these abnormalities in vivo at early stages of human development is not feasible through histological methods. In response to this challenge, a number of magnetic resonance imaging (MRI) studies have attempted to characterize biomarkers of FASD.

MRI studies can be applied non-invasively, both ex vivo and in vivo, in animals and in humans, making MRI an ideal methodology for translational research. Much of the MRI work that has been accomplished in FASD focuses on early childhood through adulthood. For instance, studies using two different sub-types of MRI, functional MRI (fMRI) and magnetic resonance spectroscopy (MRS), have been able to characterize abnormal activity patterns during cognitive tasks (Malisza 2005, Fryer 2007, Astley 2009, O'Hare 2009, Coles 2011), as well as abnormal levels of neurometabolites in the brain (Astley 1995, Fagerlund 2006, Astley 2009), respectively. Additionally, studies using another sub-type of MRI imaging, commonly referred to as structural imaging, in children and adolescents have been able to characterize abnormal cortical volume and thickness in affected individuals (Sowell 2001, Sowell 2008, Astley 2009, Nardelli 2011, Yang 2011; see Toga 2006, Lebel 2011 for review).

More recently, work has been done in animal models at stages of development that occur during time periods relative to gestation in humans (Parnell 2009, O'Leary-Moore 2010). Currently, these studies have been able to identify cortical volume and cortical thickness abnormalities in animals affected

by fetal alcohol exposure at specific time points during development. Cortical volume is commonly thought of as a product of cortical thickness and surface area. Cortical thickness and surface area are both thought to be affected by cell number and by the organization of cortical columns in the developing cerebral cortex. As cellular generation, proliferation and organization in the developing cerebral cortex have been shown via histology to be affected by ethanol exposure during gestation (Miller 1986, Miller 1988, Miller 1990, Miller 1996, Dunty 2001, Medina 2005, Mooney 2005, Granato 2006, Miller 2007, Burke 2009), these structural MRI studies are the first evidence that MRI may be useful in detecting FASD during gestation in humans. However, a systematic analysis of volume, thickness and surface area changes at multiple developmental time-points has yet to be accomplished.

Studies utilizing a sub-type of MRI, called diffusion tensor imaging (DTI), have been done in both humans and animals, showing patterns of development of DTI measures that mirror cellular-level changes in the developing cerebral cortex defined by histological methods (see Chapter 3, Leigland 2011 for review). Therefore, it is possible that DTI measurements could be used to detect anatomical abnormalities in FASD. However, no direct relationship between DTI measurements and neuronal morphology has been defined, and DTI measurements in the developing cerebral cortex investigating the effects of prenatal exposure to ethanol have not yet been performed.

DTI is particularly well suited to study the cellular-level bases of tissue changes associated with development and pathology. In DTI experiments, the

image intensity recorded by MRI is rendered sensitive to diffusion-mediated displacement of water molecules over distances of approximately 10  $\mu\text{m}$  in the immature cerebral cortex (Le Bihan 2003, Mori 2006). These measurements are extremely powerful because biological membranes impede water displacement due to diffusion (Beaulieu 2002), and thus the cellular-scale structure of tissue is reflected in water diffusion measurements. In tissue that is highly ordered on the cellular scale, water diffusion exhibits a directional dependence (Moseley 1990). Directional dependence in water diffusion within the context of DTI is termed diffusion anisotropy (Basser 1994a, Basser 1994b, Basser 1996). The extent of diffusion anisotropy reflects the degree of cellular-scale order in tissue and is frequently quantified in terms of fractional anisotropy (FA), a parameter that ranges from 0 (isotropic diffusion, unstructured tissue) to 1 (extremely anisotropic diffusion, well-ordered tissue). In the early developing cerebral cortex, FA measurements in the isocortical gray matter begin high and decrease with age, while at later stages, FA in cerebral white matter increases with maturity (Huppi 1998, Neil 1998) concurrently with the differentiation of neurons and maturation of axons and axon bundles, respectively.

Current strategies that utilize DTI to characterize the neurobiological basis of several neurodevelopmental disorders have mostly focused on cerebral white matter of affected individuals at maturity, or stages of development subsequent to the loss of cortical FA. Reduced white matter FA relative to controls has been reported within the context of FASD (Ma 2005, Wozniak 2006, Lebel 2008, Sowell 2008), suggesting a disruption in mature white matter integrity and

organization. However, a DTI-based approach aimed at detecting abnormal morphological characteristics of FASD at earlier time points within the developing cerebral cortex could potentially provide a new strategy that would extend the capabilities of DTI toward identification of anatomical abnormalities prior to the end of critical developmental periods.

Due to the major impact that prenatal exposure has on the developing brain, and the proposed consequences that these effects have on behavioral and cognitive symptoms associated with FASD (CDC, Riley 2011), a great deal of research has focused on identifying developmental cortical abnormalities associated with FASD, as discussed above. However, models used to investigate these abnormalities have varied greatly in terms of the time of ethanol insult, as well as the periods of time chosen for studying these insults. One cause in the variety of symptoms presented in humans with FASD is the range of gestational time periods, during which individuals were exposed alcohol. Various models of FASD have therefore attempted to study the effects of ethanol exposure during multiple time points relative to human gestation. In the research presented here, alcohol was administered during neuronal generation, proliferation and migration, and effects of this insult were investigated during periods of rapid neuronal differentiation. While immediate effects of alcohol administration have been demonstrated during cellular generation, alcohol administration at this time may also have consequences on the future development of neural circuits, such as lasting effects on cellular number and organization, as well as dendritic development. Additionally, as described

above, imaging methods present a unique ability to study the downstream effects of alcohol administration during neuronal generation and migration. Thus, the methods used here were chosen specifically to relate MRI methods to histologically-validated abnormalities in the cerebral cortex during the time corresponding to neuronal differentiation, caused by ethanol exposure during neuronal generation, proliferation and migration.

#### **4. Summary and Dissertation Goals**

Herein, MRI is employed as a quantifiable, non-invasive, in vivo method of characterizing abnormal cortical development. The ability to detect FASD using this non-invasive method, during time periods equivalent to human gestation would introduce the potential for new therapeutic and diagnostic interventions not currently available. The following research presents a new model of abnormal cortical development in a rat model of FASD. Additionally, both an analytical review, as well as an empirical comparison of histological and MRI methodology during normal and abnormal (FASD) development are presented. These experiments were done based on the theory that if MRI methods are sensitive enough to detect histologically-validated cortical abnormalities in FASD, a new non-invasive, in vivo method for diagnostic and therapeutic interventions in FASD would be introduced. This research will provide a link between traditional, histological measurements of neuroanatomical abnormalities in the developing cerebral cortex caused by prenatal exposure to ethanol and non-invasive MRI measurements. The overall hypothesis of this experiment is that MRI measurements will allow for the detection of isocortical abnormalities caused by

prenatal ethanol exposure, and that these measurements will be directly related to underlying neuroanatomy. The aims and hypotheses for the individual experiments are as follow:

Aim 1: To elaborate upon evidence of disrupted cortical formation by presenting a timeline of structural MRI outcomes throughout periods corresponding to late gestation in humans in a rat model of FASD. Defined patterns of cortical volume, thickness and surface area throughout critical periods in cortical development will allow for distinction between normal and abnormal development at multiple time-points, thus expanding the advantages of MRI methodology in terms of future diagnostic capabilities.

It was hypothesized that structural imaging throughout development would show differences in brain and cortical volumes, as well as cortical thickness and surface area between control and FASD subjects. Brain volume, cortical volume, cortical thickness and cortical surface area were expected to increase with age. However, in comparisons between control and FASD subjects, outcomes were expected to be decreased at all time points in response to prenatal ethanol exposure, corresponding to histological evidence of reduced cell numbers (Miller 1986, Miller 1988, Miller 1990, Miller 1996, Dunty 2001, Miller 2007, Burke 2009) and cortical organization (Medina 2005, Granato 2006).

Aim 2: To characterize the relationship between DTI measurements and underlying histology in the normal developing cerebral cortex. This work tests the theory that DTI is sensitive enough to detect age-related patterns of neuronal

morphology during normal cortical development. It was hypothesized that an analytical review of studies comparing cellular morphological differentiation with DTI results across multiple species would have two major implications: Comparable patterns of neurodevelopment and FA across species imply that DTI measurements can be related among species, and methods applied in non-human species can provide information about the human condition. Additionally, the ability of DTI to detect changes in neuroanatomy in the normal developing cerebral cortex introduces the potential for the use of this methodology in detecting cortical abnormalities associated with various developmental disorders.

A direct experimental comparison of DTI and histological results was conducted in a ferret model of normal development to validate a proposed quantitative relationship, providing empirical evidence for the theory that neuronal differentiation in the developing cerebral cortex underlies developmental FA patterns. It was hypothesized that cortical FA would decrease with age, in accordance with increasing neuronal differentiation (Neil 1998, McKinstry 2002). Importantly, it was hypothesized that a quantitative model relating neuronal differentiation to FA measurements, would be validated, thus providing a direct empirical relationship between FA and underlying neuroanatomy. Using this relationship, age-related FA and neuronal differentiation patterns across development are characterized, providing a comprehensive quantitative model of normal cortical development at a critical time for the formation of neural circuits, and allowing for patterns of abnormal development to be easily recognized.

Aim 3: To directly compare histological evidence of disrupted neuronal morphology to DTI measurements in a rat model of FASD. This work is a continuation of Aim 2, extending the relationship defined between DTI and underlying cortical morphology to abnormal cortical development resulting from fetal exposure to ethanol. This work tests the theory that DTI is sensitive enough to distinguish between normal and abnormal development of the cortex, and supports the ability of DTI (in addition to structural imaging) to detect FASD in human subjects. Cortical FA was expected to decrease in all subjects with age mirroring patterns of increasing neuronal differentiation. However, FA was expected to be higher in FASD than control subjects at time points corresponding to the early stages of dendritic differentiation, mirroring simplified dendritic arbors seen with prenatal exposure to ethanol FASD (Davies 1981, Hammer 1981, Stoltenburg-Didinger 1983, Fabregues 1985, Hammer 1986, Yanni 2000, Granato 2003, Cui 2010). Additionally, the quantitative model validated in Aim 2 was expected to be applicable to abnormal cortical development, thus providing quantitative evidence that DTI can be employed to detect neuronal morphological abnormalities associated with FASD.

## **Chapter 2. Early Detection of Fetal Alcohol Spectrum Disorder via Magnetic Resonance Imaging**

(This chapter will be modified for submission to the journal *Alcoholism: Clinical and Experimental Research*.)

### **1. Introduction**

It has been said that “the most profound effects of prenatal exposure to alcohol are on the developing brain and the cognitive and behavioral effects that ensue (Riley 2011)”. A main diagnostic criterion for FASD is central nervous system abnormalities including structural deficits (CDC). Additionally, common symptoms of ethanol exposure during gestation are microcephaly, observed decreases in the size of the brain, and malformation of brain structures (Clarren 1978, Clarren 1981). Thus, a great deal of research surrounding FASD has focused on characterizing reductions in brain size, and determining the specific neurobiological processes that lead to these effects.

Due to the potential to use MRI technology non-invasively in vivo, imaging research has emerged focusing on cortical development in FASD identifying new biomarkers that can be used for possible diagnostic and treatment strategies. Structural MRI studies have displayed significantly reduced brain and cortical volumes in children and adolescents with FASD (Astley 2009, Nardelli 2011). Additionally, reduced cortical thickness has been demonstrated in children and adolescents and regional variability has been suggested throughout the cortex (Sowell 2001, Sowell 2008, Yang 2011, Zhou 2011), although not all studies are

in agreement regarding effects and affected areas. MRI outcomes have also been related to behavior in children, adolescents and adults prenatally exposed to alcohol (Sowell 2008, Bjorkquist 2010, Coles 2011).

These studies have significantly added to our knowledge of the effects of alcohol on the cerebral cortex. However, MRI studies in animals at time points corresponding to human gestation can provide information on abnormal early development caused by prenatal alcohol exposure, as well as potentially link histologically-validated neuroanatomical abnormalities associated with prenatal alcohol exposure to neuroimaging data. Histological studies have shown reduced cell numbers and altered cellular organization in the developing cerebral cortex in response to ethanol exposure during gestation (Miller 1986, Miller 1988, Miller 1990, Miller 1996, Dunty 2001, Miller 2007, Burke 2009, Medina 2005, Granato 2006). Reduced brain masses, cortical masses and areas of specific cortical structures have also been reported in histological experiments of prenatal ethanol exposure (e.g. Miller 2007, Margret 2006, Chappell 2007) during periods of time relative to human gestation. Recently, MRI research has been conducted studying the effects of alcohol exposure at specific time points during gestation on cerebral cortical development (Parnell 2009, Godin 2010, O'Leary-Moore 2010) that might reflect abnormalities reported in histological research. In these MRI studies, mice were exposed to ethanol on gestational days 7, 8 or 10, and observed approximately 7 to 10 days later. Researchers found reduced body size, brain volume and cortical volume relative to controls.

The research presented here expands on this information by studying the effects of ethanol exposure throughout gestation on structural MRI outcomes throughout development. Given the concurrent incidence of observed cell and cortical area reductions in histological experiments and observations of reduced cortical thickness and volume in animals via MRI at specific time points, it was expected that measurements of brain mass, brain volume, isocortical volume, isocortical thickness and isocortical surface area would be lower in animals prenatally exposed to ethanol versus control animals. It was expected that these differences would be observed throughout the time period corresponding to late gestation in humans. This would suggest that MRI studies can be used to detect ethanol-induced abnormalities, but also reflect underlying neuroanatomy in models of FASD during cerebral isocortical development. Importantly, it was expected that these data would form a developmental profile of changes in structural MRI outcomes. Measurements were taken at 6 time points corresponding to late human gestation through adulthood in rat pups prenatally exposed to ethanol. This was accomplished to further characterize the effects of prenatal exposure to ethanol, but also to define specific patterns of cortical maturation resulting from prenatal exposure to alcohol for potential use with future diagnostic techniques. The ability to differentiate between normal and abnormal development at multiple time points expands the diagnostic capabilities of MRI.

## 2. Methods

### Animal Care

Long-Evans rats were purchased from Harlan Laboratories (Livermore, CA), and were delivered to the Department of Comparative Medicine at Oregon Health & Science University. Virgin female dams (N=18) were ages 9 – 10 weeks and body masses were approximately 200 – 224 g. Proven breeder males (N=4) were ages 14 – 15 weeks, and body masses were approximately 325 – 349 g. All animals received standard chow, and participated in approximately one week of handling before experimental procedures began. All possible measures were taken to minimize animal pain or discomfort. All experiments were carried out in accordance with the NIH “*Guide for the Care and Use of Laboratory Animals*” (NIH publication no. 86-23, revised 1987).

### Breeding

Each male was assigned to 3 to 6 dams. At the start of each experimental day, vaginal lavages were taken to determine day of the estrous cycle. The dam that was nearest to estrous was placed in the same cage as the male. Vaginal lavages were taken twice daily (once in the morning and once in the afternoon), and observed for day of cycle and presence of sperm. Males and females would share the same cage for up to one full cycle (approximately 5 days). If, after one cycle, there was no presence of sperm detected via any of the lavages, the male and female were separated and the male was bred with another female (although an additional attempt to breed would be made at a later date). Gestational day

(G) 1 was defined as the same day a morning lavage was found positive for sperm or the day after an afternoon lavage was found positive for sperm. Pregnant dams were assigned to one of three treatment groups: Ethanol-treated (E; n=7), Maltose/Dextrin-treated (M/D; n=5) or untreated (C; n=6).

#### Alcohol administration

In E and M/D groups, dams were administered 4.5 g/kg of a 25% (w/v) ethanol solution or a calorie matched maltose/dextrin solution, respectively. In terms of caloric content, ethanol has 7 kCal/g, while maltose/dextrin has 3.8 kCal/g. Solutions were administered daily from G1 through G20 via intragastric gavage (birth typically occurred at G23). Control groups received no treatment and minimal handling, limited to morning weights and removal for cage cleanings. Control and ethanol animals received food ad libitum throughout gestation. Each M/D animal received food that was matched in mass to food that one other E animal received. For E and M/D animals, food was removed in the morning, and gavages were administered 5 hours after food was removed. Gavages were administered in two doses, one hour apart, in order to minimize the volume of solution in the stomachs of the dams. Body masses of rat dams were measured each morning for all three groups.

#### Blood Ethanol Concentration

On G13 and G20, blood samples were collected via a saphenous vein. Approximately 20  $\mu$ l were taken at one, three and four hours after the last gavage (on G13) or one, two and four hours after the last gavage (on G20). Blood was

only collected from dams treated with ethanol as it was thought the procedures would be relatively more stressful for the M/D and C animals, thus introducing a confound in the data. However, blood collection from the saphenous vein causes minimal pain to animals (Hoff 2000), and given the subdued nature of the animals after ethanol treatment, these procedures caused minimal behavioral stress (or had minimal impact on the mental well-being of the animals). Blood ethanol concentrations were calculated via a gas chromatograph/mass spectrometer.

### Tissue Collection

At 6 postnatal time points (P0, P3, P6, P11, P19 and P60), pups from the dams were sacrificed, and their brains collected for analysis (n = 4 – 6 /age/group). Pups were given an i.p. injection of approximately 0.5 mL euthasol (pentobarbital sodium and phenytoin sodium; Butler-Schein Animal Health Supply, Dublin, OH). Heparin (0.01 mL/10 mL), with phosphate buffered saline (1x PBS), was injected into the left cardiac ventricle until the fluid of the right cardiac atrium was clear. Paraformaldehyde (2%, approximately 40 mL, pH 11) was then injected into the left cardiac ventricle. The brains were extracted and placed in paraformaldehyde (2%, approximately 40 mL) for 24 hours. Samples were then transferred to 1X PBS at 4°C. After at least 48 hours in 1X PBS at 4°C, olfactory bulbs were removed from the brains at the lateral olfactory tract, and remaining spinal cord was severed between the C1 dorsal root of the spinal cord and the medulla. Brain masses were measured, and the left and right hemispheres were separated. Left hemispheres of each brain were utilized for

all subsequent procedures (with the exception of one right hemisphere Control brain, due to a damaged left hemisphere from perfusion procedures; Right hemispheres were collected for a different set of experiments: See Chapter 5).

### MRI procedures

Hemispheres were placed in a modified 5 mL conical tube filled with 1X PBS, and allowed to equilibrate to room temperature. Samples were placed into a one-turn solenoid radio frequency (RF) coil manufactured in the laboratory (transmit/receive, tuned and matched to 500MHz), and the entire apparatus was placed in the isocenter of an 11.7 Tesla magnet (Bruker, Germany) interfaced with a 9 cm inner-diameter magnetic field gradient coil insert (maximum gradient strength of 70 G/cm per x, y and z axis). Whole-hemisphere images were acquired. A T2-weighted imaging sequence was employed (TR = 4000 – 5000, TE = 42.7 ms, FOV = 5.20 x 1.28 cm, Matrix = 250 x 64, Voxel size = 0.2 mm<sup>3</sup>, Averages = 6, Scan time = 4 hours). In some cases, fractional anisotropy (FA) maps acquired from Diffusion Tensor Imaging (DTI) methods were used to help with image analysis (see Chapter 5 for DTI acquisition and analysis details).

### Structural analyses

Anatomical images were transferred into ITK-SNAP (Yushkevich 2006) where the cerebellar area was removed from individual images. Total hemisphere volume was calculated based on the number of voxels within these images, not including the cerebellar region. Masks of the isocortex were made on individual images. Although data were collected throughout the entire

cerebral cortex, allocortical regions do not undergo the same sequence of cellular differentiation throughout development as the isocortex (Sidman 1973, Sidman 1982). Therefore, only data from the isocortex was used for analysis. The isocortex/allocortex boundary was defined laterally by the rhinal fissure, and rostrally by the lateral olfactory tract. The medial boundary of the isocortex was identified at the junction with the corpus callosum. Isocortical volumes in the hemisphere were calculated based on the number of voxels in the isocortical masks. Both brain and isocortical volume throughout the whole brain was estimated by multiplying hemispheric values by a factor of 2. This was done to more closely compare volumes estimated here to brain masses. In order to calculate isocortical thickness, outer and inner boundaries were defined on the isocortical mask (based upon the junction with the pial surface and the white matter, respectively). Mean isocortical thickness values were calculated based on a technique developed by Lerch and colleagues, which involved iteratively solving Laplace's equation using the Jacobi method, and computing streamlines between the inner and outer boundaries using Euler's method (Lerch 2008). In order to visualize cortical thickness results, and calculate surface area of the cortex, mid-cortical surface models were created from the isocortical mask. These surface models (created from a boundary half-way between the pial surface and gray-white matter boundary as determined by the technique described by Lerch 2008) were created to most accurately calculate the isocortical surface area, as it was thought that the surface models created from the pial surface or the gray-white matter boundary would either over- or

underestimate the true cortical surface area. This was accomplished using standard functions in the CARET software package (Van Essen 2001, [www.brainvis.wustl.edu/caret](http://www.brainvis.wustl.edu/caret), St. Louis, MO). A random target surface for each age was selected, and each individual cortical surface was registered to the target surface for visualization purposes. Mean cortical thickness for E, M/D and C groups at each age at each target cortical surface node was calculated and projected onto the target cortical surface for visualization. Cortical surface area was calculated by re-defining the isocortical boundary on the target surface model within the CARET software program, and utilizing regions of interest operations. This involved determining the number of nodes on each individual cortical surface model that the specified area on the target surface corresponded to. Surface area measurements are presented for the left hemisphere only. Threshold Free Cluster Enhancement (TFCE; Smith 2009) capabilities in the Linux compatible Caret version 6.0 were used to define regions on cortical surface models where mean cortical thickness differences between groups were significantly different.

### Statistics

A one-way ANOVA was used to determine the effect of group on maternal body mass at gestational day 22. A two-way mixed effects ANOVA (analysis of variance) model was used to determine effects of the independent variables, treatment group (E, C and M/D) and age group (P0, P3, P6, P11, P19 and P60), on dependent variables: brain mass, brain volume, cortical volume, overall cortical thickness and cortical surface area. Upon determining main effects of

the analysis, one-way ANOVAs were used to determine the separate effects of age and group on the dependent variables. Finally, unpaired t-tests were used to determine differences between specific pairs of treatment groups at each age. As mentioned earlier, TFCE analyses were used to determine significant regional patterns of cortical thickness among the treatment groups at each age. Uncorrected alpha was set at  $p=0.05$  for all analyses. Statistics were implemented in Statview [SAS, Cary, NC].

### **3. Results**

#### Maternal Body Mass

Mean mass values at birth for C (N = 6, mean = 312.21 g, standard error (se) = 9.474), M/D (N = 5, mean = 307.76 g, se = 15.575) and E dams (N = 5, mean = 311.940 g, se = 15.640) did not differ significantly ( $F_{2,13} = 0.020$ ,  $p = 0.98$ ).

#### Blood Ethanol Concentrations

The average blood ethanol concentration, calculated from blood samples taken 1 hour after the last gavage on G13, was 1.7 mg/ml. The average blood ethanol concentration, calculated from blood samples taken 4 hours after the last gavage on G13, was 1.0 mg/ml. The average blood ethanol concentration, calculated from blood samples taken 1 hour after the last gavage on G20, was 1.7 mg/ml. The average blood ethanol concentration, calculated from blood samples taken 4 hours after the last gavage on G20, was 1.3 mg/ml. These levels are in accordance with other studies of alcohol administration throughout gestation (i.e. Maciejewski-Lenoir 1993). Additionally, alcohol administration was

sufficient to elicit altered behavior (slow movement and altered motor coordination; qualitative examinations) in pregnant rat dams.

### Summary of Main Effects of Ethanol on Brain Mass, Brain Volume, Isocortical Volume, Isocortical Thickness and Isocortical Surface Area

For all of the dependent variables (brain mass, brain volume, isocortical volume, isocortical thickness and isocortical surface area), there was a main effect of age (measures were significantly different among age groups at all 6 ages; Brain Mass:  $F_{5,58}=1061.628$ ,  $p<0.0001$ , Brain Volume:  $F_{5,58}=642.738$ ,  $p<0.0001$ , Isocortical Volume:  $F_{5,58}=793.793$ ,  $p<0.0001$ , Isocortical Thickness:  $F_{5,58}=316.345$ ,  $p<0.0001$ , Isocortical Surface Area:  $F_{5,58}=1057.644$ ,  $p<0.0001$ ). Additionally, there was a main effect of treatment group (measures were significantly different among age groups across all three treatment groups; Brain Mass:  $F_{2,58}=55.654$ ,  $p<0.0001$ , Brain Volume:  $F_{2,58}=32.005$ ,  $p<0.0001$ , Isocortical Volume:  $F_{2,58}=38.053$ ,  $p<0.0001$ , Isocortical Thickness:  $F_{2,58}=20.890$ ,  $p<0.0001$ , Isocortical Surface Area:  $F_{2,58}=38.734$ ,  $p<0.0001$ ). There was no significant interaction between age and treatment groups on any of the dependent measures (Brain Mass:  $F_{10,58}=1.726$ ,  $p=0.10$ , Brain Volume:  $F_{10,58}=1.032$ ,  $p=0.43$ , Isocortical Volume:  $F_{10,58}=1.027$ ,  $p=0.43$ , Isocortical Thickness:  $F_{10,58}=0.669$ ,  $p=0.75$ , Isocortical Surface Area:  $F_{10,58}=1.077$ ,  $p=0.39$ ). All dependent measures increased significantly with age. With the exception of cortical thickness and surface area measures between P19 and P60, every age group differed significantly from every other age group across treatment groups;  $p<0.001$  for all

analyses. In all analyses, dependent measures were overall highest in the M/D group, and lowest in the E group.

### Brain Mass

As shown in Figure 2A, mass values were significantly different among the treatment groups at each age (asterisks; P0:  $F_{2,9}=7.719$ ,  $p<0.05$ , P3:  $F_{2,9}=9.681$ ,  $p<0.01$ , P6:  $F_{2,11}=13.138$ ,  $p<0.01$ , P11:  $F_{2,11}=33.157$ ,  $p<0.0001$ , P19:  $F_{2,9}=6.153$ ,  $p<0.05$ , P60:  $F_{2,9}=7.719$ ,  $p<0.01$ ). Between the E and C groups, there was a significant difference at P0 and P11. Between the C and M/D groups, there was a significant difference at P3, P6, P11 and P60. Between the E and M/D groups, there was a significant difference at each age.

Figure 2

### Brain Volumes

Paralleling brain mass results, as shown in Figure 2B, brain volumes were significantly different among the treatment groups at P0 through P11 (asterisks; P0:  $F_{2,9}=4.284$ ,  $p<0.05$ , P3:  $F_{2,9}=5.985$ ,  $p<0.05$ , P6:  $F_{2,11}=17.995$ ,  $p<0.001$ , P11:  $F_{2,11}=16.777$ ,  $p<0.001$ ). Additionally, there was a statistical trend towards a significant difference among treatment groups at P19 (cross symbol;  $F_{2,9}=3.697$ ,  $p=0.07$ ). Between the E and C groups, there was a significant difference at P6 and P11. Between the C and M/D groups, there was a significant difference at

P6. Between the E and M/D groups, there was a significant difference at all ages except P60.

### Isocortical volumes

Similar patterns were seen with isocortical volumes. As shown in Figure 2C, isocortical volumes were significantly different among the treatment groups at P0 through P19 (asterisks; P0:  $F_{2,9}=7.055$ ,  $p<0.05$ , P3:  $F_{2,9}=11.434$ ,  $p<0.01$ , P6:  $F_{2,11}=12.460$ ,  $p<0.01$ , P11:  $F_{2,11}=13.550$ ,  $p<0.01$ , P19:  $F_{2,9}=6.736$ ,  $p<0.05$ ), with a trend towards significance at P60 (cross symbol; P60:  $F_{2,9}=3.991$ ,  $p=0.06$ ). Between the E and C groups, there was a significant difference at P0, P6 and P11. Between the C and M/D groups, there was a significant difference at P3 and P60. Between the E and M/D groups, there was a significant difference at all ages.

### Isocortical Thickness

As shown in Figure 3A, isocortical thickness was significantly different among the treatment groups at P0 through P6 (asterisks; P0:  $F_{2,9}=12.948$ ,  $p<0.01$ , P3:  $F_{2,9}=7.918$ ,  $p<0.05$ , P6:  $F_{2,11}=8.127$ ,  $p<0.01$ ), with a trend towards significance at P19 (cross symbol; P19:  $F_{2,9}=4.024$ ,  $p=0.06$ ). Between the E and C groups, there was a significant difference at P0. Between the C and M/D groups, there was a significant difference at P3 and P6. Between the E and M/D groups, there was a significant difference at all ages except P60. [Note that despite the significant difference between E and M/D groups at P11, the

statistical comparison among all three groups at P11 did not reach significance ( $F_{2,11}=1.932$ ,  $p=0.19$ ).]

### Isocortical Surface Area

As shown in Figure 3B, isocortical surface area was significantly different among the treatment groups at P3 through P11 (asterisks; P3:  $F_{2,9}=5.642$ ,  $p<0.05$ , P6:  $F_{2,11}=21.720$ ,  $p<0.001$ , P11:  $F_{2,11}=16.724$ ,  $p<0.001$ ), with a trend towards significance at P19 and P60 (cross symbols; P19:  $F_{2,9}=3.453$ ,  $p=0.08$ , P60:  $F_{2,9}=3.558$ ,  $p=0.07$ ). Between the E and C groups, there was a significant difference at P6 and P11. Between the C and M/D groups, there was a significant difference at P3, P6 and P11. Between the E and M/D groups, there was a significant difference at P3, P6 and P11.

Figure 3

### Regional Patterns in Cortical Thickness

Specific regions where regional thickness was significantly different between E and M/D groups were identified via the TFCE method at all ages. At P60 there were no regional significant differences seen between the E and C or C and M/D groups. In a comparison between E and C groups at P0 and P11, significant clusters were present. Additionally, significant clusters were apparent in a comparison between C and M/D groups at P3 and P6. At all other ages

there were no significant regional differences found between groups. In the E versus M/D and C versus M/D comparisons, these regions covered primary motor, somatosensory, and visual cortices. Differences between C and E animals were focused mainly on primary motor and somatosensory areas (Figure 4).

Figure 4

#### **4. Discussion**

Overall, the E group displayed the lowest values on all of the measures presented here, which was expected. Histological studies of gray matter reduction (Miller 2007) as well as MRI studies of reduced brain and cortical volume (Parnell 2009, O'Leary-Moore 2010) support these findings. Additionally, these data extend previous findings in terms of suggesting specific developmental abnormalities in cortical thickness and surface area, and defines the time period during which these cortical abnormalities can be seen. Importantly, these data present the first evidence of developmental patterns in reduced brain volumes, cortical volumes, cortical thickness and cortical surface corresponding to late gestation in humans.

In the research presented here in response to prenatal exposure to maltose/dextrin (administered as a caloric control for ethanol), brain mass, brain

volume, isocortical volume, isocortical thickness and isocortical surface area were all higher than in C or E groups. While these differences were not expected, and have not been demonstrated previously, it is possible that nutritional or environmental enrichment effects of administering maltose/dextrin to these animals may have been present.

It is difficult to determine a consensus among studies of FASD in terms of effects of control treatments, as not all studies employ isocaloric controls, and those studies that use isocaloric controls vary in terms of a number of experimental parameters. In addition to the different time periods of exposure, the actual solution often differs (sucrose versus maltose/dextrin), the administration of the solution differs (gavage versus injection), some studies use only a sucrose control (and do not include an untreated control; e.g. Miller 1999), some studies use liquid diets only (in comparison to liquid diet with chow supplementation; e.g. Hammer 1981) and in a number of studies, the control groups are combined (e.g. Cui 2010).

Previous research is also inconsistent in terms of effects of isocaloric controls on brain mass. Research employing isocaloric controls for ethanol administration during gestation range from reporting no effects on brain and body mass (e.g. Davies 1981, Margret 2005) to decreased body and brain masses (e.g. Cook 1997) in response to isocaloric control treatment. One study examining the effects of ethanol on brain development in BALB/c mice found that administration of a sucrose solution throughout gestation reduced body masses and corpus callosum lengths but not brain masses compared to either ethanol-

treated or untreated control animals (Wainwright 1985). However, increases in brain masses are not reported. Additionally, comparison to the studies of the effects of ethanol on brain volume measurements in mice taken at specific time points during development (Parnell 2009, Godin 2010, O'Leary-Moore 2010) are not possible as control animals in these studies were given injections of Ringers solution (typically consisting of sodium chloride, potassium chloride, calcium chloride and sodium bicarbonate); not an isocaloric solution.

Recent studies provide support for the theory that high-fat, high-calorie diets during gestation may be harmful to offspring (e.g. Zhang 2011). However, while calories are not typically reported in studies of this kind, animals given high-fat, high-calorie diets during gestation tend to gain more mass than untreated control animals, and this was not observed in the present study. Given that the M/D dams did not necessarily experience increased fat intake, and did not show increased body mass compared to ethanol or control animals, the M/D dams and their offspring may not have experienced the harmful effects of high-fat, high-calorie diets. Food intake between the M/D and E dams was matched, as was calorie content of the M/D versus ethanol solutions. However, the M/D dams received both standard chow as well as maltose/dextrin compared to the C dams that just received standard chow. Thus, it is possible that the overall diet of the M/D dams could have had benefits not elicited by the diet of the C dams. By ingesting additional carbohydrates, the M/D group may have had an additional source of energy that the C group was not exposed to.

Additionally, the effects on the experimental variables could be due to environmental enrichment in the sense that the immature brain is being stimulated by a novel environmental factor, or maltose/dextrin. While administration of maltose/dextrin during gestation would be an unexpected form of environmental enrichment, it is possible that similar benefits in terms of increased cortical thickness are being seen here (see Greenough 1984, Hannigan 2000, The National Academies 2005 for review).

It is important to note that the increase in the measurements performed here in M/D animals does not necessarily reflect a benefit. However, these results emphasize the importance of including a calorie-matched control in experiments investigating prenatal exposure to alcohol, and suggest that further experimentation may be needed to explore the specific effect of maltose/dextrin administration.

Patterns of brain volume and isocortical volume measurements corresponded to brain mass as expected. In each treatment group, measurements increased with age, and treatment groups differed among each other at the earlier time points. Isocortical volumes showed more significant differences among groups at later ages than brain volumes. One explanation for these discrepancies could be that isocortical volume is differentially affected by prenatal exposure to ethanol. Previous work in structural MRI has shown a differential effect of prenatal ethanol exposure on cortical volume as opposed to brain volumes (O'Leary-Moore 2010). While this work was conducted with a very limited exposure to ethanol, and at earlier time points than those studied here,

there is a possibility that longer exposure to ethanol causes differences in brain and cortical volume to be seen specifically at later ages.

Cortical volume is geometrically defined as a product of cortical thickness and cortical surface area. Additionally, recent research suggests that cortical thickness and surface area provide independent information about the development of the cerebral cortex (Raznahan 2011), and the importance of looking at all three of these measurements cannot be overlooked. The results presented here are particularly interesting in this respect, as cortical thickness differences among groups are seen mostly at earlier ages (P0 through P3), while surface area differences among groups are slightly later (P3 through P11). An interaction between cortical thickness and cortical surface area supports the results found in isocortical volume at these ages. Isocortical thickness and surface area are also thought to be affected by cell number and cortical organization. Histological studies providing evidence of reduced cell numbers and altered neuronal orientation and organization with prenatal ethanol exposure (Miller 1988, Dunty 2001), specifically around the time of birth in rats (Miller 1988) also support the differences in isocortical volume, thickness and surface area seen specifically at the earlier time points investigated here.

Isocortical volume differences among the three groups were statistically significant at P19 with a trend towards significance at P60, while there were only trends toward significance in cortical thickness differences among the groups at P19, and surface area differences among the groups at P19 and P60. One possible explanation for these discrepancies could be explained by the sensitivity

of the different measurements. As in earlier ages, there might be an interaction between cortical thickness and surface area that could explain the isocortical volume measurements. Additionally, the isocortical volume measurements are purely voxel-based, while calculating cortical thickness and surface area relies on surface-based methods. In voxel-based measurements, the main sources of error arise from the delineation of the boundaries of the cortex, as well as partial volume effects. The surface-based methods used to calculate thickness and surface area rely on additional manual segmentations of the volumetric data, and algorithms used to create surfaces may also introduce additional error to the measurements. Thus, it is possible that at the later ages, the sensitivity of the thickness and surface area measurements prevented differences among the groups from reaching statistical significance. Additionally, a mid-cortical surface was chosen to most accurately represent the true isocortical surface area. While this prevents over- or underestimation in surface area measurements that would be caused by using the pial surface or the surface of the gray-white matter boundary, this could be an additional source of the discrepancy between isocortical volume and isocortical surface area data. Overall, the research presented here supports the concept that volume, thickness and surface area can provide important, independent information, and suggests that measures of both cortical thickness and surface area should be considered in relation to cortical volume. Additionally, it is suggested that prenatal exposure to ethanol may have specific, independent effects on these measures.

In an attempt to determine the areas of the cortex most affected by prenatal exposure to ethanol, statistical differences across the whole isocortex were compared across groups using a TFCE analysis. The fact that the largest cortical thickness differences were seen specifically in primary motor, somatosensory and visual areas is important in terms of interpreting symptoms of FASD. These areas are vital for the processing of environmental information, and specific abnormalities in these areas during cortical formation could lead to symptoms commonly associated with FASD. Additionally, previous structural MRI studies have related neuroimaging outcomes to behavior (Willoughby 2008, Coles 2011). While these studies did not focus specifically on the cerebral cortex, and were performed in human children and adults, results from these studies suggest that the MRI outcomes caused by prenatal exposure to ethanol presented here could potentially be related to future behavioral abnormalities.

The regional patterns presented here also mirror histological data suggesting specific deficits in cortical formation in the somatosensory cortex (Margret 2005, Margret 2006, Granato 2006) caused by prenatal exposure to ethanol. Additionally, these data expand upon previous work by suggesting specific insult to the primary motor, somatosensory and visual cortices. It is important to note that not all MRI studies examining the effects of gestational alcohol exposure are in consensus in terms of specific regional patterns of cortical thickness. For instance, studies in children and adolescents have suggested that there might be an increase in parietal thickness relative to brain size caused by exposure to ethanol during gestation (i.e. Sowell 2008, Yang

2011). However, the processes that occur during gestation in the human, and during childhood and adolescence may not be the same, and ethanol exposure during gestation may have differential effects on brain development during these time periods.

Overall, this research corresponds to histological evidence, suggesting that MRI could be used to detect cortical abnormalities caused by prenatal exposure to ethanol. Additionally, by utilizing MRI to define a specific pattern of abnormal development over a range of time points, this research could contribute to early diagnosis of FASD via imaging methods in the future.

## **Chapter 3. A Comparative Analysis of DTI Patterns to Species-Specific Time Courses of Development**

(This chapter has been adapted from Leigland and Kroenke 2011.)

### **1. A Review of DTI Studies with Reference to Neuroanatomical Development**

As mentioned in Chapter 1, a great deal of histological research has focused on attempting to quantify brain development as a measurable progression through a defined series of milestones in the developing cerebral cortex. Additionally, research has been conducted using MRI paralleling histological studies. However, it is difficult to link these approaches given the different modalities (i.e. histology versus imaging) and the different models employed (i.e. animal versus human studies). A timeline defining normal and abnormal development, linking research modalities, would allow for MRI to be related to underlying neuroanatomy, as well as for MRI and histological research done in animal models to be related to the human condition. In pursuit of this goal, the following research was conducted to link both animal and human imaging studies utilizing DTI to a series of defined neuroanatomical events in the developing cerebral cortex.

Several recent studies of brain development have provided evidence that DTI strategies are of potential utility for characterizing maturation of the cerebral cortex. Immediately following migration of pyramidal neurons from ventricular zones of the forebrain to the cortical plate, neurons exhibit simple morphology

characterized by elongated cell somas and undifferentiated, radially-oriented apical dendrites (Juraska 1979, Sidman 1982). As the cerebral cortex matures, obliquely-oriented collaterals of apical dendrites, basilar dendrites, and axons arborize to provide a scaffold for the formation of functional synapses (Conel 1939). Changes in water diffusion anisotropy take place along with these cellular-level morphological transformations. In the immature cortex, preferential restriction of diffusion in directions parallel to the pial surface, and relative lack of restriction in directions perpendicular to the pial surface are thought to play a role in prominent diffusion anisotropy seen at this time (Baratti 1997, Thornton 1997, Neil 1998, Mori 2001, McKinstry 2002). As morphological differentiation occurs within the developing cerebral cortex, cortical FA decreases (McKinstry 2002). Additionally, diffusion within the mature cortex (at a time when neurons are highly differentiated) is nearly uniformly restricted in all directions, and diffusion anisotropy is measurable but subtle (Bhagat 2004, McNab 2009).

The component of cerebral cortex termed the neuropil, which consists of axons, dendrites, and associated extracellular space, represents 70-80% of the cerebral cortical volume fraction at maturity (Miller 1990, Granger 1995). Given the relative sizes (volume fractions) of other elements such as glial cells (3.6%), vasculature (4.3%) and neuron cell somas (22%) (Miller 1990), it has been proposed that the loss of cortical diffusion anisotropy with brain maturation can be attributed to morphological differentiation of the neuropil (McKinstry 2002).

If cortical FA reflects the degree of differentiation of the neuropil rather than some other anatomical transformation, then FA would be expected to

depend directly on the age of neurons within a given cortical region. Laminar (Rakic 1995) and regional (Bayer 1991, Caviness 2003) patterns of neurogenesis have been extensively characterized in several species and are known to produce gradients in neuron age throughout the cerebral cortex. Laminar and regional patterns of cortical FA have also been examined at multiple stages of development following neurogenesis that help in evaluating whether morphological properties of the neuropil determine cortical FA values in the immature cortex.

Pyramidal neurons of the cerebral cortex are generated in an inside-out manner; neurons of deep cortical layers are born on earlier dates than neurons of more superficial layers (Rakic 1995). As a result, there is a laminar gradient in the age of these cells. Correspondingly, at early stages of cortical development, neurons of deep cortical cell layers have developed more extensive networks of obliquely-oriented collateral branches of apical and basal dendrites than have neurons of superficial cell layers (Conel 1939, Juraska 1979). Based on these observations, a laminar gradient in cortical diffusion anisotropy would be expected, with superficial layers exhibiting higher anisotropy than deeper layers. In support of this theory, the laminar dependence of cortical FA in fetal baboon brain provides evidence that a superficial-to-deep, high-to-low intracortical FA gradient exists (Kroenke 2005, Kroenke 2007). Laminar gradients in FA have also been documented in rat cerebral cortex (Sizonenko 2007, Huang 2008).

In addition to laminar patterns in neurogenesis, a regional gradient has been described, in which neurons of a given cortical lamina are born earlier near

the source of a transverse neurogenic gradient (TNG; Bayer 1991, Caviness 2003, Suter 2007) than at distal extremes of the cerebral cortical sheet. The TNG is a gradient in the time course of neuronal production emanating from a site in the proliferative ventricular neuroepithelium, opposite the internal capsule (Smart 1973, Marin-Padilla 1978, McSherry 1984, Miyama et al. 1997). The neurodevelopmental mechanism giving rise to the TNG of cortical pyramidal neurons has not yet been elucidated. However, the TNG source within the cortical sheet has been mapped onto models of the cortical surface for rodent species (Smart 1983, Bayer 1991), carnivores (ferrets (McSherry 1984, McSherry 1986), cats (Marin-Padilla 1978)), and primates (Sidman 1982). In ferrets and cats, the TNG gives rise to a 5-day age difference between neurons of a given lamina located at the TNG source and neurons located at the occipital pole (Marin-Padilla 1978, McSherry 1984, McSherry 1986). FA patterns have also been found that mirror this pattern. In the ferret (Kroenke 2009), cortical FA values measured at ages P6 through adulthood were fitted to a model in which FA decreases exponentially with postnatal age following migration of pyramidal neurons to the cortical plate. From this analysis, it was found that the difference in FA between the TNG source and occipital pole corresponds to an age difference of 5.0 days, in agreement with previous histological estimates (Marin-Padilla 1978, McSherry 1984, McSherry 1986), and in close correspondence to differences in the ages of layer II neurons estimated by autoradiographic cell-birthdating studies of ferret somatosensory and visual cortical areas (Jackson 1989, Noctor 1997). Similar rostral/lateral to caudal/dorsal cortical FA patterns

corresponding to the TNG have also been observed in rat (Huang 2007), baboon (Kroenke 2007), and human (delpolyi 2005).

Quantitative characterizations of laminar and regional patterns of cortical FA have thus established a correspondence with the age of pyramidal neurons within ferrets and baboons. This association is suggestive that a relationship exists between changes in cortical FA and morphological development of the neuropil. However, an independent experimental confirmation that changes in cortical diffusion anisotropy occur along a time course that is consistent with the time course of morphological differentiation of the cerebral cortex across species has yet to be established.

In an effort to provide this confirmation, herein a systematic comparison of the time course of FA changes to the species-specific time course of brain development, estimated from comparative analyses of developmental event timings reported in classical anatomical studies (Finlay 1995, Darlington 1999, Clancy 2007), is described. The first hypothesis of this experiment was that FA patterns can be modeled as an exponential decay with development across species, suggesting a common mechanism underlying changes in isocortical FA. The second hypothesis of this experiment was that the time during which isocortical FA decreases exponentially within the developing cerebral cortex directly corresponds to the same, specific neuroanatomical events across all species evaluated. The results of this comparison provide a novel, detailed association between FA and underlying neuroanatomy. Additionally, results of

this comparison will enable researchers to relate both FA and histological results across species as well as across various stages of cortical development.

## 2. Methods

Indices of cortical diffusion anisotropy have been characterized throughout early development in five species: mouse (*Mus musculus*), rat (*Rattus norvegicus*), ferret (*Mustela putorius furo*), baboon (*Simia hamadryas*), and human (*Homo sapiens*) (McKinstry 2002, delpolyi 2005, Gupta 2005, Kroenke 2007, Larvaron 2007, Sizonenko 2007, Bockhorst 2008, Huang 2008, Baloch 2009, Barnette 2009, Kroenke 2009). For the subset of studies suitable for the analysis described here, the species-dependent time course of reduction in cortical FA is quantified in terms of an exponential decay time constant,  $\tau_{FA}$ . The estimated  $\tau_{FA}$  values are compared to independently-estimated time courses of brain development for these species using a model developed by Finlay et al. (Finlay 1995, Darlington 1999, Clancy 2007).

It is well-recognized that the length of gestation is highly variable relative to other aspects of development across species (Finlay 1995, Darlington 1999, Clancy 2007). As a result the relevant measure of age is relative to conception rather than to birth. Gestation lengths of 18.5, 21.5, 41, 185, and 270 for mouse, rat, ferret, baboon, and human, respectively (Darlington 1999), have been assumed for purposes of converting postnatal to post-conceptual age.

An additional convention adopted herein is the use of the term cerebral cortex synonymously with the terms “isocortex” or “neocortex.” The inclusion of

isocortical regions was a criterion for inclusion of published studies in this analysis due to differences between the allocortex and isocortex mentioned in Chapter 1. The isocortex shows consistent cortical developmental patterns versus areas in the allocortex. Importantly, non-isocortical gray matter structures also do not exhibit high-to-low changes in FA with development (Kroenke 2007, Kroenke 2009).

Criteria for review were that cortical FA values during the fetal and/or perinatal periods are reported in graphical or tabular format, on healthy (or experimental control) individuals, and that no redundancy in the set of individuals may occur between data sets. Diffusion anisotropy values were obtained from these articles either directly from the authors, from data values listed in the published paper in a tabular format, or by estimating data values from published graphs. Many of the reports included here were directed at different regions of interest within the isocortex. If the entire isocortex was not studied (e.g. in a surface-based analysis), all regions of interest studied were averaged at each developmental time point for the analysis presented here to provide an approximation of overall isocortical FA. Mean FA values incorporate several cortical lamina, and thus represent a heterogeneous set of FA values across the cortical depth. In cases where values were reported for different layers, data were collected only from superficial layers.

For one of the studies conducted on human subjects (deLpolyi 2005), it was not feasible to extract FA values from the published graphs. However, in this case, FA changes were modeled as a linear decrease with age within four

distinct cortical areas. Cortical FA values were thus obtained by averaging the four reported slope and intercept values, and interpolating FA values along a line described by the mean slope and intercept values over the age range reported for individuals in this study.

As different measures of cortical diffusion anisotropy were used among the studies reviewed here, all measures were converted to FA.

$$- \frac{\lambda_1 - \lambda_2}{\lambda_1 + \lambda_2 + \lambda_3} \quad [3.1]$$

$$[3.2]$$

In equations [3.1] and [3.2], ADC is the apparent diffusion coefficient, and  $\lambda_1$ ,  $\lambda_2$ , and  $\lambda_3$  are eigenvalues of the diffusion tensor (Basser 1994, Basser 1994). Two alternative rotationally invariant measures of diffusion anisotropy are  $A_\sigma$  and relative anisotropy (RA). The conversion of  $A_\sigma$  to FA is

$$\frac{\lambda_1 - \lambda_2}{\lambda_1 + \lambda_2 + \lambda_3} \quad [3.3]$$

and the conversion of RA to FA is (Kingsley 2005, Le Bihan 2001)

$$= \frac{\dots}{\dots} \quad [3.4]$$

It has been previously proposed that, for a single position with respect to the regional cortical FA gradient, cortical FA decreases exponentially from a maximal value ( $FA_{max}$ ) observed immediately following migration of immature neurons to the cortical plate, toward an asymptotic value characterizing cortical FA at maturity ( $FA_{min}$ ) along a time-course that can be characterized by the time constant  $\tau_{FA}$  (Kroenke 2009)

$$. [3.5]$$

In equation [3.5],  $t_{init}$  is the post-conceptual age at which FA begins to decrease, and is associated with the initiation of morphological differentiation within a given cortical area.

The majority of studies reviewed here do not provide an analytical expression to model FA changes with age. Exceptions are the ferret study in which the equation [3.5] expression was proposed (Kroenke 2009), a study of

human subjects in which FA changes were considered to decrease linearly with age (delpolyi 2005), and a study of human post-mortem brains in which cortical FA was approximated using a quadratic function of age (Gupta 2005, Trivedi 2009). A drawback to linear and quadratic models of cortical FA changes with age is they do not asymptotically converge to a value that is reflective of differentiated cortex. Thus, for reports reviewed here that produced data suitable for analysis using equation [3.5],  $\tau_{FA}$  values were calculated to provide comparisons to independently measured species-specific time courses of brain development.

Three of the studies reviewed could not be analyzed using equation [3.5]. For one of these cases, cortical FA was reported at two ages (Sizonenko 2007), and an additional study reported cortical FA at four ages (Larvaron 2007). For these two studies, an analysis using equation [3.5] is underdetermined because there are as many (or more) adjustable parameters in the model as there are measured data values. The study of delpolyi et al. (delpolyi 2005) was also not used for the equation [3.5] analysis because extraction of FA values required reference to a model in which FA linearly decays with age, and this step in the data analysis would introduce systematic error in subsequent fitting using the exponential function in equation [3.5]. Data from studies not analyzed using equation [3.5] are plotted as open symbols in Figure 5.

Data reported in the remaining eight studies reviewed were fitted using the equation [3.5] model and the nonlinear least squares optimization routine

implemented in Matlab (The Mathworks, Boston, MA). Results of these analyses are represented as solid curves in Figure 5.

For species in which more than one study is available (rat, ferret, and human), analyses were performed such that  $t_{\text{init}}$  values were constrained to a common species-specific value. Due to the lack of data at early and/or late ages for a subset of species, it was necessary to impose educated guesses as constraints in some optimization calculations. For the primate species, unconstrained optimization yielded  $t_{\text{init}}$  values of 125 and 195 days for baboon and human, respectively. Such values are considered unrealistically high because cortical FA is known to decrease in baboon following gestational day 100 (unpublished observations), and data from human studies indicate cortical FA decreases over the period from 175 to 195 days gestation (Neil 1998, delpolyi 2005, Huang 2009, Mukherjee 2006). Thus, optimizations were performed by constraining  $t_{\text{init}}$  values to 100 and 175 days in baboon and human species, respectively. Additionally, optimizations performed, in which  $FA_{\text{min}}$  was not constrained produced unrealistically small values for this parameter of approximately 0.05 in human studies. Although a realistic estimate of  $FA_{\text{min}}$  will depend on experimental conditions, previous estimates of cortical FA at maturity are on the order of 0.2 (Bhagat 2004). Thus,  $FA_{\text{min}}$  values for the studies of human subjects were constrained to be 0.1 or greater.

### 3. Results

Figure 5

A translational model of brain development (Finlay 1995, Darlington 1999, Clancy 2007) was used to obtain a quantitative measure of the time course of neuroanatomical development in each species. The translating time model (<http://www.translatingtime.net/>) relates post-conceptual age to a species score, an event score, an interactive term, and a constant factor of 4.34 through the expression

$$\text{Post-conceptual age} = \exp(\text{species score} + \text{event score} + \text{interaction term}) + 4.34. \quad [3.6]$$

The species score reflects the time course of development of particular species; species which develop relatively slowly will have higher scores. The event score reflects the timing of specific neural events (e.g. the appearance of the external capsule) with events occurring later in development having higher scores. The interaction term reflects a slower time course of cortical development in primates; it equals 0.249 for events occurring within the cerebral cortex in primate species and equals 0 otherwise. The constant factor represents the amount of time over which extremely early developmental events (i.e. blastulation) occur.

For each of the five species included in this review, the period of time between the end of neurogenesis in cortical layers II/III (characterized by an

event score of 1.929) and eye opening (characterized by an event score of 2.546) was calculated. This time is defined here as  $t_{\text{event}}$  and is expressed in units of days. To obtain a  $t_{\text{event}}$  for baboon (a species not explicitly included in the translating time model (Finlay 1995, Darlington 1999, Clancy 2007)), a correction factor, which is the ratio of the lengths of gestation for baboon divided by that for macaque (185/165 days) was multiplied by  $t_{\text{event}}$  for macaque. The baboon  $t_{\text{event}}$  derived is in qualitative agreement with observations reported in a histological study of baboon brain development (Dieni 2004).

Figure 6 provides a graphical comparison of  $t_{\text{event}}$  and  $\tau_{\text{FA}}$  for the five species. Generally, variation in the  $t_{\text{event}}$  is matched by a proportional variation in  $\tau_{\text{FA}}$ , which reflects agreement in the estimation of the time course of brain development between cortical FA changes and specific cortical developmental events. The line intersecting the origin, fit to the Figure 6 data (dashed line), has a slope of 0.454, indicating that the time constant associated with cortical FA decay with age is 45.4% the length of time elapsed between cortical layers II/III neurogenesis and eye opening. In this comparison, there was a significant correlation between  $\tau_{\text{FA}}$  and  $t_{\text{event}}$  ( $r = 0.996$ ,  $p < 0.0001$ ; statistics implemented in Statview [SAS, Cary, NC]).

Figure 6

#### 4. Discussion

The most notable potential deviation from a proportional relationship between  $\tau_{FA}$  and  $t_{event}$  in Figure 6 is observed for humans, in that the  $\tau_{FA}$  values for both human studies are larger than predicted based on the human  $t_{event}$ . Two potential sources of difference between data for humans and other species may be contributing to this deviation. First, the difficulty of obtaining measurements of “normal” human individuals should be acknowledged. The *in vivo* studies (McKinstry 2002, delpolyi 2005) utilized prematurely delivered human infants that showed no overt signs of neurological disorder as subjects. However, it could be argued that premature birth in itself predisposes individuals to heightened risk of abnormal brain development, and the inflated  $\tau_{FA}$  values observed here reflect reduced time courses of development relative to control individuals in this population. A similar argument could be made that the brain tissue obtained in the post-mortem analysis (Gupta 2005) is not representative of “normal” brain. A second, related potential source of discrepancy between human  $\tau_{FA}$  and  $t_{event}$  values is a species-specific mechanistic difference between biophysical determinants of cortical FA and development milestones used to build the translating time model. The authors that developed this model (Finlay 1995, Darlington 1999, Clancy 2007) have also stated that human data points used in the translating time model were limited due to the variation in measurements used as well as the ages studied in humans.

Despite this variability, patterns of cortical diffusion anisotropy during early developmental stages, found among studies both within and across species, are

strikingly similar. Changes in FA can be accurately approximated using an empirical mathematical expression (equation [3.5]), and the time periods, over which the decreases in FA occur correspond to similar neuroanatomical developmental events across species. This suggests that there is a common mechanism underlying DTI measurements among these studies. The time periods reviewed correspond to periods of neuronal differentiation, specifically a period wherein neuritic arbors become increasingly complex. Therefore, inferences about cortical microanatomy should be possible based on studies employing DTI methodology. The comparisons between time constants calculated from exponential decreases in FA and time periods characterizing specific neuroanatomical events across five different species support this concept.

The significant correlation between  $\tau_{FA}$  and  $t_{event}$  values suggests that the time course of reduction in FA corresponds to the time course of neural development for these species. In addition to suggesting that DTI methodology can infer neuroanatomical differentiation in the cerebral cortex, this comparison suggests that utilizing DTI methodology in animal species should allow for results to be applicable to humans.

## **Chapter 4. Validation of a Quantitative Model Relating DTI to Cellular Morphology in a Ferret Model of Normal Development**

(Parts of this section have been adapted from Jespersen, Leigland, Cornea and Kroenke. IEEE Trans Med Imaging. 2012.)

### **1. Introduction**

The previous chapter suggests that common neuroanatomical events across species underly the loss of diffusion anisotropy in the cerebral cortex. Additional evidence to support interpreting FA values within the developing cerebral cortex in terms of the underlying anatomical properties of brain tissue is presented here by directly examining the link between FA changes and specific cellular morphological changes. Recent research has proposed a quantitative expression relating water diffusion anisotropy, as measured by DTI, to neurite complexity, as reflected in the width of neurite orientation distributions (Jespersen 2007, Jespersen 2012). Theory and experimental validation for this expression employing a ferret model of normal cortical development is described here.

In Chapters 1 and 3, the unique ability to use DTI to study cortical development on a cellular-level basis was discussed. Cell membranes restrict water diffusion in the developing cerebral cortex. The directional dependence of water diffusion, measured in DTI experiments, can in principle reveal structure of cellular membranes. In DTI, images are formed of 3-dimensional voxels. Within each voxel, water diffusion is measured in a number of directions. This

information is characterized by the diffusion tensor (a 3 x 3 symmetrical matrix). From the diffusion tensor, the dominant water diffusion magnitude and direction, as well as the magnitude of water diffusion in directions orthogonal to the dominant direction are calculated. These values are classified as the eigenvalues (dominant magnitude =  $\lambda_1$ , orthogonal magnitudes =  $\lambda_2$  and  $\lambda_3$ ) and eigenvectors (directions) of the diffusion tensor. Using these parameters, FA is defined (providing an indication of the directional dependence of water diffusion) (Basser 1994). Given the restriction of water diffusion by cell-membranes, as well as evidence suggesting a direct relationship between cellular morphology and FA (Chapter 3), measurements of FA should provide an indication of the level of cellular morphology present in areas examined.

A recent model was proposed to quantify both the distribution of neuronal processes in the developing cerebral cortex, as well as determine a quantitative relationship between neuronal processes and FA measurements (Jespersen 2007, Jespersen 2012). This model takes into account water diffusion within neuronal processes, as well as the effect of the orientations of ensembles of neuronal processes on water diffusion. To this effect, water diffusion within the intracellular compartment of neuronal processes is characterized here by water diffusion parallel to the local axis of the neuronal processes, or longitudinal diffusion ( $D_L$ ), and water diffusion perpendicular to the local axis of the neuronal processes, or transverse diffusion ( $D_T$ ).  $D_L$  and  $D_T$  are distinct from axial and radial diffusivity in that water diffusion within the intracellular compartment is being described. Intrinsic water diffusion is defined as  $D_A$  or the difference  $D_L$ -

$D_T$ . Additionally, similar to the calculation of the diffusion tensor, this model defines a fiber orientation tensor that is based upon the dominant number (or magnitude) and orientation of neuronal processes, and the numbers of processes in directions orthogonal to the dominant direction (or eigenvalues  $[O_1, O_2, O_3]$  and eigenvectors of the orientation tensor). From this information, the anisotropy present in neurite orientations, herein termed NA, was calculated. Lastly, the water diffusion signal originates both from the volume fraction of cylindrically-structured cellular components, such as neuronal processes, as well as from the extra-cylindrical volume fraction (Jespersen 2010, Jespersen 2007). Thus the volume fraction of cylindrically structured components, such as axons and dendrites, is defined as  $v$ . The quantitative relationship developed relates water diffusion anisotropy (and the eigenvalues of the diffusion tensor) to anisotropy in fiber orientations (and the eigenvalues of the orientation tensor), specifically taking into account the contribution made to the water diffusion signal by anisotropic diffusion and the volume fraction of cylindrical processes. This relationship is defined here:

$$FA \sqrt{\sum_i \lambda_i^2} = v D_A NA \sqrt{\sum_i O_i^2} \quad [4.1]$$

In the present study, experimental validation for this model is provided by characterizing age-dependent diffusion anisotropy and neuronal differentiation in the ferret.

In an attempt to relate histology with MRI measurements, studies have been conducted in white matter comparing white matter integrity to measurements of DTI (Ding 2003, Sun 2007, Sun 2008, Zhang 2009, Leergaard 2010, Budde 2011). Additionally, quantitative measurements of demyelination and axonal degeneration have been related to diffusion measurements in a number of these studies (Ding 2003, Leergaard 2010, Budde 2011). In the developing cerebral cortex, studies have compared histological measures of laminar organization during early human gestation (Kostovic 2002), cell number in response to hypoxia-ischemia in the rat (Sizonenko 2007), gliosis in response to traumatic brain injury in the rat (Budde 2011) as well as neuronal complexity in response to neonatal enucleation in the ferret (Bock 2010) to DTI results. However, a direct quantitative relationship between DTI measurements and neuronal differentiation in the developing cerebral cortex has not been defined until this point. A quantitative link is necessary to use FA to define specific neurobiological structures and processes in the developing cerebral cortex. Additionally, defining this relationship could be particularly useful in detecting developing cerebral cortical abnormalities. Thus, the goal of this experiment was to use empirical evidence, specifically changes with development in neuronal morphology and water diffusion anisotropy in the same tissue, to validate a novel quantitative expression (equation [4.1]) defining the relationship between the orientation distribution of neuronal processes and FA.

In order to perform such a quantitative comparison, histological staining and analysis techniques were necessary to provide a representative measure of

cellular morphology. Additionally, it was important that this investigation take into account the three-dimensional properties of both water diffusion and neuronal differentiation in order to properly define the cellular morphological restrictions to water diffusion. Golgi-staining procedures were used for the research here due to the sparse, unbiased nature of the staining, as well as the ability to visualize neuronal differentiation via confocal imaging in Golgi-stained tissue. While confocal imaging of Golgi-stained neurons has been accomplished before (Tredici 1993, Freire 1995, Al-Kofahi 2002), this study presents a unique extension of these techniques to determine a quantitative estimate of neuronal arborization. Specific image registration between Golgi-stained and DTI images was performed to directly compare FA with the anisotropy of neuronal processes in identical tissue areas. An investigation was then performed examining the relationship described above (equation [4.1]) that quantitatively relates measurements of neuronal complexity to FA measurements.

The specific hypotheses of this experiment were that FA would decrease with age as described in Chapter 3, neuronal complexity would increase with age in accordance with previous literature, and that the distribution of neuronal processes could be quantitatively related to FA values using equation [4.1]. This would provide the first experimental validation that neuronal morphological complexity can be directly calculated from DTI measurements of FA.

## 2. Methods

### Animal Care

Ferret litters were purchased from Marshall Bioresources (North Rose, NY) and delivered to the Oregon Health & Science University Department of Comparative Medicine on postnatal day 5 (P5). Ferrets were supplied with food (Purina, St. Louis, MI) and water ad libitum. From arrival to 2 months of age, kits were fed a high density ferret diet (5L14) mixed with kitten milk replacer. Kits were also supplemented with Nutri-Cal (EVSCO). Adults were fed the normal ferret diet (5280). All possible measures were taken to minimize animal pain or discomfort. All experiments were carried out in accordance with the NIH "*Guide for the Care and Use of Laboratory Animals*" (NIH publication no. 86-23, revised 1987).

### Tissue Collection

Three female ferrets (P13, P20, P31) were sacrificed, and their brains collected for analysis. Animals were given an i.p. injection of 0.5 mL euthasol (Butler-Schein Animal Health Supply, Dublin, OH). Heparin (0.01 mL/10 mL), with phosphate buffered saline (1x PBS), was injected into the left cardiac ventricle until the fluid of the right cardiac atrium was clear. Paraformaldehyde (4%, approximately 35 mL, pH 7) was then injected into the left cardiac ventricle. The brains were extracted and placed in paraformaldehyde (4%, approximately 30 – 45 mL) for 24 hours. Samples were then transferred to 1x PBS at 4°C from the time of extraction until DTI scanning.

### DTI scanning

Prior to performing MRI experiments, hemispheres of each brain were separated, and right hemispheres were utilized for all subsequent procedures (No differences between left and right hemispheres were predicted in terms of either FA or the orientation distribution of neuronal processes; Left hemispheres were collected for a different set of experiments). Characteristics of FA are preserved in the post-mortem brain (Sun 2003, Sun 2005). Therefore, post-mortem scanning was not expected to alter experimental hypotheses.

### MRI procedures

Hemispheres were placed in a 15 mL tube filled with Fluorinert<sup>TM</sup> Electronic Liquid FC-77 (3M<sup>TM</sup>, St. Paul, MN), and allowed to equilibrate to room temperature. Samples were placed into a one-turn solenoid RF coil manufactured in the laboratory (transmit/receive, tuned and matched to 500MHz), and the entire apparatus was placed in the isocenter of an 11.7 Tesla magnet (Bruker, Rheinstetten, Germany) interfaced with a 9 cm inner-diameter magnetic field gradient coil insert (maximum gradient strength of 70 G/cm per x, y and z axis).

A multi-slice spin-echo pulse sequence incorporating a Stejskal-Tanner diffusion sensitization gradient pair was used to acquire DTI data. Axial slices, 150  $\mu\text{m}$  thick, of the entire hemisphere were imaged (approximately 90 slices). Voxel size was 0.15 mm<sup>3</sup>, TR was approximately 10 s (115 ms per slice), TE was 0.042 s and 6 scans were averaged together. Scan time was approximately 12

hours. The b value was  $2500 \text{ s/mm}^2$ ,  $\delta = 12 \text{ ms}$  and  $\Delta = 20.958 \text{ ms}$ . Two scans were acquired in which  $b=0$ , and diffusion anisotropy was measured using a 25-direction, icosahedral sampling scheme (Batchelor 2003).

### Diffusion Analyses

Raw data from each voxel was entered into a model selection algorithm to determine whether diffusion was isotropic, axially symmetric or point-symmetric (Kroenke 2006). FA was then calculated for each voxel using the best-fit model of diffusion anisotropy as determined by Akaike's information criterion, corrected for small sample sizes (McQuarrie 1998). This was done to avoid over-fitting data by employing only the classic diffusion tensor model (Basser 1994a, Basser 1994b) to calculate the FA value for each voxel.

### Image Analyses

FA images were transferred into the CARET software package (Van Essen 2001, [www.brainvis.wustl.edu/caret](http://www.brainvis.wustl.edu/caret), St. Louis, MO) where the cerebellar region and region defining the olfactory bulb were removed from individual images. Additionally, masks of the isocortex were made on individual images, and cortical surface models were made using standard functions in the CARET software. The isocortex/allocortex boundary was defined laterally by the fundus of the rhinal fissure, and rostrally by the lateral olfactory tract (Dennis 1975, Lockard 1983, Lockard 1985). The medial boundary of the isocortex was identified at the junction with the corpus callosum. The voxel with the maximum

cortical FA value along the cortical wall at each cortical surface node was calculated.

#### Rapid Golgi staining

Tissue samples were removed from Fluorinert immediately after the completion of DTI scanning, and placed in 1x PBS until Golgi procedures were initiated. Samples were frozen in Tissue Tek<sup>®</sup> OCT (Optimal Cutting Temperature) compound (Ted Pella, Inc., Redding, CA) using a dry-ice slurry, and 150  $\mu$ m-thick axial slices were cut. Tissue samples were directly mounted onto Gelatin subbed slides (2% for P13 and P20 samples, 5% for the P31 sample), and left to dry. Slides were then processed and stained using the Rapid GolgiStain<sup>™</sup> kit (FD NeuroTechnologies, Inc., Ellicott City, MD). Staining was performed according to kit instructions with the exception of the dehydration steps. Slides were not dehydrated in order to preserve the thickness of the cut tissue samples (resulting samples showed less than 5  $\mu$ m of diminished thickness). Golgi staining has been demonstrated to label cells sparsely, and in a non-biased manner, with 1 – 10% of cells being labeled with this method (Pasternak 1975, Shanakranarayana 2004).

#### Neurite Orientation – FA comparison

Light microscope (Zeiss 510 META NLO, Carl Zeiss AG, Oberkochen, Germany, Morphology and Imaging Core, Oregon National Primate Research Center) images at 2.5X, 5X and 10X magnification were recorded at each age for visual comparisons. For quantitative comparisons of measured FA and the

orientation distributions of neuronal processes, 5 slices of the P13 hemisphere were utilized. High resolution (25X) images were obtained utilizing back-scattered light of wavelength 633 nm on a confocal microscope (Leica SP5 AOBS, Leica Microsystems, Bannockburn, IL, Morphology and Imaging Core, Oregon National Primate Research Center). For the five equally-spaced axial sections of the P13 hemisphere, 32 775 × 775 × ~100 μm fields were identified at approximately equally-spaced positions along the rostral/caudal extent of the isocortex. These fields were further separated into 4 sub-fields to more closely resemble the areas of the DTI voxels. Each of the 3D Confocal images were thresholded to produce binary 3D datasets (ImageJ, NIH), which were then transformed using a 3D skeletonization algorithm (Malandain 1992, Palagyi 2001) implemented in Matlab (Matlab, The Mathworks, Boston, MA). Branches of neuronal processes were identified within the skeleton by identifying groups of three or more connected voxels. Each branch was then segmented into sections of 10 contiguous coordinates, and the orientation of each segment was determined by computing the 3D orthogonal distance regression line from the 10 coordinates. Orientations of the fitted 3D vectors were then plotted onto a sphere to represent the neurite orientation distribution; each black mark on the sphere represents an orientation in 3D of one neuronal process (Figure 7).

Figure 7

The fiber orientation tensor of neuronal processes was measured from this distribution, and values of NA (or the anisotropy of the neuronal processes) were calculated.

### Registration of Golgi-Stained Tissue to DTI Images

For the P13 brain, the Golgi and DTI data were directly compared to each other. The overall strategy to register the two sets of images was to perform five separate landmark-based linear registration transformations (Umeyama 1991) to the DTI data to obtain slices that are coplanar to each of the five Golgi-stained sections analyzed. In order to generate landmarks to guide the five registrations, 3D surface models of the cerebral cortical surface were first constructed from the Golgi and DTI data, and these surfaces were registered to one another. From the registered 3D surface models, it was possible to utilize a set of points that outline the cerebral cortex in a given Golgi section to determine the corresponding plane in the DTI data.

To construct the 3D surface model from the Golgi data, montages of 2.5x magnification images were assembled for the 70 adjacent 150  $\mu\text{m}$  axial sections making up the P13 left hemisphere. The outline of the cortical surface was manually traced on each montage, and each contour trace was recorded as an ordered set of 2-D points (red dots, Figure 8A). The 70 contour traces were then used to construct a model of the cortical surface, using functionalities in the CARET software, following procedures described in the software documentation. In the Golgi-based cortical surface model (Figure 8B), surface nodes closest to

each of the contour trace points in Figure 8A are shown as red spheres. The operations used to generate a 3D cortical surface model from the DTI data (Figure 8C) also utilized functionalities of CARET software, and have been described previously (Kroenke 2009).

## Figure 8

Next, a surface-based registration of the Golgi and DTI models of the cerebral cortex was performed. This step was implemented using CARET software following previously-described procedures (Kroenke 2009). A set of six sulcal landmarks (coronolateral sulcus (CLS), sylvian sulcus/presylvian sulcus (SS/PSS), suprasylvian sulcus (SSS), splenial sulcus (Sps), and cruciate sulcus (CS), and the anterior rhinal fissure (aRF); shown as yellow spheres, Figure 8B,C) were used to constrain the surface-based registration. The result of the surface registration procedure is to establish a one-to-one correspondence between nodes of the Golgi surface model and nodes of the DTI surface model. Surface nodes on the DTI model that correspond to the five contour traces (red spheres, Figure 8B) are shown as green spheres in Figure 8C.

Linear transformations that specify each of the five P13 Golgi slices in the DTI frame were obtained following the method described in (Van Essen 2001) using the set of planar contour trace points (e.g., the set of red points for a given section in Figure 8A) and their associated nodes on the DTI-derived cerebral

cortical surface model (green spheres for the corresponding section, Figure 8C). Parameters that specify a rotation matrix  $R$ , a scaling parameter  $c$ , and the translation vector  $t$ , were determined that operate on an arbitrary point  $i$  in the DTI frame,  $P_i^{DTI}$ , to give the corresponding point in the Golgi frame,  $P_i^{Golgi}$  according to the expression:

$$P_i^{Golgi} = cRP_i^{DTI} + t. \quad [4.2]$$

The above expression contains four adjustable parameters; a rotation angle specifies the elements of the  $2 \times 2$  rotation matrix  $R$ ,  $c$  is a scalar, and  $t$  contains 2 adjustable parameters in a  $2 \times 1$  column vector. Vector quantities, such as the diffusion sensitization,  $q$ , can be transformed from the DTI frame to the Golgi frame according to  $q^{Golgi} = Rq^{DTI}$ . Diffusion data were expressed in each of the five P13 Golgi slice frames by re-sampling the diffusion-weighted images, and re-calculating diffusion tensors for each voxel. For the three most ventral slices analyzed, there was a subset of contour trace points along the medial boundary that overlap non-cortical tissue. These points were not included in the set of points used to determine linear registrations because the medial boundary for these slices is not easily recognized in the MRI data. The regions of contour traces used for registrations to the DTI data are overlaid on FA parameter maps for the 5 slices in Figure 9A (red dashed curves). Traces connecting the set of points in the DTI frame used to determine the linear registration parameters are also projected onto the Figure 9A FA maps (green dashed curves). To provide an estimate of the precision in the linear registration, the distance between Golgi and DTI landmark pairs was determined. The

average inter-landmark distance within the Figure 9A planes is 0.36 mm. However, as described below, manual adjustments were made to minimize in-plane mis-registration effects. An estimate of the mis-registration effects that cannot be corrected by manual adjustment is the average distance for each of the DTI landmarks (green spheres, Figure 8C) to the corresponding plane in Figure 9A, which is 0.20 mm.

## Figure 9

The locations of the 32 Golgi fields used for axonal/dendritic orientation distribution determinations are indicated in Figure 9B. As mentioned above and illustrated in Figure 9B, each Golgi field was subdivided into four quadrants so that the volumes of the quadrants approximately match the volume of a single DTI voxel. The center of each Golgi field, which is known in the Golgi reference frame common to the set of points  $P_i^{Golgi}$ , was transformed to the DTI frame using the equation [4.2] parameters (blue dots, Figure 9A). For 26 of the 32 Golgi fields, small manual adjustments to the location of the Golgi field in the DTI frame were necessary to ensure the neighborhood of DTI voxels was located in cerebral cortex that most closely corresponds to the location of the Golgi field center. For the remaining 6 Golgi fields (asterisks, Figure 9A), no manual adjustment was necessary. For each Golgi field, DTI voxels corresponding to each quadrant were identified by adding/subtracting 387.5  $\mu\text{m}$  to/from the Golgi

field center position in the DTI frame. Each set of four DTI voxels is color-coded yellow in Figure 9A.

### Statistics

Maximum cortical FA was compared across age groups. One-way, fixed effects ANOVAs were used to determine the effects of age on cortical FA. NA values were calculated from neurite orientation distributions obtained from each of the 128 regions (32 regions divided into 4 subfields) of confocal imaged Golgi data. Measured FA values were calculated for the voxel corresponding to the coordinates of each region of imaged Golgi data ( $n = 128$ , total). As no interpolation or other transformations were performed to affect voxel intensity values in the DTI data, the FA value for each voxel was treated as an independent measure in all analyses.

To quantify the relationship between FA and neurite orientation distributions in the same tissue samples in identical areas, a correlation analysis was conducted. To visualize this relationship FA values were plotted against NA values. The slope of the line in Figure 11 corresponds to the product  $vD_A$ , or 0.53.

## **3. Results**

### Temporal patterns of cortical diffusion anisotropy

Fractional anisotropy differed among the age groups ( $F_{2,12546} = 11813.8$ ,  $p < 0.0001$ ) (Figure 10, right column). FA was highest in the P13 age group (mean

= 0.561). The P20 age group had intermediate FA values (mean = 0.392), and the P31 age group had the lowest FA values (mean = 0.304). Fisher's PLSD post-hoc analyses revealed that the three groups were significantly different from each other (p values < 0.0001).

Figure 10

Relationship between anisotropy and distribution of neurite orientation distribution

Golgi-stained tissue samples were observed by light microscopy to determine if cortical neurite complexity throughout development corresponded to observed FA values. The complexity of neuronal processes in the cortex varied by age. Neuronal processes were more radially-oriented in younger brains versus older brains. In older brains neurite orientation distributions were much wider, with neuronal processes oriented both parallel and perpendicular to the pial surface. In Figure 10, the left panels show representative neurons at each age that correspond to FA maps displayed in the right column. In Figure 10E, it is evident that the neurites are no longer as radially-oriented and the extent or width of the distribution of neurite orientations is much higher than in Figure 10A or C. Paralleling these age differences were differences in FA (Figure 10 right column).

Measured FA values were quantitatively compared to values predicted from neurite orientation distribution measurements, or NA, in order to validate the previously described model for the diffusion-attenuated MRI signal (Jespersen 2007, Jespersen 2012). Using this model, it can be shown that fractional anisotropy and eigenvalues of the diffusion tensor (FA and  $\lambda_i$  for  $i=\{1,2,3\}$ , respectively) are related to the fractional anisotropy and eigenvalues of the fiber orientation distribution (NA and  $O_i$  for  $i=\{1,2,3\}$ , respectively) through equation [4.1]. The product of  $D_A$  and  $v$  was calculated by plotting the eigenvalues of the diffusion tensor against the eigenvalues of the fiber orientation tensor, and finding the line with the best robust fit to the data. This value was calculated to be 0.53, and corresponds with previous estimates (Jespersen 2012). In order to directly and quantifiably compare cortical neuronal complexity to cortical anisotropy, light microscope images of Golgi-stained tissue were non-linearly registered to DTI images of the same tissue. This involved defining contours on the light microscope images and reconstructing these contours into a cortical surface model. This cortical surface model was then registered to a cortical surface model generated from DTI images. DTI data were then re-sampled corresponding to the 5 equally-spaced axial images from which confocal data at specific regions was collected, and NA measured. The set of points defining each field in which confocal data were analyzed was then used to calculate FA, measured via DTI, in corresponding regions.

Golgi stained tissue samples were used to measure neurite orientation distributions at 128 regions within the P13 isocortex. Orientation distributions

were used to calculate NA in each region. A significant linear correlation was found ( $p < 0.0001$ ) between measured FA and anisotropy of the neuronal processes (NA, reflecting the distribution of neurite orientations) with a correlation coefficient of  $\rho = 0.40$  (Figure 11). The relationship between FA and NA is consistent with the quantitative model relating NA to FA values (equation [4.1]) with the slope of the graph in Figure 11, or  $vD_A$ , equal to 0.53.

Figure 11

#### **4. Discussion**

The temporal patterns of heterogeneity in ferret isocortex from the second to fourth weeks of life resemble previously documented patterns in other species. Over this developmental period, cortical anisotropy decreased with age. This shares similarities with cortical anisotropy patterns seen in postnatal days 4 – 10 in the rat (Huang 2008), the second to third trimester of gestation in baboons (Kroenke 2005, Kroenke 2007), and the third trimester of gestation in humans (delpolyi 2005). This gives further support to the consistent developmental gradient in FA among various species presented in Chapter 3, suggesting an underlying common mechanism of cortical development.

Due to the fact that ferrets are a popular animal model for studying cortical development, extension of the analysis of cortical anisotropy to this species

enables these observations to be placed within the context of other developmental events. Neurogenesis is mostly complete by embryonic day 36 in the ferret (McSherry 1986, Jackson 1989), followed by early stages of synaptic development occurring from birth to postnatal day 6 (Voigt 1993). The decline in cortical anisotropy with age reaches a minimum asymptote around P31, and subsequent to this (P36 to P38), ferrets exhibit a mature state of axonal clustering, similar to adult levels (Callaway 1990). These findings in the context of other developmental events, as well as the suggested common mechanism of development among different species, add to knowledge of normal neurite development in the cortex.

Here a direct comparison that confirms the involvement of neuronal differentiation in changes in cortical diffusion anisotropy is provided. As discussed in Chapters 2 and 3, theoretical considerations prompted the development of a quantitative model (Jespersen 2007, Jespersen 2012), which was hypothesized to relate cortical FA to the distribution in the orientation of cortical neuronal processes. The quantitative analysis of Golgi data presented here is consistent with previous qualitative descriptions of dendritic development in ferrets (Zervas 1999). Findings were that cortical FA reductions coincide in time with increases in the width in the orientation distribution of neuronal processes in the same tissue samples, which provides support for the quantitative model utilized in this study. Further, a significant association between cortical FA and underlying neuroanatomy, defined by the quantitative model presented here was shown.

Although a highly significant correlation was observed between FA and NA, which supports the hypothesized relationship, there was also considerable variability present in measured in the Figure 11 plot. This variability could be due to a number of factors including variations in the volume fraction of neuronal processes,  $v$ , or intrinsic diffusion anisotropy,  $D_A$ , among the different Golgi fields. Additionally, slight mis-registrations might also have contributed to this variability. The nature of the Golgi-staining procedures may introduce deformations to the tissue not accounted for by the linear registration performed here. However, manual in-plane adjustments were made to help correct for these discrepancies. Despite the variations seen in NA and FA values, a significant statistical correlation was found. Future studies investigating the potential biological or technical sources of deviation from the proposed relationship will likely contribute further to our ability to interpret cortical DTI measurements in terms of underlying anatomical structure.

In helping to elucidate characteristics of normal neuronal differentiation, and in validating the model relating cortical FA to the orientation distribution of neuronal processes, these findings link neuronal development, traditionally studied in animal model systems, to a systematic analysis of DTI data, which can be currently used in human fetuses in utero (Jiang 2007) and within prematurely delivered human infants in a neonatal intensive care environment (Mukherjee 2006). Thus, DTI is introduced as a potential tool for providing information about neuroanatomical structure in a human, in vivo setting. This also suggests the

possibility of detecting disorders associated with dendritic anomalies, such as FASD, through this non-invasive, quantitative method.

## **Chapter 5. Characterizing Early Dendritic Development in FASD via DTI:**

### **A Histological Comparison**

(This chapter will be modified for submission to the journal *Cerebral Cortex*.)

#### **1. Introduction**

The preceding results have shown that DTI is sensitive enough to show age-related differences in FA in the normal developing cortex, reflective of neuronal complexity. Additionally, it has been shown that the model described by Jespersen and colleagues (Jespersen 2012) can be used to directly compare FA and neuronal differentiation. The remaining research presented herein expands upon the patterns found in the developing cerebral cortex, and helps further characterize the quantitative relationship between FA and cortical development, specifically in FASD.

It has been shown that cell production, migration and organization are disrupted in rats prenatally exposed to ethanol (Miller 1986, Miller 1988, Miller 1990, Miller 1996, Dunty 2001, Medina 2005, Mooney 2005, Granato 2006, Miller 2007, Burke 2009). Additionally, in studies of the effects of ethanol administration during times corresponding with gestation in humans, disorganized cellular structures and dendritic anomalies have been observed in the early developing cerebral cortex that potentially contribute to cognitive and behavioral problems associated with these disorders (Davies 1981, Hammer 1981, Stoltenburg-Didinger 1983, Fabregues 1985, Yanni 2000, Cui 2010).

In one such study, ethanol was administered throughout gestation in rats, at a time corresponding to the generation and migration of neurons, and dendritic development was investigated using Golgi-staining techniques at birth, corresponding to early neuronal differentiation. This study found that animals exposed to ethanol showed decreased arborization, particularly in the somatosensory cortex in relation to other areas of the brain (Hammer 1981). A similar study in mice, using a Dil DiOlistic technique, and investigating mice at various postnatal time points (P0 – P30), corresponding to the time period over which rapid dendritic differentiation is seen, showed decreased numbers of spines, and decreased lengths of pyramidal neurons in the visual cortex. Additionally, synaptic ultrastructure over this time period was altered (Cui 2010).

Studies have also been conducted to investigate ethanol insult at times specifically relative to dendritic differentiation in the cortex. For instance, one study administered ethanol throughout gestation in the guinea-pig, and used Golgi techniques to investigate dendritic development at birth. This study found that dendrites in the somatosensory cortex were fewer and shorter than in controls (Fabregues 1985). Another study used similar techniques in a rat model of FASD, administering ethanol at birth specifically to affect early dendritic elaboration. This study also found that the extent of dendritic arborization was decreased in response to ethanol (Davies 1981).

This perturbation of normal cortical maturation during critical periods of development could lead to permanent dysfunction, causing the cognitive and behavioral deficits seen in FASD. Given the sensitivity to neuronal morphology

seen with DTI, this methodology has the potential to detect biomarkers of FASD at critical, early time periods during development. Thus, herein changes in FA as well as neuronal morphology with development in response to prenatal exposure to ethanol were investigated. Additionally, the validity of the quantitative relationship between FA and the orientation distribution of neuronal processes described in Chapter 4 in the context of a rat model of FASD was examined.

The model of ethanol administration used here in the rat, coinciding with neuronal generation and migration, was chosen to investigate disruption in cellular generation and organization (see Chapter 2), as well as neuronal differentiation. Rat dams were administered ethanol throughout most of gestation (G1- G20), and rat pups were examined at 6 postnatal time points. DTI imaging was conducted on post-mortem ex vivo samples. Subsequently, tissue was stained using DiOlistic and Hoechst staining techniques. Hoechst stained tissue was used for histologically-based calculations of cortical thickness used for comparison to cortical thickness calculated from DTI images (as well as thickness calculations reported in Chapter 2). DiOlistic techniques were chosen for use here as neurons are labeled sparsely and non-biasedly (the amount of cells stained is similar to that in Golgi-stained tissue, with approximately 1 – 10% of cells stained (Pasternak 1975, Shanakranarayana 2004)). Additionally, higher confocal resolution can be achieved with DiOlistic methods, and these methods can more easily be combined with other staining techniques than with Golgi staining techniques (Staffend 2011). The complexity of Dil-stained neurons was visually compared to FA data in the same tissue areas. Distributions of neuronal

processes were also measured from Dil stained tissue, and the anisotropy in neuronal processes was calculated. Finally, the relationship validated in Chapter 4 was used to compare the anisotropy in neuronal processes to FA measured via DTI.

One hypothesis of the following research was that these data would provide a timeline of normal versus ethanol-affected developmental changes in FA. Additionally, it was expected that prenatal ethanol exposure would cause abnormal differentiation of cerebral isocortical neurons, and that this would be reflected in higher FA values compared to control groups. Lastly, the quantitative relationship between the width of the orientation distribution of neuronal processes and FA validated in normal development in Chapter 4 was expected to be consistent in abnormal development caused by prenatal exposure to ethanol. The research presented here shows that abnormal neuronal differentiation caused by prenatal exposure to ethanol, specifically a disruption in the formation and development of neuronal processes such as axons and dendrites in the developing cerebral cortex, can be detected by DTI measurements. More specifically, this research suggests that abnormal neuronal morphology can be detected by DTI in experimental versus control animals at ages corresponding to late gestation in humans. Additionally, by validating the quantitative relationship between FA and NA previously presented, potential diagnostic capabilities of DTI are introduced.

## **2. Methods**

(Animal care, breeding, alcohol administration and blood ethanol concentration procedures are the same as those used in Chapter 2.)

### Tissue Collection

At 3 postnatal time points (P0, P3, P6), pups from the dams were sacrificed, and their brains collected for analysis (n = 2 /age/group). Pups were given an i.p. injection of approximately 0.5 mL euthasol (Butler-Schein Animal Health Supply, Dublin, OH). Heparin (0.01 mL/10 mL), with phosphate buffered saline (1x PBS), was injected into the left cardiac ventricle until the fluid of the right cardiac atrium was clear. Paraformaldehyde (2%, approximately 40 mL, pH 11) was then injected into the left cardiac ventricle. The brains were extracted and placed in paraformaldehyde (2%, approximately 40 mL) for 24 hours. Samples were then transferred to 1X PBS at 4°C. After at least 48 hours in 1X PBS at 4°C, olfactory bulbs were removed from the brains at the lateral olfactory tract, and remaining spinal cord was severed between the C1 dorsal root of the spinal cord and the medulla. Left and right hemispheres were separated, and right hemispheres of each brain were utilized for all subsequent procedures (Left hemispheres were collected for a different set of experiments: See Chapter 2).

### MRI procedures

Hemispheres were placed in a modified 5 mL conical tube filled with 1X PBS, and allowed to equilibrate to room temperature. Samples were placed into a one-turn solenoid RF coil manufactured in the laboratory (transmit/receive,

tuned and matched to 500MHz), and the entire apparatus was placed in the isocenter of an 11.7 Tesla magnet (Bruker, Germany) interfaced with a 9 cm inner-diameter magnetic field gradient coil insert (maximum gradient strength of 70 G/cm per x, y and z axis).

A multi-slice spin-echo pulse sequence incorporating a Stejskal-Tanner diffusion sensitization gradient pair was used to acquire DTI data. Axial slices, 200  $\mu\text{m}$  thick, of the entire hemisphere were imaged (TR = 4000 – 5000, TE = 42.7 ms, FOV = 5.20 x 1.28 cm, Matrix = 250 x 64, Voxel size = 0.2  $\text{mm}^3$ , Averages=6, Scan time = 12 hours). The b value was 2500  $\text{s}/\text{mm}^2$ ,  $\delta$  = 12 ms and  $\Delta$  = 20.958 ms. Two scans were acquired in which b=0, and diffusion anisotropy was measured using a 25-direction, icosahedral sampling scheme (Batchelor 2003). Scanning time was approximately 12 hours total per sample. Additionally, characteristics of FA are preserved in the post-mortem brain (Sun 2003, Sun 2005). Therefore, post-mortem scanning was not expected to alter experimental hypotheses.

### DTI analyses

FA maps were generated from DTI data using the software provided by Bruker (Bruker, Rheinstetten, Germany). FA images were transferred into ITK-SNAP (Yushkevich 2006) where the cerebellar area was removed from individual images. Masks of the isocortex were made on individual images. Only data from the isocortex was used for analysis for reasons previously described. The isocortex/allocortex boundary was defined laterally by the rhinal fissure, and

rostrally by the lateral olfactory tract. The medial boundary of the isocortex was identified at the junction with the corpus callosum. Mean FA values over the entire isocortex were calculated. In order to calculate isocortical thickness, outer and inner boundaries were defined on the isocortical mask (based upon the junction with the pial surface and the white matter, respectively). Mean isocortical thickness values were calculated based on a technique developed by Lerch and colleagues, which involved iteratively solving Laplace's equation using the Jacobi method, and computing streamlines between the inner and outer boundaries using Euler's method (Lerch 2008). In order to visualize FA results, mid-cortical surface models were created from the isocortical mask as in Chapter 2. This was accomplished using standard functions in the CARET software package (Van Essen 2001, [www.brainvis.wustl.edu/caret](http://www.brainvis.wustl.edu/caret), St. Louis, MO). A random target surface for each age was selected, and each individual cortical surface was registered to the target surface for visualization purposes. Mean FA for E, M/D and C groups at each age at each target cortical surface node was calculated and projected onto the target cortical surface for visualization.

### Histological methods

Subsequent to DTI scanning, hemispheres were sectioned coronally on a vibratome at a thickness of 200  $\mu\text{m}$ . In order to minimize the amount of tissue being examined, a method of systematic uniform random sampling was adopted (see Boyce 2010 for review). Mid-coronal sections, at 8 points corresponding to the middle of the rostral to caudal extent of the hemisphere were obtained throughout the brain, 200  $\mu\text{m}$  apart, the first section chosen randomly. These

sections were stained using a Hoechst stain (Invitrogen, Molecular Probes). The two sections corresponding to the middle of the rostral to caudal extent of the hemisphere were additionally stained using DiOlistic techniques (Gan 2000, Seabold 2010). Sections were mounted on slides using Prolong Antifade Gold mounting medium (Invitrogen, Molecular Probes).

Mid-coronal sections were chosen specifically to represent somatosensory areas of the cortex (see Hjernevik 2007). Histological studies have demonstrated reduced gray matter volumes (Margret 2005, Margret 2006, Miller 2007), disrupted organization of neurons (Granato 2006), and altered dendritic morphology (Hammer 1981, Fabregues 1985) specifically in somatosensory areas of the cortex in response to prenatal exposure to ethanol. Additionally, structural MRI studies investigating cortical thickness in children and adolescents have suggested that the somatosensory cortex may be particularly affected in FASD (Sowell 2001, Sowell 2008, Yang 2011, Zhou 2011). The results presented in Chapter 2 also demonstrate that the thickness of the somatosensory cortex is predominantly altered after prenatal ethanol exposure. Thus, differences in cortical thickness and neuronal differentiation between control and ethanol groups were expected to be greatest in the somatosensory cortex, and histological measurements were focused on this particular area.

Cortical thickness values for three hemispheres (one in each treatment group) at P6 were investigated using the 8 Hoechst-stained sections for each brain. Histological estimates included calculating the volume of brain and cortex via the Cavalieri method. Estimates of surface area were additionally made

using the Weibel probe. Isocortical thickness was calculated from brain volume, isocortical volume and surface area estimates. These methods were chosen to eliminate the potential bias introduced by the plane of the section, and optimally examine the areas of interest, and were implemented using Stereoinvestigator software (MBF Bioscience, Williston, VT). Hoechst stain images were viewed on a dedicated stereology microscope (Zeiss 510 META NLO, Carl Zeiss AG, Oberkochen, Germany, Morphology and Imaging Core, Oregon National Primate Research Center), using fluorescent stimulation. All estimates involved identifying the area of the brain or cortex by drawing a contour defining the region of interest. Estimates of the cortical thickness also involved drawing a contour of the mid-line surface (half-way between the pial and white matter surfaces) to obtain the most accurate thickness measurements of the cortex. The Cavalieri method involved placing a grid of 250  $\mu\text{m}$  over the entire tissue section. All points that were determined to be inside the contour of the whole brain or cortex were counted (again to determine brain and cortical volume). The Weibel probe involved placing a grid of lines (length 1mm, spacing 1mm) over the entire section. Intersections of any point on the grid line with the mid-cortical surface were counted. Additionally, occurrences of the left-most point of any grid line within the area defined by the brain contour were counted. Thickness was determined by the following formula:  $\text{thickness} = \text{isocortical volume} / ((2 * \text{number of intersections with mid cortical contour}) / \text{total length of lines in the brain} * \text{brain volume})$ .

DiOlistic techniques were adopted from methodology used in the lab of Dr. Veronica Alvarez (NIH, Maryland; Seabold 2010). This technique involves coating tungsten beads with Dil (Dil[1,1'-Diocadecyl-3,3,3',3'-tetramethylindocarbocyanine; Anaspec) stain. Beads are then diced, loaded into special tubing, and administered to the tissue using the Helios® Gene Gun system (Bio-Rad, USA). This technique was used to stain the tissue in a sparse, non-biased manner, in an attempt to visualize individual processes of neurons (Gan 2000, Seabold 2010).

#### Neurite Orientation – FA comparison

For visual comparisons of measured FA and neurite orientation distributions, 2 mid-coronal slices of each hemisphere (2/age/group) were utilized. Superior and inferior fields on each slice were imaged. High resolution (40X, oil immersion) images were obtained utilizing fluorescent techniques at a wavelength 561 nm on a confocal microscope (Resolution: 512x512, Speed: 400 Hz, Zoom: 1, FOV: 387.5 microns<sup>2</sup>, Voxel size: 758.32 nm x 758.32 nm x 755.31 nm, Laser for Dil visualization: 561 (17-33%)) (Leica SP5 AOBS, Leica Microsystems, Bannockburn, IL, Morphology and Imaging Core, Oregon National Primate Research Center). Maximum projection images were utilized to visualize Dil staining in these fields.

For a comparison of measured FA to a quantitative estimation of the extent of the orientation distribution of neuronal processes, one inferior field from a mid-coronal section of one hemisphere each in the C and E groups was used.

For this purpose, methods similar to those described in Chapter 4 were used. For each field, 3D confocal images were thresholded to produce binary 3D datasets, which were then transformed using a 3D skeletonization algorithm (Malandain and Bertrand 1992, Palagyi et al. 2001) implemented in Matlab (Matlab, The Mathworks, Boston, MA). Branches of neuronal processes were identified within the skeleton by identifying groups of three or more connected voxels. Each branch was then segmented into sections of 10 contiguous coordinates, and the orientation of each segment was determined by computing the 3D orthogonal distance regression line from the 10 coordinates. The fiber orientation tensor of neuronal processes was measured from this distribution, and values of NA (or the anisotropy of the neuronal processes) were calculated using methods described previously (see Chapter 4, Jespersen 2007, Jespersen 2012).

### Statistics

A two-way mixed effects ANOVA (analysis of variance) model was used to determine effects of the independent variables, treatment group (E, C and M/D) and age group (P0, P3, P6), on dependent variables: FA and cortical thickness. Upon determining main effects of the analysis, one-way ANOVAs were used to determine the separate effects of age and group on the dependent variables. Finally unpaired t-tests were used to determine differences between specific pairs of treatment groups at each age. Uncorrected alpha was set at  $p=0.05$  for all analyses. Statistics were implemented in Statview [SAS, Cary, NC].

### 3. Results

(Blood ethanol concentration results are reported in Chapter 2.)

#### Cortical FA and Thickness

As seen in Figure 12, expected patterns of decreases in FA, as well as expected laminar patterns were present in each group (FA maps and cortical surfaces for one individual in the ethanol group are shown for demonstration in Figure 12). FA was highest at P0 and lowest at P6 in all groups. Additionally, at all ages FA values in the outer layers of the cortex (nearest the pial surface) were higher than in deeper layers (though this was not directly quantified).

#### Figure 12

There was a significant main effect of age group and treatment group on isocortical FA (Age Group:  $F_{2,9}=1096.009$ ,  $p<0.0001$ , Treatment Group:  $F_{2,9}=73.605$ ,  $p<0.0001$ ). There was also a significant interaction of age and treatment group ( $F_{4,9}=13.849$ ,  $p<0.001$ ). FA was highest in the E group, and lowest in the M/D group. Fractional anisotropy differed among the age groups at P0 and P3, but not P6 (Figure 13, asterisks;  $p<0.05$ ). At P0, E versus M/D as well as C versus M/D comparisons were significantly different ( $p<0.05$ ). At P3, E versus M/D groups were significantly different ( $p<0.05$ ), with a trend for a

significant difference between E versus C, as well as C versus M/D groups ( $p=0.05$ ).

There was a significant main effect of age group and treatment group on isocortical thickness (Age Group:  $F_{2,9}=180.197$ ,  $p<0.0001$ , Treatment Group:  $F_{2,9}=12.315$ ,  $p<0.01$ ). There was no interaction between age group and treatment group ( $F_{4,9}=2.696$ ,  $p=0.10$ ). Cortical thickness was highest in the M/D group, and lowest in the E group. There was a trend for significance among the treatment groups at P3 and P6 (Figure 13, cross symbols; P3:  $p=0.08$ , P6:  $p=0.06$ ). Individual comparisons between groups at each age did not reach significance.

Figure 13

Figure 14 shows the overall patterns that were observed among the groups, with brain size and cortical thickness generally being lowest in the E group, and highest in the M/D group. Additionally, FA was generally highest in the E group, and lowest in the M/D group (FA maps and cortical surfaces are shown for one subject per group at P3 for demonstration).

Figure 14

### Stereological Estimates of Cortical Thickness

Estimates of cortical thickness in the E, C, and M/D hemispheres at P6 were 1.3, 2.0 and 2.2 mm, respectively. These are higher than estimates made by DTI in the same subjects from similar mid-coronal (rostral to caudal) extents of the brain (E=1.2 mm, C=1.3 mm, M=1.4 mm). These discrepancies could be explained by different experimental error introduced by the different measurements, as well as by different error introduced by the separate delineations of the isocortical boundaries. However, the same patterns of the M/D subject having the highest isocortical thickness, with the E subject having the lowest isocortical thickness are observed. These patterns are also the same as those observed with larger subject numbers using DTI measurements of isocortical thickness presented in the results above and in Chapter 2.

### Neurite Orientation – FA comparison

As expected, in all groups, the complexity of neuronal processes appeared to increase with age mirroring cortical FA patterns. Additionally, there appeared to be differences in neuronal complexity across treatment groups. As shown in Figure 15, maximum intensity projection images of 3D confocal data measured in superior and inferior regions of mid-cortical areas showed that neurite distribution was lowest (simpler dendritic arbors) at earlier time points compared to later time points, and that simpler neuronal arbors were present in the E group compared to the C and M/D groups (E and C groups shown in Figure 15 for comparison).

## Figure 15

In an attempt to compare FA values to values of anisotropy in the neuronal processes (or NA), NA was calculated for two inferior fields on a mid-coronal slice of a control and ethanol hemisphere at P6. Figure 16 demonstrates the original maximum intensity images of these fields, as well as the line segments used to determine the neurite orientation distribution in these fields. Using a method described previously (see Chapter 4, Jespersen 2007, Jespersen 2012), NA values were calculated from the orientation distributions of neuronal processes. The NA value for the P6 C field (with visibly more complex neuronal arbors) was higher (NA = 0.624) than the NA value for the P6 E field (with visibly simpler neuronal arbors) (NA = 0.416). Additionally, the FA values measured at these sites in the same P6 hemispheres were higher in the E (FA = 0.2) than the C animal (FA = 0.1). Applying the correction factor of 0.53 defined by the quantitative model in Chapter 4 (representing  $vD_A$ , and accounting for the contribution made to the water diffusion signal by anisotropic diffusion and the volume fraction of cylindrical processes) to NA values, E values would be expected to be slightly higher. However, FA values in the maps here are slightly lower than normal due to perfusion with an alkaline PFA solution, and the differences between the FA values in the E and C groups directly correspond to the differences in the NA values between groups.

Figure 16

#### **4. Discussion**

In all groups, visual evidence of laminar patterns were present wherein FA was highest in newer layers of the cortex nearest the pial surface, and lowest in older, deeper layers. Additionally, quantitative evidence showed a decrease in FA with age in all groups. Laminar patterns in the data presented here support histological evidence of laminar patterns in dendrite morphology (Conel 1939, Juraska 1979), as well as evidence of laminar patterns in FA data at similar time points in the fetal baboon (Kroenke 2005, Kroenke 2007) and rat cerebral cortex (Sizonenko 2007, Huang 2008). Age patterns shown here also support evidence of increasing dendritic complexity described in Chapter 4 and supported by previous research (Conel 1939), as well as evidence of decreasing FA with age (see Chapter 4; Baratti 1997, Thornton 1997, Neil 1998, Mori 2001, McKinstry 2002).

The thickness increases with age, and overall decreases in cortical thickness caused by ethanol exposure shown here support results described in Chapter 2. Additionally, lower cortical thickness overall in the E group is supported by histological evidence of reduced cell numbers and altered neuronal orientation and organization with prenatal ethanol exposure (Miller 1988, Dunty 2001), specifically around the time of birth in rats (Miller 1988). Calculations of

thickness via histological methods confirmed thickness results obtained via MRI, with the E hemisphere displaying the lowest cortical thickness, and the M/D hemisphere showing the highest cortical thickness, further validating the theory that MRI results are a reflection of underlying neuroanatomy.

There was evidence that FA measurements were lower, and thickness measurements higher, in the M/D group than in the C or E groups. While this was not expected, these results are in agreement with the structural MRI results found in Chapter 2. As described in Chapter 2, this may reflect a nutritional or environmental enrichment effect. In studies examining dendrite morphology in animals prenatally exposed to ethanol, no differences in dendritic arbors were reported (Davies 1981, Hammer 1981). However, in one of these studies, camera lucida drawings of Golgi-Cox stained hippocampal CA1 pyramidal cells displayed altered horizontal arrangements of dendritic branches in the sucrose-control versus chow-control groups. While this may not be reflected in overall dendritic length or number, abnormal dendritic arrangement would be reflected in the width of the orientation distribution of neuronal processes and could be affecting FA in the present experiment. It is important to recognize that this may not necessarily reflect a benefit of administering maltose/dextrin during gestation. However, this further supports the use of a caloric control in FASD experiments, and investigating M/D administration during gestation in more detail in future experiments.

Importantly, this is the first evidence that there are disruptions in cortical developmental FA patterns seen in response to prenatal exposure to ethanol,

and that these disruptions are directly related to neuronal morphology and differentiation. FA was lower in the E group at P0 and P3, corresponding to the period of early neuronal differentiation in the cerebral cortex. Images of neuronal structure obtained through DiOlistic staining and confocal imaging displayed shorter arbors and limited extent of neuronal arborization in E animals compared to the C and M/D groups. This is in accordance with past literature that has shown dendritic abnormalities in response to pre and perinatal exposure to ethanol in animals at time points corresponding to those studied here (Stoltenburg-Didinger 1983, Davies 1981, Hammer 1981, Fabregues 1985, Yanni 2000, Cui 2010). Neuronal arborization was quantified using methods previously described (Jespersen 2007, Jespersen 2012), and compared to DTI measurements. Neuronal arborization was highest in the C group compared to the E group corresponding to visual evidence of increased neuronal complexity and FA measured via DTI. This demonstrates that decreases in FA caused by prenatal exposure to ethanol are directly related to neuronal differentiation in the developing cerebral cortex.

Given that previous research suggests the dosing used in this study is sufficient to elicit cognitive abnormalities (see Driscoll 1990, Schneider 2011 for review), and that dendritic abnormalities have been related to mental retardation (see Stoltenburg-Didinger 1983, Kaufmann 2000 for review), it is possible that the ethanol-induced neuronal morphological abnormalities seen in the developing cerebral cortex, and reflected in FA, could lead to cognitive and behavioral deficits similar to those seen in the human condition. Many recent studies have

attempted to use structural and diffusion tensor imaging in children exposed to ethanol during gestation to relate brain volume and white matter connectivity to behavioral and cognitive performance (Willoughby 2008, Sowell 2008, Astley 2009, Lebel 2010). In one such study, white matter microstructure in the left parietal region of the brain was positively correlated with mathematical ability in children (Lebel 2010). Thus, while additional work should be done to use the specific measures presented here to find correlates to behavior, evidence suggests that behavioral deficits would be seen with this paradigm.

In respect to the isocortical thickness increases and FA decreases seen in the M/D group, it is more difficult to determine what the expected effects on behavior would be. Research suggests that environmental enrichment causes increased dendritogenesis. Additionally, thicker cortices have been observed in animals exposed to environmental enrichment. Environmental enrichment has also been suggested to be beneficial in terms of cognitive and behavioral tasks (see Greenough 1984, Hannigan 200, The National Academies 2005 for review). If neuronal differentiation is truly advanced in the M/D group, and affected in a similar way by maltose/dextrin as by environmental enrichment, then one might expect better performance on cognitive and behavioral tasks. However, as mentioned previously, it is possible that the altered patterns of neuronal branching and lower FA values in the M/D group, may not necessarily be beneficial. Thus, future research should be done to determine the neurobehavioral outcomes of maltose/dextrin administration during gestation.

This research confirms that the quantitative relationship that has been developed relating FA to underlying neuroanatomy (Chapter 4) can be used in a model of FASD. This has significant implications for the study of FASD in humans. DTI measurements can currently be performed non-invasively, in vivo, in humans at early stages of development (Mukherjee 2006, Jiang 2007). Given the sensitivity of DTI to detect abnormalities caused by ethanol exposure during gestation, and the direct relationship between abnormal FA measurements and abnormal neuronal differentiation, DTI is introduced as a potential diagnostic methodology for FASD.

## **Chapter 6. Summary and Conclusions**

Fetal alcohol syndrome and related disorders (commonly referred to as Fetal Alcohol Spectrum Disorder, or FASD) cause significant hardships to the individuals affected. The objective of the research presented here was to assess whether magnetic resonance imaging (MRI) techniques (specifically structural and diffusion tensor imaging) are sufficiently sensitive to detect neuroanatomical effects of fetal ethanol exposure on development of the cerebral cortex during the period of time corresponding to late gestation in humans. Currently, the mean age of diagnosis of FASD is years after disease onset. For example, Elliott and colleagues (Elliott 2008) report a mean age of 3.3 years at diagnosis. If MRI techniques could be used to aid in the diagnosis of FASD, these disorders could potentially be identified at much earlier ages, thus reducing the impact of these disorders (Streissguth 2004, Olson 2007).

Structural deficits in the central nervous system are commonly associated with FASD, and considered to be one of the most important factors in the development of symptomology associated with FASD, such as cognitive deficits (CDC, Riley 2011). By characterizing the specific insults to brain structure, a better understanding of the effects of fetal ethanol exposure can be gained. More precise knowledge of the exact anatomy affected, and the timeline along which these insults occur could elucidate novel diagnostic and treatment options for FASD.

As described in the chapters presented here, multiple sources of histological research have demonstrated isocortical developmental abnormalities caused by exposure to ethanol during time points corresponding to late gestation in humans. However, applying this research to the human condition has been classically difficult due to both an inability to non-invasively investigate early human development in vivo through histological means, as well as difficulties in translating research performed in animal models to humans. Due to the ability to apply MRI to both animals and humans, as well as the ability to employ MRI techniques non-invasively in vivo, MRI could provide the link necessary for diagnosis during human gestation. Indeed, work has been done using MRI techniques to determine the impact of fetal ethanol exposure on the developing cerebral cortex. However, in many cases, timelines defining normal and abnormal development have not been developed. Additionally, in many cases, a link between anatomy and MRI results has not been established.

There were three main goals of the research presented here. The first goal was to characterize developmental patterns of structural MRI results in a model of FASD, and relate these results to underlying neuroanatomy. A specific pattern of cortical structural development in FASD could help differentiate between normal appearance of the cerebral cortex and abnormal manifestations of these disorders at multiple time points. This would allow for diagnoses to be more easily obtained without the need for examination at specific ages. Additionally, by linking MRI results to histological evidence of abnormal neuroanatomy, a more clear understanding of the processes being affected by

prenatal ethanol exposure can be established. Brain volume, isocortical volume, isocortical thickness and isocortical surface area were all demonstrated to be affected by prenatal exposure to ethanol. Patterns in these measurements were defined across a period relative to late human gestation, during which time abnormal cell numbers and structure have been identified via histological methods to also be affected by prenatal ethanol exposure. Thus, a developmental timeline for prenatal ethanol effects on structural MRI measurements has been established. Additionally, evidence is provided that structural MRI methods can be used to identify large-scale effects of prenatal ethanol exposure on the developing cortex, specifically in terms of cell numbers and organization.

The second goal of this research was to specifically define the relationship between diffusion tensor imaging (DTI) measurements and the differentiation of neurons in the developing cerebral cortex. DTI, specifically measures of FA, are particularly sensitive to the restriction of water diffusion by cellular membranes. Given the structure and specific pattern of maturation of neurons during cortical formation, DTI has the potential to provide information about cortical development at a cellular level, specifically during time periods corresponding to neuronal differentiation. Multiple histological studies have provided information about the processes that take place during this time period. Additionally, multiple studies of normal cortical development have characterized FA during this time. However, these studies focus on a range of time points, and have been conducted using various animal species as well as humans, making it difficult to

form a clear view of the timeline of events and how they relate to each other and to the human condition. Additionally, no quantitative link among these studies has been developed to form a comprehensive view of how MRI relates to the neurobiological processes occurring in the cerebral cortex. A quantitative link would not only allow for MRI to be useful in diagnoses of cortical developmental abnormalities in the human by relating animal and human research, but also allow for the definition of these abnormalities in terms of the specific neurobiological structures and processes affected. The research presented here establishes a timeline of neurodevelopmental events, and relates studies of FA patterns during cortical development across species to this timeline. This provides a foundation for relating FA and underlying neuroanatomy, and allows for studies of FA conducted in animal models to be translated to human research. Additionally, a quantitative relationship between FA and neuronal differentiation was validated. This allows for measurements of FA to be definitive of the extent of neuronal arborization in the developing cerebral cortex.

The final goal of this research was to determine the effects of prenatal ethanol exposure on FA measurements, and directly compare FA to neuronal differentiation in a model of FASD. As described previously, histological studies have demonstrated disrupted dendritic formation in response to prenatal exposure to ethanol. Given the relationship established among studies of FA and the time period in which rapid dendritic differentiation occurs, as well as the empirically validated quantitative relationship relating FA to the extent of neuronal complexity, it was expected that measurements of FA would reflect histologically-

validated effects of prenatal ethanol exposure on dendritic arborization. Prenatal ethanol exposure caused significant decreases in FA values. In the same samples, DiOlistically labeled neurons had shorter processes, and the extent of neuronal arborization was decreased. Quantification of the arborization of neuronal processes in histologically stained tissue showed higher anisotropy of the neuronal processes in animals prenatally exposed to ethanol relative to controls, mirroring FA values in identical areas of the tissue. Thus, DTI measurements of FA were shown to be sufficiently sensitive to detect cortical abnormalities in a model of FASD, and FA measurements were directly and quantitatively linked to neuronal morphology.

Collectively, these results present evidence that structural imaging and DTI methods can potentially be used to diagnose FASD in humans. A developmental timeline was presented for the effects of prenatal exposure to ethanol on structural MRI measures. Additionally, structural MRI measures were shown to be indicative of large-scale cortical developmental anomalies, such as abnormal cell number and organization, caused by prenatal ethanol exposure. A comprehensive analysis of DTI measurements of FA in relation to neuroanatomical events was presented allowing for research in FA to be related to specific cortical processes, to be comparable across species, and to be applicable to the human condition. Additionally, FA was quantitatively related to neuronal differentiation both in normal development and in a model of FASD, suggesting potential diagnostic and therapeutic capabilities of imaging techniques.

## Future Directions

While the preceding results strongly support the ability of MRI to detect and define neuroanatomical processes in the developing cerebral cortex, there are a number of ways this research could be supported and expanded upon in the future.

- While there is a strong relationship between the structural imaging results presented here and cortical cell number and organization, future studies should attempt to quantify this relationship. Histological methods have been developed that would enable quantification of cell numbers, and the techniques developed here for quantifying neuronal complexity could, in theory, be applied to columnar organization. Directly comparing structural MRI measurements to histological estimates of cell number and organization in identical tissue would further strengthen the diagnostic capabilities of imaging techniques.
- One limitation of conducting this research utilizing a rat model of FASD is that cortical gyration cannot be measured. As the human brain is gyroencephalic, this could be an important consideration in terms of how structural and diffusion tensor imaging results are affected by the folding of the brain. Therefore, another potential avenue of research could focus

on the effects of prenatal exposure to ethanol on cortical gyration, and the neuronal processes that effect gyration in the brain.

- Potentially important results in the research presented here were the effects of administration of calorie-matched maltose/dextrin to rat dams during gestation, included as a separate control from untreated animals. Both structural and diffusion tensor imaging measurements showed unexpected effects in this group, with maltose/dextrin treated animals displaying apparently advanced development relative to both untreated controls and ethanol-treated animals. Future imaging, histological, pharmacological and behavioral research could help to determine the exact effects of this treatment.
- In all groups, future behavioral experiments would be a helpful addition to the experiments presented here. While structural deficits are commonly associated with future cognitive and behavioral deficits in children prenatally exposed to ethanol, studies comparing imaging and histological results to specific cognitive and behavioral impairments could aid in the diagnosis and treatment of FASD.
- While FA across the cortex was affected in the model of FASD presented here, regional and laminar analyses of the effects of prenatal exposure to ethanol on FA would help to both characterize FASD, as well as

potentially distinguish FASD from other disorders associated with abnormalities in neuronal differentiation.

- An important step in using DTI as a diagnostic tool will be to examine the effects on the measurements presented here of a range of doses of ethanol, as well as a range of time periods during which ethanol is administered. The dose of ethanol used in this study was high, and administration of ethanol occurred throughout rat gestation. As prenatal exposure in the human varies greatly in terms of amounts of alcohol consumed by mothers and time periods of consumption during gestation, a range of doses and time periods of ethanol administration will help relate this research to the human condition.
- Lastly, future studies should take advantage of the relationships defined here between imaging techniques and neuroanatomy in the setting of human gestation. DTI experiments have been conducted in fetuses in utero (Jiang 2007) and within prematurely delivered human infants in a neonatal intensive care environment (Mukherjee 2006). Thus, the potential exists for DTI research to be used as a diagnostic tool for FASD in human studies.

## **References**

1. Alexander, A.L., J.E. Lee, M. Lazar, R. Boudos, M.B. DuBray, T.R. Oakes, J.N. Miller, J. Lu, E.K. Jeong, W.M. McMahon, E.D. Bigler, and J.E. Lainhart, Diffusion Tensor Imaging of the Corpus Callosum in Autism. *NeuroImage*, 2007. 41: p. 15-30.
2. Al-Kohafi, K.A., S. Lasek, D.H. Szarowski, C.J. Pace, G. Nagy, J.N. Turner, and B. Roysam, Rapid Automated Three-Dimensional Tracing of Neurons From Confocal Image Stacks. *IEEE Transactions on Information Technology in Biomedicine*, 2002. 6(2): p. 171-187.
3. Almli, C.R., M.J. Rivkin, and R.C. McKinstry, The NIH MRI Study of Normal Brain Development (Objective-2): Newborns, infants, toddlers, and preschoolers. *NeuroImage*, 2007. 35: p. 308-325.
4. Anjari, M., L. Srinivasan, J.M. Allsop, J.V. JHajnal, M.A. Rutherford, A.D. Edwards, and S.J. Counsell, Diffusion Tensor Imaging With Tract-Based Spatial Statistics Reveals Local White Matter Abnormalities in Preterm Infants. *NeuroImage*, 2007. 35: p. 1021-1027.
5. Arias, C. and M.G. Chotro, Interactions Between Prenatal Ethanol Exposure and Postnatal Learning About Ethanol in Rat Pups. *Alcohol*, 2006. 40: p. 51-59.
6. Armstrong, D.D., K. Dunn, and B. Antalffy, Decreased Dendritic Branching in Frontal Motor and Limbic Cortex in Rett Syndrome Compared With Trisomy 21. *Journal of Neuropathology and Experimental Neurology*, 1998. 57: p. 1013-1017.
7. Astley, S., H. Carmichael-Olson, K. Kerns, A. Brooks, E.H. Aylward, T.E. Coggins, J. Davies, S. Dorn, B. Gendler, T. Jirikowic, P. Kraegel, K. Maravilla, and T. Richards, Neuropsychological and Behavioral Outcomes From a Comprehensive Magnetic Resonance Study of Children with Fetal Alcohol Spectrum Disorders. *Canadian Journal of Clinical Pharmacology*, 2009. 16(1): p. e178-e201.
8. Astley, S.J., E.H. Aylward, H. Carmichael-Olson, K. Kerns, A. Brooks, T.E. Coggins, J. Davies, S. Dorn, B. Gendler, T. Jirikowic, P. Kraegel, K. Maravilla, and T. Richards, Functional Magnetic Resonance Imaging Outcomes From a Comprehensive Magnetic Resonance Study of Children With Fetal Alcohol Spectrum Disorders. *Journal of Neurodevelopmental Disorders*, 2009. 1: p. 61-80.
9. Astley, S.J., E.H. Aylward, H. Carmichael-Olson, K. Kerns, A. Brooks, T.E. Coggins, J. Davies, S. Dorn, B. Gendler, T. Jirikowic, P. Kraegel, K. Maravilla, and T. Richards, Magnetic Resonance Imaging Outcomes From a Comprehensive Magnetic Resonance Study of Children With Fetal

- Alcohol Spectrum Disorders. *Alcoholism: Clinical and Experimental Research*, 2009. 33(10): p. 1671-1689.
10. Astley, S.J., T. Richards, E.H. Aylward, H. Carmichael-Olson, K. Kerns, A. Brooks, T.E. Coggins, J. Davies, S. Dorn, B. Gendler, T. Jirikowic, P. Kraegel, and K. Maravilla, Magnetic Resonance Spectroscopy Outcomes From a Comprehensive Magnetic Resonance Study of Children with Fetal Alcohol Spectrum Disorders. *Magnetic Resonance Imaging*, 2009. 27: p. 760-778.
  11. Astley, S.J., E. Weinberger, D.W.W. Shaw, T.L. Richards, and S.K. Clarren, Magnetic Resonance Imaging and Spectroscopy in Fetal Ethanol Exposed Macaca Nemestrina. *Neurotoxicology and Teratology*, 1995. 17(5): p. 523-530.
  12. Backman, C., J.R. West, J.C. Mahoney, and M.R. Palmer, Electrophysiological Characterization of Cerebellar Neurons From Adult Rats Exposed to Ethanol During Development. *Alcoholism: Clinical and Experimental Research*, 1998. 22(5): p. 1137-1145.
  13. Baer, J.S., P.D. Sampson, H.M. Barr, P.D. Connor, and A.P. Streissguth, A 21-Year Longitudinal Analysis of the Effects of Prenatal Alcohol Exposure on Young Adult Drinking. *Archives of General Psychology*, 2003. 60: p. 377-385.
  14. Baloch, S., R. Verma, H. Huang, P. Khurd, S. Clark, P. Yarowsky, T. Abel, S. Mori, and C. Davatzikos, Quantification of Brain Maturation and Growth Patterns in C57BL/6J Mice Via Computational Neuroanatomy of Diffusion Tensor Images. *Cerebral Cortex*, 2009. 19: p. 675-687.
  15. Baratti, C., A. Barnett, and C. Pierpaoli. Comparative MRI Study of Brain Maturation Using T1, T2, and the Diffusion Tensor. in *Proceedings of the ISMRM*. 1997. Vancouver, Canada.
  16. Barnette, A.R., J.J. Neil, C.D. Kroenke, J.L. Griffith, A.A. Epstein, P.V. Bayly, A.K. Knutsen, and T.E. Inder, Characterization of Brain Development in the Ferret Via MRI. *Pediatric Research*, 2009. 66: p. 80-84.
  17. Basser, P.J., J. Mattiello, and D. Le Bihan, Estimation of the Effective Self-Diffusion Tensor From the NMR Spin Echo. *Journal of Magnetic Resonance Series B.*, 1994. 103: p. 247-254.
  18. Basser, P.J., J. Mattiello, and D. Le Bihan, MR Diffusion Tensor Spectroscopy and Imaging. *Journal of Biophysics*, 1994. 66: p. 259-567.
  19. Basser, P.J. and C. Pierpaoli, Microstructural and Physiological Features of Tissues Elucidated by Quantitative-Diffusion-Tensor MRI. *Journal of Magnetic Resonance Series B.*, 1996. 111: p. 209-219.

20. Batchelor, P.G., D. Atkinson, D.L. Hill, F. Calamante, and A. Connelly, Anisotropic Noise Propagation in Diffusion Tensor MRI Sampling Schemes. *Magnetic Resonance in Medicine*, 2003. 49: p. 1143-1151.
21. Bayer, S.A. and J. Altman, *Neocortical Development*. 1991, New York, NY: Raven Press.
22. Beaulieu, C., The Basis of Anisotropic Water Diffusion in the Nervous System - A Technical Review. *NMR in Biomedicine*, 2002. 15: p. 435-455.
23. Behrens, T.E., H.J. Berg, S. Jbabdi, M.F. Rushworth, and M.W. Woolrich, Probabilistic Diffusion Tractography With Multiple Fiber Orientations: What Can We Gain? *NeuroImage*, 2007. 34: p. 144-155.
24. Bhagat, Y.A. and C. Beaulieu, Diffusion Anisotropy in Subcortical White Matter and Cortical Gray Matter: Changes With Aging and the Role of CSF-Suppression. *Journal of Magnetic Resonance Imaging*, 2004. 20: p. 216-227.
25. Bizley, J.K., F.R. Nodal, V.M. Bajo, I. Nelken, and A.J. King, Physiological and Anatomical Evidence for Multisensory Interactions in Auditory Cortex. *Cerebral Cortex*, 2007. 17: p. 2172-2189.
26. Bjorkquist, O.A., S.L. Fryer, A.L. Reiss, S.N. Mattson, and E.P. Riley, Cingulate Gyrus Morphology in Children and Adolescents with Fetal Alcohol Spectrum Disorders. *Psychiatry Research*, 2010. 181: p. 101-107.
27. Bockhorst, K.H., P.A. Narayana, R. Liu, P. Ahobila-Vijjula, J. Ramu, M. Kamel, J. Wosik, T. Bockhorst, H. Hahn, K.M. Hasan, and J.R. Perez-Polo, Early Postnatal Development of Rat Brain: In Vivo Diffusion Tensor Imaging. *Journal of Neuroscience Research*, 2008. 86: p. 1520-1528.
28. Boyce, R.W., K.-A. Dorph-Petersen, L. Lyck, and H.J.G. Gundersen, Design-Based Stereology Introduction to Basic Concepts and Practical Approaches for Estimation of Cell Number. *Toxicology and Pathology*, 2010. 38(7): p. 1011-1025.
29. Burke, M.W., R.M. Palmour, F.R. Ervin, and M. Ptito, Neuronal Reduction in Frontal Cortex of Primates After Prenatal Alcohol Exposure. *NeuroReport*, 2009. 20: p. 13-17.
30. Bystron, I., C. Blakemore, and P. Rakic, Development of the Human Cerebral Cortex: Boulder Committee Revisited. *Nature Reviews Neuroscience*, 2008. 9: p. 110-122.
31. Calloway, E.M. and L.C. Katz, Emergence and Refinement of Clustered Horizontal Connections in Cat Striate Cortex. *Journal of Neuroscience*, 1990. 10: p. 1134-1153.

32. Caviness Jr, V.S., T. Goto, T. Tarui, T. Takahashi, P.G. Bhide, and R.S. Nowakowski, Cell Output, Cell Cycle Duration and Neuronal Specification: A Model of Integrated Mechanisms of the Neocortical Proliferative Process. *Cerebral Cortex*, 2003. 13: p. 592-598.
33. CDC, Fetal Alcohol Syndrome—United States, 1979-1992. 1993, (CDC) Centers for Disease Control and Prevention: *Morbidity and Mortality Weekly Report*. p. 239-241.
34. CDC, Update: Trends in Fetal Alcohol Syndrome —United States, 1979–1993. 1995, (CDC) Centers for Disease Control and Prevention: *Morbidity and Mortality Weekly Report*. p. 249-251.
35. CDC, Surveillance for Fetal Alcohol Syndrome Using Multiple Sources—Atlanta, Georgia, 1981-1989. 1997, (CDC) Centers for Disease Control and Prevention: *Morbidity and Mortality Weekly Report*. p. 1118-1120.
36. CDC, Fetal Alcohol Syndrome - Alaska, Arizona, Colorado and New York, 1995-1997. 2002, (CDC) Centers for Disease Control and Prevention: *Morbidity and Mortality Weekly Report*. p. 433-435.
37. Chappell, T.D., C.P. Margret, C.X. Li, and R.S. Waters, Long-Term Effects of Prenatal Alcohol Exposure on the Size of the Whisker Representation in Juvenile and Adult Rat Barrel Cortex. *Alcohol*, 2007. 41: p. 239-251.
38. Choi, B.H. and L.W. Lapham, Radial Glia in the Human Fetal Cerebrum: A Combined Golgi, Immunofluorescent and Electron Microscopic Study. *Brain Research*, 1978. 148: p. 295-311.
39. Chotro, M.G., C. Arias, and G. Laviola, Increased Ethanol Intake After Prenatal Ethanol Exposure: Studies with Animals. *Neuroscience and Behavioral Reviews*, 2007. 31: p. 181-191.
40. Chotro, M.G., C. Arias, and N.E. Spear, Binge Ethanol Exposure in Late Gestation Induces Ethanol Aversion in the Dam but Enhances Ethanol Intake in the Offspring and Affects Their Postnatal Learning About Ethanol. *Alcohol*, 2009. 43: p. 453-463.
41. Clancy, B., R.B. Darlington, and B.L. Finlay, Translating Developmental Time Across Mammalian Species. *Neuroscience*, 2001. 105(1): p. 7-17.
42. Clancy, B., B. Kersh, J. Hyde, R.B. Darlington, K.J. Anand, and B.L. Finlay, Web-Based Method for Translating Neurodevelopment From Laboratory Species to Humans. *Neuroinformatics*, 2007. 5: p. 79-94.
43. Clarren, S.K., Recognition of Fetal Alcohol Syndrome. *Journal of the American Medical Association*, 1981. 245: p. 2436-2439.

44. Clarren, S.K., E.C. Alvord Jr, S.M. Sumi, A.P. Streissguth, and D.W. Smith, Brain Malformations Related to Prenatal Exposure to Ethanol. *Journal of Pediatrics*, 1978. 92: p. 64-67.
45. Clasca, F., A. Llamas, and F. Reinoso-Suarez, Insular Cortex and Neighboring Fields in the Cat: A Redefinition Based on Cortical Microarchitecture and Connections With the Thalamus. *Journal of Comparative Neurology*, 1997. 384: p. 456-482.
46. Coles, C.D., F.C. Goldstein, M.E. Lynch, X. Chen, J.A. Kable, K.C. Johnson, and X. Hu, Memory and Brain Volume in Adults Prenatally Exposed to Alcohol. *Brain and Cognition*, 2011. 75: p. 67-77.
47. Coles, C.D. and Z. Li, Functional Neuroimaging in the Examination of Effects of Prenatal Alcohol Exposure. *Neuropsychology Review*, 2011. 21: p. 119-132.
48. Conel, J.L., *The Postnatal Development of the Human Cerebral Cortex*, Vol. 1. 1939, Cambridge, MA: Harvard University Press.
49. Cook, M.N., G.S. Marks, H.J. Vreman, D.K. Stevenson, and J.F. Brien, Heme Oxygenase Activity and Acute and Chronic Ethanol Exposure in the Hippocampus, Frontal Cerebral Cortex, and Cerebellum of the Near-Term Fetal Guinea Pig. *Alcohol*, 1997. 14(2): p. 117-124.
50. Counsell, S.J., A.D. Edwards, A.T. Chew, M. Anjari, L.E. Dyet, L. Srinivasan, J.P. Boardman, J.M. Allsop, J.V. Hajnal, M.A. Rutherford, and F.M. Cowan, Specific Relations Between Neurodevelopmental Abilities and White Matter Microstructure in Children Born Preterm. *Brain*, 2008. 131: p. 3201-3208.
51. Cui, Z., K. Zhao, H. Zhao, D. Yu, Y. Niu, J. Zhang, and J. Deng, Prenatal Alcohol Exposure Induces Long-Term Changes in Dendritic Spines and Synapses in the Mouse Visual Cortex. *Alcohol & Alcoholism*, 2010. 45(4): p. 312-319.
52. D'Arceuil, H. and A. de Crespigny, The Effects of Brain Tissue Decomposition on Diffusion Tensor Imaging and Tractography. *NeuroImage*, 2007. 36: p. 64-68.
53. D'Arceuil, H., S. Westmoreland, and A.J. de Crespigny, An Approach to High Resolution Diffusion Tensor Imaging in Fixed Primate Brain. *NeuroImage*, 2007. 35: p. 553-565.
54. Darlington, R.B., S.A. Dunlop, and B.L. Finlay, Neural Development in Metatherian and Eutherian Mammals: Variation and Constraint. *The Journal of Comparative Neurology*, 1999. 411: p. 359-368.

55. Davies, D.L. and D.E. Smith, A Golgi Study of Mouse Hippocampal CA1 Pyramidal Neurons Following Perinatal Ethanol Exposure. *Neuroscience Letters*, 1981. 26: p. 49-54.
56. delpolyi, A.R., P. Mukherjee, K. Gill, R.G. Henry, S.C. Partridge, S. Veeraraghavan, H. Jin, Y. Lu, S.P. Miller, D.M. Ferriero, D.B. Vigneron, and A.J. Barkovich, Comparing Microstructural and Macrostructural Development of the Cerebral Cortex in Premature Newborns: Diffusion Tensor Imaging Versus Cortical Gyration. *NeuroImage*, 2005. 27: p. 579-586.
57. Dennis, B.J. and D.I. Kerr, Olfactory Bulb Connections With Basal Rhinencephalon in the Ferret: An Evoked Potential Neuroanatomical Study. *Journal of Comparative Neurology*, 1975. 159: p. 129-148.
58. Dieni, S., T. Inder, B. Yoder, T. Briscoe, E. Camm, G. Egan, D. Denton, and S. Rees, The Pattern of Cerebral Injury in a Primate Model of Preterm Birth and Neonatal Intensive Care. *Journal of Neuropathology and Experimental Neurology*, 2004. 63: p. 1297-1309.
59. Ding, Z., J.C. Gore, and A.W. Anderson, Classification and Quantification of Neuronal Fiber Pathways Using Diffusion Tensor MRI. *Magnetic Resonance in Medicine*, 2003. 49(4): p. 716-721.
60. Dreher, B. and S.R. Robinson, Development of the Retinofugal Pathway in Birds and Mammals: Evidence for a Common 'Timetable'. *Brain, Behavior and Evolution*, 1988. 31: p. 369-390.
61. Driscoll, C.D., A.P. Streissguth, and E.P. Riley, Prenatal Alcohol Exposure: Comparability of Effects in Humans and Animal Models. *Neurotoxicology and Teratology*, 1990. 12: p. 231-237.
62. Dunty, W.C.J., S. Chen, R.M. Zucker, D.B. Dehart, and K.K. Sulik, Selective Vulnerability of Embryonic Cell Populations to Ethanol-Induced Apoptosis: Implications for Alcohol-Related Birth Defects and Neurodevelopmental Disorder. *Alcoholism: Clinical and Experimental Research*, 2001. 25(10): p. 1523-1535.
63. Elliott, E.J., J. Payne, A. Morris, E. Haan, and C. Bower, Fetal Alcohol Syndrome: A Prospective National Surveillance Study. *Archives of Disease in Childhood*, 2008. 93(9): p. 732-737.
64. Fabregues, I., I. Ferrer, J.M. Gairi, A. Cahuana, and P. Giner, Effects of Prenatal Exposure to Ethanol on the Maturation of the Pyramidal Neurons in the Cerebral Cortex of the Guinea-Pig: A Quantitative Golgi Study. *Neuropathology and Applied Neurobiology*, 1985. 11: p. 291-298.
65. Fagerlund, A., S. Heikkinen, L. Autti-Ramo, M. Korkman, M. Timonen, T. Kuusi, E.P. Riley, and N. Lundbom, Brain Metabolic Alterations in

- Adolescents and Young Adults With Fetal Alcohol Spectrum Disorders. *Alcoholism: Clinical and Experimental Research*, 2006. 30(12): p. 2097-2104.
66. Fields, R.D., White Matter in Learning, Cognition and Psychiatric Disorders. *Trends in Neuroscience*, 2008. 31: p. 361-370.
  67. Finlay, B.L. and R.B. Darlington, Linked Regularities in the Development and Evolution of Mammalian Brains. *Science*, 1995. 268: p. 1578-1584.
  68. Flynn, S.W., D.J. Lang, A.L. Machay, V. Goghari, I.M. Vavasour, K.P. Whittall, G.N. Smith, V. Arango, J.J. Mann, A.J. Dwork, P. Falkai, and W.G. Honer, Abnormalities of Myelination in Schizophrenia Detected In Vivo With MRI, and Post-Mortem With Analysis of Oligodendrocyte Proteins. *Molecular Psychiatry*, 2003. 8: p. 811-820.
  69. Frank, L.R., Anisotropy in High Angular Resolution Diffusion-Weighted MRI. *Magnetic Resonance in Medicine*, 2001. 45: p. 935-939.
  70. Freire, M. and A. Boyde, Stereoscopic and Biplanar Microphotography of Golgi-Impregnated Neurons: A Correlative Study Using Conventional and Real-Time, Direct-Image Confocal Microscopies. *Journal of Neuroscience Methods*, 1995. 58: p. 109-116.
  71. Fryer, S.L., S.F. Tapert, S.N. Mattson, M.P. Paulus, A.D. Spadoni, and E.P. Riley, Prenatal Alcohol Exposure Affects Frontal-Striatal BOLD Response During Inhibitory Control. *Alcoholism: Clinical and Experimental Research*, 2007. 31(8): p. 1415-1424.
  72. Gan, W.-B., J. Grutzendler, W.T. Wong, R.O.L. Wong, and J.W. Lichtman, Multicolor "DiOlistic" Labeling of the Nervous System Using Lipophilic Dye Combinations. *Neuron*, 2000. 27: p. 219-225.
  73. Giedd, J.N., J. Blumenthal, N.O. Jeffries, F.X. Castellanos, H. Liu, A. Zijdenbos, T. Paus, A.C. Evans, and J.L. Rapoport, Brain Development During Childhood and Adolescence: A Longitudinal MRI Study. *Nature Neuroscience*, 1999. 2(10): p. 861-863.
  74. Godin, E.A., S.K. O'Leary-Moore, A.A. Khan, S.E. Parnell, J.J. Ament, D.B. Dehart, B.W. Johnson, G.A. Johnson, M.A. Styner, and K.K. Sulik, Magnetic Resonance Microscopy Defines Ethanol-Induced Brain Abnormalities in Prenatal Mice: Effects of Acute Insult on Gestational Day 7. *Alcoholism: Clinical and Experimental Research*, 2010. 34(1): p. 98-111.
  75. Gogtay, N., J.N. Giedd, L. Lusk, K.M. Hayashi, D. Greenstein, A.C. Vaituzis, T.F. Nugent III, D.H. Herman, L.S. Clasen, A.W. Toga, J.L. Rapoport, and P.M. Thompson, Dynamic Mapping of Human Cortical

Development During Childhood Through Early Adulthood. Proceedings of the National Academy of Science, 2004. 101(21): p. 8174-8179.

76. Granato, A., Altered Organization of Cortical Interneurons in Rats Exposed to Ethanol During Neonatal Life. *Brain Research*, 2006. 1069: p. 23-30.
77. Granato, A. and J. Van Pelt, Effects of Early Ethanol Exposure on Dendrite Growth of Cortical Pyramidal Neurons: Inferences From a Computational Model. *Brain Research. Developmental Brain Research*, 2003. 142: p. 223-227.
78. Granger, B., F. Tekaia, A.M. Le Sourd, P. Rakic, and J.P. Bourgeois, Tempo of Neurogenesis and Synaptogenesis in the Primate Cingulate Mesocortex: Comparison with the Neocortex. *Journal of Comparative Neurology*, 1995. 360: p. 363-376.
79. Greenough, W.T., Structural Correlates of Information Storage in the Mammalian Brain: A Review and Hypothesis. *Trends in Neuroscience*, 1984. 7: p. 229-233.
80. Guilfoyle, D.N., J.A. Helpern, and K.O. Lim, Diffusion Tensor Imaging in Fixed Brain Tissue at 7.0 T. *NMR in Biomedicine*, 2003. 16: p. 77-81.
81. Guldin, W.O., H.J. Markowitsch, R. Lampe, and E. Irle, Cortical Projections Originating From the Cat's Insular Area and Remarks on Claustrocortical Connections. *Journal of Comparative Neurology*, 1986. 243: p. 468-487.
82. Gupta, R.K., K.M. Hasan, R. Trivedi, M. Pradhan, V. Das, N.A. Parikh, and P.A. Narayana, Diffusion Tensor Imaging of the Developing Human Cerebrum. *Journal of Neuroscience Research*, 2005. 81: p. 172-178.
83. Hammer Jr., R.P., Alcohol Effects on Developing Neuronal Structure, in *Alcohol and Brain Development*, J.R. West, Editor. 1986, Oxford Press: New York, NY. p. 184-203.
84. Hammer Jr., R.P. and A.B. Scheibel, Morphologic Evidence For a Delay of Neuronal Maturation in Fetal Alcohol Exposure. *Experimental Neurology*, 1981. 74: p. 587-596.
85. Hannigan, J.H. and R.F. Berman, Amelioration of Fetal Alcohol-Related Neurodevelopmental Disorders in Rats: Exploring Pharmacological and Environmental Treatments. *Neurotoxicology and Teratology*, 2000. 22: p. 103-111.
86. Hjernevik, T., T.B. Leergaard, D. Darine, O. Moldestad, A.M. Dale, F. Willoch, and I.G. Bjaalie, Three-Dimensional Atlas System for Mouse and Rat Brain Imaging Data. *Frontiers in Neuroinformatics*, 2007. 1: p. 4.

87. Hoff, J., Methods of Blood Collection in the Mouse. *Lab Animal*, 2000. 29(10): p. 47-53.
88. Hofman, M.A., Size and Shape of the Cerebral Cortex in Mammals. I. The Cortical Surface. *Brain, Behavior and Evolution*, 1985. 27: p. 28-40.
89. Hofman, M.A., Size and Shape of the Cerebral Cortex in Mammals. II. The Cortical Volume. *Brain, Behavior and Evolution*, 1988. 32: p. 17-26.
90. Huang, H., R. Xue, J. Zhang, T. Ren, L.J. Richards, P. Yarowsky, M.I. Miller, and S. Mori, Anatomical Characterization of Human Fetal Brain Development With Diffusion Tensor Magnetic Resonance Imaging. *Journal of Neuroscience*, 2009. 29: p. 4263-4273.
91. Huang, H., A. Yamamoto, M.A. Hossain, L. Younes, and S. Mori, Quantitative Cortical Mapping of Fractional Anisotropy in Developing Rat Brains. *Journal of Neuroscience*, 2008. 28: p. 1427-1433.
92. Hubel, D.H., Exploration of the Primary Visual Cortex, 1955-78. *Nature*, 1982. 299: p. 515-524.
93. Huppi, P.S., S.E. Maier, S. Peled, G.P. Zientara, P.D. Barnes, F.A. Jolesz, and J.J. Volpe, Microstructural Development of Human Newborn Cerebral White Matter Assessed In Vivo by Diffusion Tensor MRI. *Pediatric Research*, 1998. 44: p. 584-590.
94. Innocenti, G.M. and D.J. Price, Exuberance in the Development of Cortical Networks. *Nature Reviews Neuroscience*, 2005. 6: p. 955-965.
95. Izbudak, I., L. Farage, D. Bonekamp, W. Zhang, G. Bibat, S. Mori, S. Naidu, and A. Horska. Diffusion Tensor Imaging Findings in Rett Syndrome Patients. in *Proceedings of the 17th ISMRM Scientific Meeting*. 2009. Honolulu, HI.
96. Jackson, C.A., J.D. Peduzzi, and T.L. Hickey, Visual Cortex Development in the Ferret. I. Genesis and Migration of Visual Cortical Neurons. *Journal of Neuroscience*, 1989. 9: p. 1242-1253.
97. Jespersen, S.N., C.R. Bjarkam, J.R. Nyengaard, M.M. Chakravarty, B. Hansen, T. Vosegaard, L. Ostergaard, D. Yablonskiy, N.C. Nielsen, and P. Vestergaard-Poulsen, Neurite Density From Magnetic Resonance Diffusion Measurements at Ultrahigh Field: Comparison With Light Microscopy and Electron Microscopy. *NeuroImage*, 2010. 49: p. 205-216.
98. Jespersen, S.N., C.D. Kroenke, L. Ostergaard, J.J.H. Ackerman, and D.A. Yablonskiy, Modeling Dendrite Density From Magnetic Resonance Diffusion Measurements. *NeuroImage*, 2007. 34: p. 1473-1486.
99. Jespersen, S.N., L.A. Leigland, A. Cornea, and C.D. Kroenke, Determination of Axonal and Dendritic Orientation Distributions Within the

- Developing Cerebral Cortex by Diffusion Tensor Imaging. *IEEE Transactions on Medical Imaging*, 2012. 31: p. 16-32.
100. Jiang, S., H. Xue, A. Glover, M. Rutherford, D. Rueckert, and J.V. Hajnal, MRI of Moving Subjects Using Multislice Snapshot Images With Volume Reconstruction (SVR): Application to Fetal, Neonatal, and Adult Brain Studies. *IEEE Transactions on Medical Imaging*, 2007. 26: p. 967-980.
  101. Juraska, J.M. and E. Fifkova, A Golgi Study of the Early Postnatal Development of the Visual Cortex of the Hooded Rat. *Journal of Comparative Neurology*, 1979. 183: p. 247-256.
  102. Kaminen-Ahola, N., A. Ahola, M. Maga, K. Mallitt, P. Fahey, T.C. Cox, E. Whitelaw, and S. Chong, Maternal Ethanol Consumption Alters the Epigenotype and the Phenotype of Offspring in a Mouse Model. *Public Library of Science: Epigenetics and Gestational Alcohol Exposure*, 2010. 6(1:e1000811): p. 1-10.
  103. Katz, L.C. and J.C. Crowley, Development of Cortical Circuits: Lessons From Ocular Dominance Columns. *Nature Reviews Neuroscience*, 2002. 3: p. 34-42.
  104. Kaufmann, W.E. and H.W. Moser, Dendritic Anomalies in Disorders Associated With Mental Retardation. *Cerebral Cortex*, 2000. 10: p. 981-991.
  105. Kingsley, P.B., Introduction to Diffusion Tensor Imaging Mathematics: Part II. Anisotropy, Diffusion-Weighting Factors, and Gradient Echo Schemes. *Concepts in Magnetic Resonance Part A*, 2005. 28A: p. 123-154.
  106. Kishi, N. and J.D. Macklis, MECP2 is Progressively Expressed in Post-Migratory Neurons and is Involved in Neuronal Maturation Rather Than Cell Fate Decisions. *Molecular and Cellular Neurosciences*, 2004. 27: p. 306-321.
  107. Kostovic, I., M. Judas, M. Rados, and P. Hrabac, Laminar Organization of the Human Fetal Cerebrum Revealed by Histochemical Markers and Magnetic Resonance Imaging. *Cerebral Cortex*, 2002. 12: p. 536-544.
  108. Krahe, T.E., W. Wang, and A.E. Medina, Phosphodiesterase Inhibition Increases CREB Phosphorylation and Restores Orientation Selectivity in a Model of Fetal Alcohol Spectrum Disorders. *Public Library of Science: One*, 2009. 4(8): p. 1-13.
  109. Kroenke, C.D., J.J. Ackerman, and D.A. Yablonskiy, On the Nature of the NAA Diffusion Attenuated MR Signal in the Central Nervous System. *Magnetic Resonance in Medicine*, 2004. 52: p. 1052-1059.

110. Kroenke, C.D., G.L. Bretthorst, T.E. Inder, and J.J. Neil, Diffusion MR Imaging Characteristics of the Developing Primate Brain. *NeuroImage*, 2005. 25: p. 1205-1213.
111. Kroenke, C.D., G.L. Bretthorst, T.E. Inder, and J.J. Neil, Modeling Water Diffusion Anisotropy Within Fixed Newborn Primate Brain Using Bayesian Probability Theory. *Magnetic Resonance in Medicine*, 2006. 55: p. 187-197.
112. Kroenke, C.D., E.N. Taber, L.A. Leigland, A.K. Knutsen, and P.V. Bayly, Regional Patterns of Cerebral Cortical Differentiation Determined By Diffusion Tensor MRI. *Cerebral Cortex*, 2009. 19: p. 2916-2929.
113. Kroenke, C.D., D.C. Van Essen, T.E. Inder, S. Rees, G.L. Bretthorst, and J.J. Neil, Microstructural Changes of the Baboon Cerebral Cortex During Gestational Development Reflected in Magnetic Resonance Imaging Diffusion Anisotropy. *Journal of Neuroscience*, 2007. 27: p. 12506-12515.
114. Kubicki, M., R. McCarley, C.F. Westin, H.J. Park, S. Maier, R.J. Kikinis, F.A., and M.E. Shenton, A Review of Diffusion Tensor Imaging Studies in Schizophrenia. *Journal of Psychiatric Research*, 2007. 41: p. 15-30.
115. Kubicki, M., H.J. Park, C.F. Westin, P.G. Nestor, R.V. Mulkern, S.E. Maier, M. Niznikiewicz, E.E. Connor, J.J. Levitt, M. Frumin, R. Kikinis, F.A. Jolesz, R.W. McCarley, and M.E. Shenton, DTI and MTR Abnormalities in Schizophrenia: Analysis of White Matter Integrity. *NeuroImage*, 2005. 26: p. 1109-1118.
116. Kumra, S., M. Ashtari, K.L. Cervellione, I. Henderson, H. Kester, D. Roofeh, J. Wu, T. Clarke, E. Thaden, J.M. Kane, J. Rhinewine, T. Lencz, A. Diamond, B.A. Ardekani, and P.R. Szeszko, White Matter Abnormalities in Early-Onset Schizophrenia: A Voxel-Based Diffusion Tensor Imaging Study. *Journal of the American Academy of Child and Adolescent Psychiatry*, 2005. 44: p. 934-941.
117. Larvaron, P., O. Boespflug-Tanguy, J.P. Renou, and J.M. Bonny, In Vivo Analysis of the Postnatal Development of Normal Mouse Brain by DTI. *NMR in Biomedicine*, 2007. 20: p. 413-421.
118. Le Bihan, D., Looking into the functional architecture of the brain with diffusion MRI. *Nature Reviews Neuroscience*, 2003. 4: p. 469-480.
119. Le Bihan, D., J.F. Mangin, C. Poupon, C.A. Clark, S. Pappata, N. Molko, and H. Cabriat, Diffusion Tensor Imaging: Concepts and Applications. *Journal of Magnetic Resonance Imaging*, 2001. 13: p. 534-546.
120. Lebel, C., C. Rasmussen, K. Wyper, G. Andrew, and C. Beaulieu, Brain Microstructure is Related to Math Ability in Children with Fetal Alcohol

- Spectrum Disorder. *Alcoholism, Clinical and Experimental Research*, 2010. 34(2): p. 354-363.
121. Lebel, C., C. Rasmussen, K. Wyper, L. Walker, G. Andrew, J. Yager, and C. Beaulieu, Brain Diffusion Abnormalities in Children With Fetal Alcohol Spectrum Disorder. *Alcoholism: Clinical and Experimental Research*, 2008. 32: p. 1732-1740.
  122. Lebel, C., F. Roussotte, and E.R. Sowell, Imaging the Impact of Prenatal Alcohol Exposure on the Structure of the Developing Human Brain. *Neuropsychology Review*, 2011. 21: p. 102-118.
  123. Leergaard, T.B., N. White, A. De Crespigny, I. Bolstad, H. D'Arceuil, J.G. Bjaalie, and A.M. Dale, Quantitative Histological Validation of Diffusion MRI Fiber Orientation Distributions in the Rat Brain. *Public Library of Science: One*, 2010. 5(1): p. e8595.
  124. Leigland, L.A. and C.D. Kroenke, A Comparative Analysis of Cellular Morphological Differentiation Within the Cerebral Cortex Using Diffusion Tensor Imaging, in *Animal Models of Behavioral Analysis*, J. Raber, Editor. 2011, Human Press c/o Springer Science: New York, NY. p. 329-251.
  125. Lerch, J.P., J.B. Carroll, A. Dorr, S. Spring, A.C. Evans, M.R. Hayden, J.G. Sled, and R.M. Henkelman, Cortical Thickness Measured From MRI in the YAC128 Mouse Model of Huntington's Disease. *NeuroImage*, 2008. 41: p. 243-251.
  126. Leuzzi, V., M. Tosetti, D. Montanaro, C. Carducci, C. Artiola, C. Carducci, I. Antonozzi, M. Burrioni, F. Carnevale, F. Chiarotti, T. Popolizio, G.M. Giannatempo, V. D'Alesio, and T. Scarabino, The Pathogenesis of the White Matter Abnormalities in Phenylketonuria: A Multimodal 3.0 Tesla MRI and Magnetic Resonance Spectroscopy (1H MRS) Study. *Journal of Inherited Metabolic Disease*, 2007. 30: p. 209-216.
  127. Lindsley, T.A., S.N. Shah, and E.A. Ruggiero, Ethanol Alters BDNF-Induced Rho GTPase Activation in Axonal Growth Cones. *Alcoholism: Clinical and Experimental Research*, 2011. 35(7): p. 1321-1330.
  128. Lockard, B.I., Telencephalon of the Ferret (*Mustela furo*), in *Comparative Correlative Neuroanatomy of the Vertebrate Telencephalon*, E.H. Crosby and H.N. Schnitzlein, Editors. 1983, Macmillan Publishing Company: New York, N.Y. p. 484-500.
  129. Lockard, B.I., The Forebrain of the Ferret. *Laboratory Animal Science*, 1985. 35: p. 216-228.
  130. Ma, C., C.D. Coles, M.E. Lynch, S.M. Laconte, O. Zurkiya, D. Wang, and X. Hu, Evaluation of Corpus Callosum Anisotropy in Young Adults With

- Fetal Alcohol Syndrome According to Diffusion Tensor Imaging. *Alcoholism: Clinical and Experimental Research*, 2005. 29: p. 1214-1222.
131. Maciejewski-Lenoir, D., Chronic Prenatal Ethanol Exposure Does Not Affect the Expression of Selected Genes in Rat Brain Development. *Alcohol and Alcoholism*, 1993. 28(4): p. 401-412.
  132. Malandain, G. and G. Bertrand, Fast Characterization of 3D Simple Points. *Pattern Recognition*, 1992. 30: p. 232-235.
  133. Malisza, K.L., A. Allman, D. Shiloff, L. Jakobson, S. Longstaffe, and A.E. Chudley, Evaluation of Spatial Working Memory Function in Children and Adults With Fetal Alcohol Spectrum Disorders: A Functional Magnetic Resonance Imaging Study. *Pediatric Research*, 2005. 58(6): p. 1150-1157.
  134. Manger, P.R., I. Masiello, and G.M. Innocenti, Areal Organization of the Posterior Parietal Cortex of the Ferret (*Mustela putorius*). *Cerebral Cortex*, 2002. 12: p. 1280-1297.
  135. Manger, P.R., H. Nakamura, S. Valentiniene, and G.M. Innocenti, Visual Areas in the Lateral Temporal Cortex of the Ferret (*Mustela putorius*). *Cerebral Cortex*, 2004. 14: p. 676-689.
  136. Margret, C.P., C.X. Li, T.D. Chappell, A.J. Elberger, S.G. Matta, and R.S. Waters, Prenatal Alcohol Exposure Delays the Development of the Cortical Barrel Field in Neonatal Rats. *Experimental Brain Research*, 2006. 172: p. 1-13.
  137. Margret, C.P., C.X. Li, A.J. Elberger, S.G. Matta, T.D. Chappell, and R.S. Waters, Prenatal Alcohol Exposure Alters the Size, But Not the Pattern, of the Whisker Representation in Neonatal Rat Barrel Cortex. *Experimental Brain Research*, 2005. 165: p. 167-178.
  138. Marin-Padilla, M., Prenatal and Early Postnatal Ontogenesis of the Human Motor Cortex: A Golgi Study. I. The Sequential Development of the Cortical Layers. *Brain Research*, 1970. 23: p. 167-183.
  139. Marin-Padilla, M., Prenatal and Early Postnatal Ontogenesis of the Human Motor Cortex: A Golgi Study. II. The Basket Pyramidal System. *Brain Research*, 1970. 23: p. 185-191.
  140. Marin-Padilla, M., Dual Origin of the Mammalian Neocortex and Evolution of the Cortical Plate. *Anatomy and Embryology*, 1978. 152: p. 109-126.
  141. Mattson, S.N., N. Crocker, and T.T. Nguyen, Fetal Alcohol Spectrum Disorders: Neuropsychological and Behavioral Features. *Neuropsychology Review*, 2011. 21: p. 81-101.

142. McAllister, A.K., Cellular and Molecular Mechanisms of Dendrite Growth. *Cerebral Cortex*, 2000. 10(963-973): p. 963.
143. McKinstry, R.C., A. Mathur, J.P. Miller, A.O. Ozcan, A.Z. Snyder, G.L. Schefft, C.R. Alml, S.I. Shiran, T.E. Conturo, and J.J. Neil, Radial Organization of Developing Human Cerebral Cortex Revealed By Non-Invasive Water Diffusion Anisotropy MRI. *Cerebral Cortex*, 2002. 12: p. 1237-1243.
144. McLaughlin, D.F. and S.L. Juliano, Developmental Regulation of Plasticity in the Forepaw Representation of Ferret Somatosensory Cortex. *Journal of Neurophysiology*, 2003. 89: p. 2289-2298.
145. McLaughlin, D.F., R.V. Sonty, and S.L. Juliano, Organization of the Forepaw Representation in Ferret Somatosensory Cortex. *Somatosensory & Motor Research*, 1998. 15: p. 253-268.
146. McNab, J.A., S. Jbabdi, S.C. Deoni, G. Douad, T.E. Behrens, and K.L. Miller, High Resolution Diffusion-Weighted Imaging in Fixed Human Brain Using Diffusion-Weighted Steady State Free Precession. *NeuroImage*, 2009. 46: p. 775-785.
147. McQuarrie, A.D.R. and C.L. Tsai, *Regression and Time Series Model Selection*. 1998, Singapore: World Scientific.
148. McSherry, G.M., Mapping of Cortical Histogenesis in the Ferret. *Journal of Embryology and Experimental Morphology*, 1984. 81: p. 239-252.
149. McSherry, G.M., Cell Production Gradients in the Developing Ferret Isocortex. *Journal of Anatomy*, 1986. 144: p. 1-14.
150. Medina, A.E. and T.E. Krahe, Neocortical Plasticity Deficits in Fetal Alcohol Spectrum Disorders: Lessons From Barrel and Visual Cortex. *Journal of Neuroscience Research*, 2008. 86: p. 256-263.
151. Medina, A.E., T.E. Krahe, D.M. Coppola, and A.S. Ramoa, Neonatal Alcohol Exposure Induces Long-Lasting Impairment of Visual Cortical Plasticity of Visual Cortical Plasticity in Ferrets. *The Journal of Neuroscience*, 2003. 23(31): p. 10002-10012.
152. Medina, A.E., T.E. Krahe, and A.S. Ramoa, Early Alcohol Exposure Induces Persistent Alteration of Cortical Columnar Organization and Reduced Orientation Selectivity in the Visual Cortex. *Journal of Neurophysiology*, 2005. 93: p. 1317-1325.
153. Meyer, G., J.P. Schaaps, L. Moreau, and A.M. Goffinet, Embryonic and Fetal Development of the Human Neocortex. *The Journal of Neuroscience*, 2000. 20(5): p. 1858-1868.

154. Mihalick, S.M., J.E. Crandall, J.C. Langlois, J.D. Krienke, and W.V. Dube, Prenatal Ethanol Exposure, Generalized Learning Impairment, and Medial Prefrontal Cortical Deficits in Rats. *Neurotoxicology and Teratology*, 2001. 23: p. 453-462.
155. Miller, M.W., Effects of Alcohol on the Generation and Migration of Cerebral Cortical Neurons. *Science*, 1986. 233(4770): p. 1308-1311.
156. Miller, M.W., Effect of Prenatal Exposure to Ethanol on the Development of Cerebral Cortex: I. Neuronal Generation. *Alcoholism: Clinical and Experimental Research*, 1988. 12(3): p. 440-449.
157. Miller, M.W., Limited Ethanol Exposure Selectively Alters the Proliferation of Precursor Cells in the Cerebral Cortex. *Alcoholism: Clinical and Experimental Research*, 1996. 20(1): p. 139-144.
158. Miller, M.W., Exposure to Ethanol During Gastrulation Alters Somatosensory-Motor Cortices and the Underlying White Matter in the Macaque. *Cerebral Cortex*, 2007. 17: p. 2961-2971.
159. Miller, M.W., S. Astley, and S.K. Clarren, Number of Axons in the Corpus Callosum of the Mature Macaca Nemestrina: Increases Caused by Prenatal Exposure to Ethanol. *The Journal of Comparative Neurology*, 1999. 412: p. 123-131.
160. Miller, M.W. and G. Potempa, Numbers of Neurons and Glia in Mature Rat Somatosensory Cortex: Effects of Prenatal Exposure to Ethanol. *Journal of Comparative Neurology*, 1990. 293: p. 92-102.
161. Miyama, S., T. Takahashi, R.S. Nowakowski, and V.S. Caviness Jr, A Gradient in the Duration of the G1 Phase in the Murine Neocortical Proliferative Epithelium. *Cerebral Cortex*, 1997. 7: p. 678-689.
162. Mori, S., R. Itoh, J. Zhang, W.E. Kaufmann, P.C. van Zijl, M. Solaiyappan, and P. Yarowsky, Diffusion Tensor Imaging of the Developing Mouse Brain. *Magnetic Resonance in Medicine*, 2001. 46: p. 18-23.
163. Mori, S. and J. Zhang, Principles of Diffusion Tensor Imaging and its Applications to Basic Neuroscience Research. *Neuron*, 2006. 51: p. 527-539.
164. Moseley, M.E., Y. Cohen, J. Mintorovich, L. Chileuitt, H. Shimizu, J. Kucharczyk, M.F. Wendland, and P.R. Weinstein, Early Detection of Regional Cerebral Ischemia in Cats: Comparison of Diffusion- and T2-Weighted MRI and Spectroscopy. *Magnetic Resonance in Medicine*, 1990. 14: p. 330-346.
165. Moser, H.W., Dendritic Anomalies in Disorders Associated With Mental Retardation. *Developmental Neuropsychology*, 1999. 16(3): p. 369-371.

166. Mukherjee, P. and R.C. McKinstry, Diffusion Tensor Imaging and Tractography of Human Brain Development. *Neuroimaging Clinics of North America*, 2006. 16: p. 19-43.
167. Naidu, S., W.E. Kaufmann, M.T. Abrams, G.D. Pearlson, D.C. Lanham, K.A. Fredericksen, P.B. Barker, A. Horska, X. Golay, S. Mori, D.F. Wong, M. Yablonski, H.W. Moser, and M.V. Johnston, Neuroimaging Studies in Rett Syndrome. *Brain Development*, 2001. 23(Suppl 1): p. S62-S71.
168. Nardelli, A., C. Lebel, C. Rasmussen, G. Andrew, and C. Beaulieu, Extensive Deep Gray Matter Volume Reductions in Children and Adolescents With Fetal Alcohol Spectrum Disorders. *Alcoholism: Clinical and Experimental Research*, 2011. 35(8): p. 1404-1417.
169. The National Academies (publisher), *Enrichment Strategies for Laboratory Animals*. Institute for Laboratory Animal Research Journal, 2005. 46(2).
170. Neil, J.J., S.I. Shiran, R.C. McKinstry, G.L. Schefft, A.Z. Snyder, C.R. Almlie, E. Akbudak, J.A. Aaronovitz, J.P. Miller, B.C.P. Lee, and T.E. Conturo, Normal Brain in Human Newborns: Apparent Diffusion Coefficient and Diffusion Anisotropy Measured Using Diffusion Tensor Imaging. *Radiology*, 1998. 209: p. 57-66.
171. Nitkin, R.M., *Dendritic Mechanisms in Brain Function and Developmental Disabilities*. *Cerebral Cortex*, 2000. 10(10): p. 925-926.
172. Noctor, S.C., N.J. Scholnicoff, and S.L. Juliano, Histogenesis of Ferret Somatosensory Cortex. *Journal of Comparative Neurology*, 1997. 387: p. 179-193.
173. O'Hare, E.D., L.H. Lu, S.M. Houston, S.Y. Bookheimer, S.N. Mattson, M.J. O'Connor, and E.R. Sowell, Altered Frontal-Parietal Functioning During Verbal Working Memory in Children and Adolescents with Heavy Prenatal Alcohol Exposure. *Human Brain Mapping*, 2009. 30: p. 3200-3208.
174. O'Leary-Moore, S.K., S.E. Parnell, E.A. Godin, D.B. Dehart, J.J. Ament, A.A. Khan, G.A. Johnson, M.A. Styner, and K.K. Sulik, Magnetic Resonance Microscopy-Based Analyses of the Brains of Normal and Ethanol-Exposed Fetal Mice. *Birth Defects Research. Part A, Clinical and Molecular Teratology*, 2010. 88(11): p. 953-964.
175. Olson, H.G., T. Jirikowic, D. Kartin, and S. Astley, Responding to the Challenge of Early Intervention for Fetal Alcohol Spectrum Disorders. *Infants & Young Children*, 2007. 20(2): p. 172-189.
176. Palagyi, K., E. Sorantin, E. Balogh, A. Kuba, C. Halmai, B. Erdohelyi, and K. Husegger, A Sequential 3D Thinning Algorithm and its Medical Applications. *Lecture Notes in Computer Science*, 2001. 2082: p. 409-415.

177. Parnell, S.E., S.K. O'Leary-Moore, E.A. Godin, D.B. Dehart, B.W. Johnson, G.A. Johnson, M.A. Styner, and K.K. Sulik, Magnetic Resonance Microscopy Defines Ethanol-Induced Brain Abnormalities in Prenatal Mice: Effects of Acute Insult on Gestational Day 8. *Alcoholism: Clinical and Experimental Research*, 2009. 33(6): p. 1001-1011.
178. Pasternak, J.F. and T.A. Woolsey, On the "Selectivity" of the Golgi-Cox Method. *The Journal of Comparative Neurology*, 1975. 160(3): p. 307-312.
179. Pfefferbaum, A., E.V. Sullivan, E. Adalsteinsson, T. Garrick, and C. Harper, Postmortem MR Imaging of Formalin-Fixed Human Brain. *NeuroImage*, 2004. 21: p. 1585-1595.
180. Rakic, P., Specification of Cerebral Cortical Areas. *Science*, 1988. 241: p. 170-176.
181. Rakic, P., A Small Step for the Cell, a Giant Leap for Mankind: A Hypothesis of Neocortical Expansion During Evolution. *Trends in Neuroscience*, 1995. 18: p. 383-388.
182. Ramakers, G.J.A., Neuronal Network Formation, in *Progress in Brain Research*, M.K. J. van Pelt, C.N. Levelt, A. van Ooyen, G.J.A. Ramakers, P.R. Roelfsema, Editor. 2005, Elsevier Academic Press: San Diego, CA. p. 3-12.
183. Raznahan, A., P. Shaw, F. Lalonde, M. Stockman, G.L. Wallace, D. Greenstein, L. Clasen, N. Gogtay, and J.N. Giedd, How Does Your Cortex Grow? *The Journal of Neuroscience*, 2011. 31(19): p. 7174-7177.
184. Rice, F.L., C.M. Gomez, S.S. Leclerc, R.W. Dykes, J.S. Moon, and K. Pourmoghadam, Cytoarchitecture of the Ferret Suprasylvian Gyrus Correlated with Areas Containing Multiunit Responses Elicited by Stimulation of the Face. *Somatosensory & Motor Research*, 1993. 10: p. 161-188.
185. Riley, E.P., M.A. Infante, and K.R. Warren, Fetal Alcohol Spectrum Disorders: An Overview. *Neuropsychology Review*, 2011. 21(2): p. 73-80.
186. Robinson, S.R. and B. Dreher, The Visual Pathways of Eutherian Mammals and Marsupials Develop According to a Common Timetable. *Brain, Behavior and Evolution*, 1990. 36: p. 177-195.
187. Schneider, M.L., C.F. Moore, and M.M. Adkins, The Effects of Prenatal Alcohol Exposure on Behavior: Rodent and Primate Studies. *Neuropsychology Review*, 2011. 21: p. 186-203.
188. Seabold, G.K., J.B. Daunais, A. Rau, K.A. Grant, and V.A. Alvarez, DiOLISTIC Labeling of Neurons From Rodent and Non-Human Primate Brain Slices. *Journal of Visualized Experiments*, 2010. 41: p. e2081.

189. Shanakranarayana, R.B.S. and T.R. Raju, The Golgi Techniques for Staining Neurons, in *Brain and Behavior*, T.R. Raju, et al., Editors. 2004: Bangalore, India. p. 102-111.
190. Shaw, P., N.J. Kabani, J.P. Lerch, K. Eckstrand, R. Lenroot, N. Gogtay, D. Greenstein, L. Clasen, A. Evans, J.L. Rapoport, J.N. Giedd, and S.P. Wise, Neurodevelopmental Trajectories of the Human Cerebral Cortex. *The Journal of Neuroscience*, 2008. 28(14): p. 3586-3594.
191. Sheperd, T.M., J.J. Flint, P.E. Thelwall, G.J. Stanisiz, T.H. Mareci, A.T. Yachnis, and S.J. Blackband, Postmortem Interval Alters the Water Relaxation and Diffusion Properties of Rat Nervous Tissue - Implications for MRI Studies of Human Autopsy Samples. *NeuroImage*, 2009. 44: p. 820-826.
192. Sheperd, T.M., P.E. Thelwall, G.J. Stanisiz, and S.J. Blackband, Aldehyde Fixative Solutions Alter the Water Relaxation and Diffusion Properties of Nervous Tissue. *Magnetic Resonance in Medicine*, 2009. 62: p. 26-34.
193. Sidman, R.L. and P. Rakic, Neuronal Migration, with Special Reference to Developing Human Brain: A review. *Brain Research*, 1973. 62: p. 1-35.
194. Sidman, R.L. and P. Rakic, Development of the Human Central Nervous system, in *Histology and Histopathology of the Nervous System*, R.D.A. W. Haymaker, Editor. 1982, C.C. Thomas: Springfield, IL. p. 3-145.
195. Sizonenko, S.V., E.J. Camm, J.R. Garbow, S.E. Maier, T.E. Inder, C.E. Williams, J.J. Neil, and P.S. Huppi, Developmental Changes and Injury Induced Disruption of the Radial Organization of the Cortex in the Immature Rat Brain Revealed By In Vivo Diffusion Tensor MRI. *Cerebral Cortex*, 2007. 17: p. 2609-2617.
196. Smart, I.H.M., Proliferative Characteristics of the Ependymal Layer During the Early Development of the Mouse Neocortex: A Pilot Study Based on Recording the Number, Location and Plane of Cleavage of Mitotic Figures. *Journal of Anatomy*, 1973. 116: p. 67-91.
197. Smart, I.H.M., Three Dimensional Growth of the Mouse Isocortex. *Journal of Anatomy*, 1983. 137: p. 683-694.
198. Smith, S.M. and T.E. Nichols, Threshold-Free Cluster Enhancement: Addressing Problems of Smoothing, Threshold Dependence and Localization in Cluster Inference. *NeuroImage*, 2009. 44(1): p. 83-98.
199. Sowell, E.R., A. Johnson, E. Kan, L.H. Lu, J.D. Van Horn, A.W. Toga, M.J. O'Connor, and S.Y. Bookheimer, Mapping White Matter Integrity and Neurobehavioral Correlates in Children With Fetal Alcohol Spectrum Disorders. *Journal of Neuroscience*, 2008. 28: p. 1313-1319.

200. Sowell, E.R., S.N. Mattson, E. Kan, P.M. Thompson, E.P. Riley, and A.W. Toga, Abnormal Cortical Thickness and Brain-Behavior Correlation Patterns in Individuals With Heavy Prenatal Alcohol Exposure. *Cerebral Cortex*, 2008. 18(1): p. 136-144.
201. Sowell, E.R., P.M. Thompson, C.M. Leonard, S.E. Welcome, E. Kan, and A.W. Toga, Longitudinal Mapping of Cortical Thickness and Brain Growth in Normal Children. *The Journal of Neuroscience*, 2004. 24(38): p. 8223-8231.
202. Sowell, E.R., P.M. Thompson, S.N. Mattson, K.D. Tessner, T.L. Jernigan, E.P. Riley, and A.W. Toga, Voxel-Based Morphometric Analyses of the Brain in Children and Adolescents Prenatally Exposed to Alcohol. *Cognitive Neuroscience and Neuropsychology*, 2001. 12(35): p. 515-523.
203. Staffend, N.A. and R.L. Meisel, DiOlistic Labeling of Neurons in Tissue Slices: A Qualitative and Quantitative Analysis of Methodological Variations. *Frontiers in Neuroanatomy*, 2011. 5: p. 14.
204. Stoltenburg-Didinger, G. and H.L. Spohr, Fetal Alcohol Syndrome and Mental Retardation: Spine Distribution of Pyramidal Cells in Prenatal Alcohol-Exposed Rat Cerebral Cortex; A Golgi Study. *Developmental Brain Research*, 1983. 11: p. 119-123.
205. Streissguth, A.P., F.L. Bookstein, H.M. Barr, P.D. Sampson, K. O'Malley, and J.K. Young, Risk Factors for Adverse Life Outcomes in Fetal Alcohol Syndrome and Fetal Alcohol Effects. *Developmental and Behavioral Pediatrics*, 2004. 25(4): p. 228-238.
206. Sun, S.W., H.F. Liang, A.H. Cross, and S.K. Song, Evolving Wallerian Degeneration After Transient Retinal Ischemia in Mice Characterized by Diffusion Tensor Imaging. *NeuroImage*, 2008. 40: p. 1-10.
207. Sun, S.W., H.F. Liang, R.E. Schmidt, A.H. Cross, and S.K. Song, Selective Vulnerability of Cerebral White Matter in a Murine Model of Multiple Sclerosis Detected Using Diffusion Tensor Imaging. *Neurobiological Disorders*, 2007. 28: p. 30-38.
208. Sun, S.W., J.J. Neil, H.F. Liang, Y.Y. He, R.E. Schmidt, C.Y. Hsu, and S.K. Song, Formalin Fixation Alters Water Diffusion Coefficient Magnitude But Not Anisotropy in Infarcted Brain. *Magnetic Resonance in Medicine*, 2005. 53: p. 1447-1451.
209. Sun, S.W., J.J. Neil, and S.K. Song, Relative Indices of Water Diffusion Anisotropy Are Equivalent in Live and Formalin-Fixed Mouse Brains. *Magnetic Resonance in Medicine*, 2003. 50: p. 743-748.
210. Suter, B., R.S. Nowakowski, P.G. Bhide, and V.S. Caviness, Navigating Neocortical Neurogenesis and Neuronal Specification: A Positional

- Information System Encoded by Neurogenetic Gradients. *Journal of Neuroscience*, 2007. 27: p. 10777-10784.
211. Thelwall, P.E., T.M. Sheperd, G.J. Stanis, and S.J. Blackband, Effects of Temperature and Aldehyde Fixation on Tissue Water Diffusion Properties, Studied in an Erythrocyte Ghost Tissue Model. *Magnetic Resonance in Medicine*, 2006. 56: p. 282-289.
  212. Thornton, J.S., R.J. Ordidge, J. Penrice, E.B. Cady, P.N. Amess, S. Punwani, M. Clemence, and J.S. Wyatt, Anisotropic Water Diffusion in White and Gray Matter of the Neonatal Piglet Brain Before and After Transient Hypoxia-Ischaemia. *Magnetic Resonance Imaging*, 1997. 15: p. 433-440.
  213. Toga, A.W., P.M. Thompson, and E.R. Sowell, Mapping Brain Maturation. *Trends in Neuroscience*, 2006. 29(3): p. 148-159.
  214. Travis, K., K. Ford, and B. Jacobs, Regional Dendritic Variation in Neonatal Human Cortex: A Quantitative Golgi Study. *Developmental Neuroscience*, 2005. 27: p. 277-287.
  215. Tredici, G., A.D. Francesco, A.J. Miani, and G. Pizzini, Real Complete Three-Dimensional Reconstruction of Golgi-Impregnated Neurons by Means of a Confocal Laser Scanning Microscope. *NeuroImage*, 1993. 1: p. 87-93.
  216. Trivedi, R., R.K. Gupta, N. Husain, R.K. Rathore, S. Saksena, S. Srivastava, G.K. Malik, V. Das, M. Pradhan, M.K. Sarma, C.M. Pandey, and P.A. Narayana, Region-Specific Maturation of Cerebral Cortex in Human Fetal Brain: Diffusion Tensor Imaging and Histology. *Neuroradiology*, 2009. 51: p. 567-576.
  217. Tuch, D.S., Q-ball Imaging. *Magnetic Resonance in Medicine*, 2004. 52: p. 1358-1372.
  218. Tuch, D.S., T.G. Reese, M.R. Wiegell, N. Makris, J.W. Belliveau, and V.J. Wedeen, High Angular Resolution Diffusion Imaging Reveals Intravoxel White Matter Fiber Heterogeneity. *Magnetic Resonance in Medicine*, 2002. 48: p. 577-582.
  219. Umeyama, S., Least-Squares Estimation of Transformation Parameters Between Two Point Patterns. *IEEE Transactions on Pattern Analysis and Machine Intelligence*, 1991. 13: p. 376-380.
  220. Van Essen, D.C., J. Dickson, J. Harwell, D. Hanlon, C.H. Anderson, and H.A. Drury, An Integrated Software System for Surface-Based Analysis of Cerebral Cortex. *Journal of the American Medical Informatics Association*, 2001. 41: p. 1359-1378.

221. Voigt, T., A.D. De Lima, and M. Backmann, Synaptophysin Immunohistochemistry Reveals Inside-Out Pattern of Early Synaptogenesis in Ferret Cerebral Cortex. *Journal of Comparative Neurology*, 1993. 330: p. 48-64.
222. Wainwright, P. and G. Fritz, Effect of Moderate Prenatal Ethanol Exposure on Postnatal Brain and Behavior Development in BALB/c Mice. *Experimental Neurology*, 1985. 89(1): p. 237-249.
223. Wedeen, V.J., P. Hagmann, W.Y. Tseng, T.G. Reese, and R.M. Weisskoff, Mapping Complex Tissue Architecture With Diffusion Spectrum Magnetic Resonance Imaging. *Magnetic Resonance in Medicine*, 2005. 54: p. 1377-1386.
224. Wiesel, T.N., Postnatal Development of the Visual Cortex and the Influence of Environment. *Nature*, 1982. 299: p. 583-591.
225. Willoughby, K.A., E.D. Sheard, K. Nash, and J. Rovet, Effects of Prenatal Alcohol Exposure on Hippocampal Volume, Verbal Learning, and Verbal and Spatial Recall in Late Childhood. *Journal of the International Neuropsychological Society*, 2008. 14: p. 1022-103.
226. Wozniak, J.R., B.A. Mueller, P.N. Chang, R.L. Muetzel, L. Caros, and K.O. Lim, Diffusion Tensor Imaging In Children With Fetal Alcohol Spectrum Disorders. *Alcoholism: Clinical and Experimental Research*, 2006. 30: p. 1799-1806.
227. Yang, Y., F. Roussotte, E. Kan, K.K. Sulik, S.N. Mattson, E.P. Riley, K.L. Jones, C.M. Adnams, P.A. May, M.J. O'Connor, K.L. Narr, and E.R. Sowell, Abnormal Cortical Thickness Alterations in Fetal Alcohol Spectrum Disorders and Their Relationships With Facial Dysmorphology. *Cerebral Cortex*, 2011: p. 1-10.
228. Yanni, P.A. and T.A. Lindsley, Ethanol Inhibits Development of Dendrites and Synapses in Rat Hippocampal Pyramidal Neuron Cultures. *Developmental Brain Research*, 2000. 120: p. 233-243.
229. Youngentob, S.L., J.C. Molina, N.E. Spear, and L.E. Youngentob, The Effect of Gestational Ethanol Exposure on Voluntary Ethanol Intake in Early Postnatal and Adult Rats. *Behavioral Neuroscience*, 2007. 121(6): p. 1306-1315.
230. Yushkevich, P.A., J. Piven, H.C. Hazlett, R.G. Smith, S. Ho, J.C. Gee, and G. Gerig, User-Guided 3D Active Contour Segmentation of Anatomical Structures: Significantly Improved Efficiency and Reliability. *NeuroImage*, 2006. 31(3): p. 1116-1128.

231. Zervas, M. and S.U. Walkley, Ferret Pyramidal Cell Dendritogenesis: Changes in Morphology and Ganglioside Expression During Cortical Development. *Journal of Comparative Neurology*, 1999. 413: p. 429-448.
232. Zhang, J., M. Jones, C.A. DeBoy, D.S. Reich, J.A.D. Farrell, P.N. Hoffman, J.W. Griffin, K.A. Sheikh, M.I. Miller, S. Mori, and P.A. Calabresi, Diffusion Tensor Magnetic Resonance Imaging of Wallerian Degeneration in Rat Spinal Cord After Dorsal Root Axotomy. *The Journal of Neuroscience*, 2009. 29(10): p. 3160-3171.
233. Zhang, Z.Y., J.J. Zeng, M. Kjaergaard, N. Guan, K. Raun, C. Nilsson, and M.W. Wang, Effects of a Maternal Diet Supplemented With Chocolate and Fructose Beverage During Gestation and Lactation on Rat Dams and Their Offspring. *Clinical and Experimental Pharmacology and Physiology*, 2011. 38(9): p. 613-622.
234. Zhou, D., C. Lebel, C. Lepage, C. Rasmussen, A. Evans, K. Wyper, J. Pei, G. Andrew, A. Massey, D. Massey, and C. Beaulieu, Developmental Cortical Thinning in Fetal Alcohol Spectrum Disorders. *NeuroImage*, 2011. 58: p. 16-25.
235. Zilles, K., Architecture of the Human Cerebral Cortex, in *The Human Nervous System*, J.K. G. Paxinos, Mai, Editor. 2004, Elsevier Academic Press: San Diego, CA. p. 997-1055.

## **Figure Legends**

Figure 1. A timeline of critical events during cortical formation (neuronal generation, migration, differentiation and synaptogenesis) is presented for a number of mammalian species relative to humans. The top table represents human gestation. T = Trimester, W = week, D = Gestational Day, PC = Embryonic/Post-Conceptional Day. The bottom table lists post-conceptional time points (and postnatal time points in red) that correspond to a specific period of time in the human, relevant to neuronal generation proliferation, migration, differentiation and synaptogenesis. Estimated starting points for these events are marked by blue arrows. \*Mouse development is temporally advanced by approximately 1 day compared to the rat.

Figure 2. Rat brain masses (A), brain volumes (B) and isocortical volumes (C) in all treatment groups increased significantly with age (N = 4 – 6/age/group). Additionally, across age groups, the maltose/dextrin (M/D) had the highest mean brain mass, brain volume and isocortical volumes, while the ethanol (E) group had the lowest means (compared to the control (C) group). There was a significant difference in brain mass among treatment groups at all ages (asterisks). Additionally, there were significant differences among groups at postnatal day (P)0 through P11 (with a trend for significance at P19) and at P0 through P19 (with a trend for significance at P60) for brain volume and cortical volume, respectively. Asterisks and cross symbols represent levels of significance (p-values are listed in the figure legend).

Figure 3. Rat isocortical thickness (A) and isocortical surface area (B) in all treatment groups increased significantly with age (N = 4 – 6/age/group). Additionally, across age groups, the maltose/dextrin (M/D) had the highest mean isocortical thickness and isocortical surface area, while the ethanol (E) group had the lowest means (compared to the control (C) group). There were significant differences among groups at postnatal day (P)3 through P6 (with a trend for significance at P19) and at P3 through P11 (with trend for significance at P19 and P60) for isocortical thickness and surface area, respectively. Asterisks and cross symbols represent levels of significance (p-values are listed in the figure legend).

Figure 4. Results of the Threshold Free Cluster Enhancement (TFCE) analysis. 3 of the 6 age groups (postnatal day (P)0, P6 and P11) are presented for demonstration (N = 4 – 6/age/group). Mean cortical thickness per group in the rat are projected onto target cortical surfaces at each age, and pictured in the center row of each image. TFCE results are pictured in dark red in the first and last rows of each image representing regions, in which mean cortical thickness between groups is significantly different ( $p < 0.05$ ). D = Dorsal, V = Ventral, Cd = Caudal, R = Rostral. Specific regional differences, centered on the primary motor, somatosensory and visual cortices, were found among ethanol (E) and maltose/dextrin (M/D) groups at all ages except P60. Regions of significant difference were also found in comparisons between E and control (C) groups at P0 and P11, and between C and M/D groups at P3 and P6. Note: Colorbars at P0 represent thicknesses from 0 – 1.0 mm, while colorbars at P6 and P11 represent thicknesses from 0 – 2.0 mm. This was done to provide the best visual comparison among groups at each age.

Figure 5. Isocortical fractional anisotropy (FA) is plotted as a function of post-conceptual age in five different species (A through E). Data from 11 independent studies were fit to the empirical mathematical model expressed in equation [3.5]. Fractional anisotropy across species shows an exponential decline with development over the age ranges pictured. Data in A - E are pictured for mouse, rat, ferret, baboon and human species, respectively. Squares indicate data collected in vivo, while circles represent data collected from post-mortem samples. Open shapes indicate data that were insufficient for modeling a time constant for an exponential decline in FA ( $\tau_{FA}$ ); 1=(Larvaron 2007), 2=(Baloch 2009), 3=(Sizonenko 2007), 4=(Huang 2008), 5=(Bockhorst 2008), 6=(Kroenke 2009), 7=(Barnette 2009), 8=(Kroenke 2007), 9=(Deipolyi 2005), 10=(McKinstry 2002), 11=(Gupta 2005). (This figure is adapted from Leigland 2011.)

Figure 6. Time constants (units=days) for the exponential decrease in fractional anisotropy ( $\tau_{FA}$ ) are plotted as a function of neuroanatomical development times ( $t_{event}$ ; units=days) for five different species. Time constants for decreases in fractional anisotropy were calculated based on the empirical mathematical model expressed in equation [3.5]. Neurodevelopmental event times were calculated based on the days between the end of neurogenesis in cortical layer II/III and eye opening for each species (Clancy 2007, Darlington 1999, Finlay 1995). A high degree of correlation was found between time constants among and across

species, suggesting that neuroanatomical development in the isocortex underlies patterns in diffusion anisotropy seen with age. The dashed line was obtained by fitting a line intersecting the origin to the eight data values. The slope of this line is 0.454. Squares indicate data collected in vivo, while circles represent data collected from post-mortem samples. References are numbered as in Figure 5. (This figure is adapted from Leigland 2011.)

Figure 7. The object in red is a 3D model of a neuron made from 3D confocal images of Golgi-staining data. Black lines represent the set of line segments used to approximate the neuronal processes, and estimate the neuronal orientation distribution. In the inset, the 3D orientation distribution of the line segments is visualized on a unit sphere. Each black mark on the sphere represents an orientation in 3D of one neuronal process. From this distribution, the fiber orientation tensor is measured, and anisotropy in the neuronal processes, or NA is calculated. (This figure is adapted from Jespersen 2011.)

Figure 8. Surface models of the postnatal day (P)13 ferret cerebral cortex facilitate co-registration of the Golgi and DTI data. Montages of the five axial Golgi-stained sections used for comparisons with DTI data are shown in (A). Manually-traced contour outlines were drawn for each of 70 montages, as illustrated with red lines/points for the five sections in (A). The Golgi-based model of the cortical surface (B) is generated from the 70 adjacent contour outlines using CARET software (see text for details). Surface model coordinates corresponding to the contour outline points are displayed as red spheres in (B). A surface model of the cerebral cortex is also generated from the DTI data, shown in (C) (see text for details). Sulcal landmarks were used to constrain surface-based registration procedures implemented using CARET software. Sulcal landmarks that are visible on the lateral views of (B) and (C) are indicated with yellow spheres. Surface nodes corresponding to red spheres on the Golgi-based model in (B) are shown as green spheres on the DTI-based model in (C). Abbreviations: aRF anterior rhinal fissure, Cd caudal, CLS coronolateral sulcus, CS cruciate sulcus, D dorsal, L lateral, M medial, PSS presylvian sulcus, R rostral, SSS suprasylvian sulcus, SS sylvian sulcus, V ventral. Scale bar = 2 mm. (This figure is adapted from Jespersen 2011.)

Figure 9. Co-registration results for DTI and Golgi images. In (A), five FA parameter maps that result from re-sampling diffusion weighted images to be co-

planar with each of the sets of surface nodes corresponding to each set of green spheres in Figure 8C are shown. The outline of these points are projected onto each FA map, and overlaid as the green dashed traces. For comparison, contour outline points derived from the Golgi data are displayed as red dashed traces. For the bottom three planes, contour outline points along the medial wall were not included in the registration and are therefore not included in the dashed green and red traces (see text for details). Panels in (B) show the corresponding montages of Golgi-stained tissue sections. The boundaries of each Golgi field, with its four quadrants, are shown as an overlay. Each Golgi field center was projected onto the FA parameter maps in (A), and is illustrated as a blue filled circle. For six Golgi fields (asterisks in (A)), no manual adjustment was needed to provide a match between Golgi and DTI locations. For the remaining fields, manual adjustments were necessary to ensure the field center specified in the FA maps was consistent with the center shown in the Golgi images, relative to gyral and sulcal landmarks. 128 DTI voxels (shown in yellow in (A)) were chosen based on distance from the Golgi field center for comparisons between the DTI data and each Golgi quadrant. Abbreviations are as in Figure 3. Scale bars = 2 mm. (This figure is adapted from Jespersen 2011.)

Figure 10. A. Postnatal day (P)13 ferret Golgi-stained neurons B. P13 ferret left hemisphere FA map in an axial orientation C. P20 ferret Golgi-stained neuron D. P20 ferret left hemisphere FA map in an axial orientation E. P31 ferret Golgi-stained neuron F. P31 ferret left hemisphere FA map in an axial orientation. Gray scale for FA maps is 0 – 0.7. Scale bars in Golgi-stained images represent 50  $\mu\text{m}$ . The scale bar in B. is representative for all FA maps and is equal to 4 mm. Radial organization is lost with age, and neuritic branches become more complex. Corresponding decreases in FA are seen with age.

Figure 11. Measurements were made in 128 total regions in five equally-spaced axial sections of a postnatal day (P)13 ferret hemisphere. DTI data were registered to histological data, and identical regions of tissue were compared in terms of FA (or water diffusion anisotropy) and NA (or anisotropy in the neuronal processes). A highly significant ( $p < 0.0001$ ), linear correlation was found between these measurements, with the correlation coefficient,  $\rho = 0.40$ . This relationship is consistent with the quantitative model relating NA to FA values (equation [4.1]) with the slope of the graph, or  $vD_A$ , equal to 0.53. (This figure is adapted from Jespersen et al. 2011.)

Figure 12. A. FA map for one ethanol (E) hemisphere in the rat at postnatal day (P)3. The red line represents the pial surface, the green line approximates the mid-cortical surface and the blue line represents the gray/white matter boundary. Visual inspection of FA maps in all groups at all ages verified a laminar pattern in FA, with higher FA seen in superficial (closer to the pial surface) than deeper layers. B. The top row of images are laterally-facing cortical surface models of one ethanol hemisphere at each of 3 ages (P0, P3 and P6), on which cortical FA at each cortical surface node is projected. The bottom row represents mid-sagittal FA maps for each hemisphere at each age. Cortical FA decreased with age, and cortical thickness increased with age.

Figure 13. A. Isocortical FA in the rat in all treatment groups decreased significantly with age ( $N = 2/\text{age}/\text{group}$ ). Additionally, across age groups, the maltose/dextrin (M/D) had the lowest mean isocortical FA, while the ethanol (E) group had the largest FA (compared to the control (C) group). There were significant differences among groups at postnatal day (P)0 and P3 (asterisks). B. Isocortical thickness in all treatment groups increased significantly with age. Additionally, across age groups, the maltose/dextrin (M/D) displayed the highest mean isocortical thickness, while the ethanol (E) group showed the smallest thickness (compared to the control (C) group). There were trends for significant differences among groups at P3 and P6 (cross symbols). Asterisks and cross symbols represent levels of significance ( $p$ -values are listed in the figure legend).

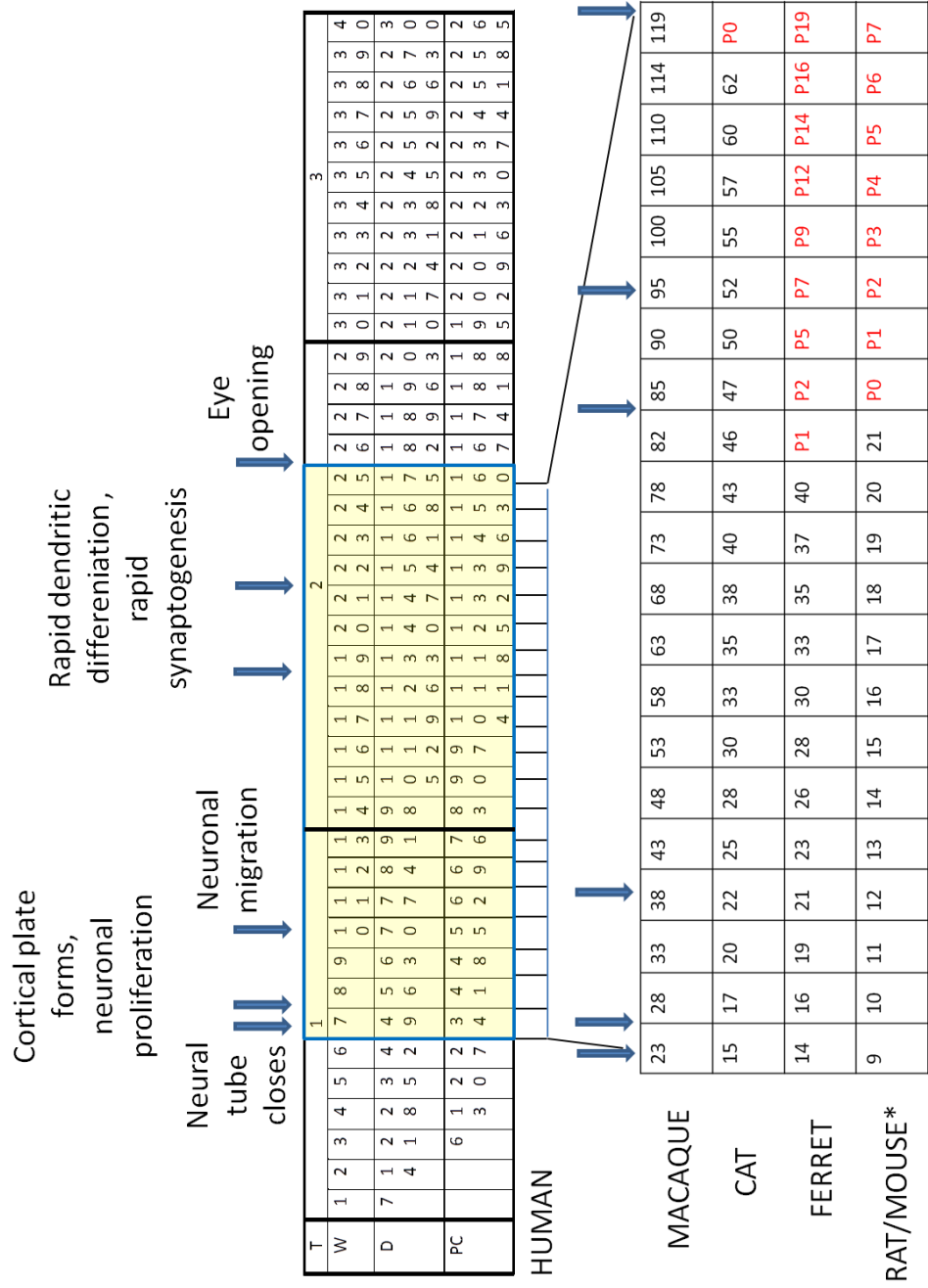
Figure 14. The top row of images are laterally-facing cortical surface models of one rat postnatal day (P)3 hemisphere for each of the 3 treatment groups (ethanol (E), control (C) and maltose/dextrin (M/D)), on which cortical FA at each cortical surface node is projected. The bottom row represents mid-sagittal FA maps for hemispheres of each treatment group. Cortical FA was largest, and cortical thickness smallest, in the E group compared to the C and M/D groups. Cortical FA was smallest, and cortical thickness largest, in the M/D group.

Figure 15. The left panel displays a schematic illustration provided for reference to cerebral cortex location. The yellow square represents the region from which the images in the right panel were taken. The right panel displays maximum intensity projection images of 3D confocal images of DiOlistically stained neurons

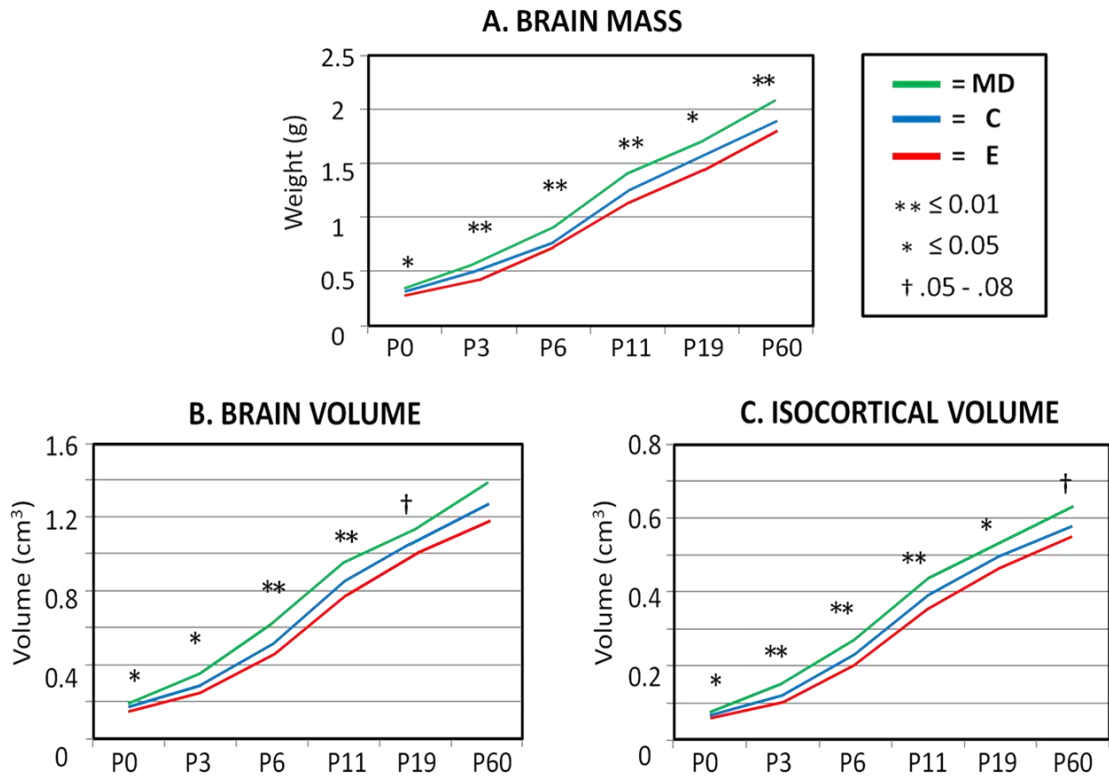
at two different time points in the ethanol (E) and control (C) groups in the rat. Neuronal arbors were found to be less complex at earlier ages such as the postnatal day (P)0 relative to P3 ages displayed here, and less complex in the E compared to C and maltose/dextrin (M/D) groups (E and C groups displayed here).

Figure 16. Rat tissue was stained using a DiOlistic technique. The anisotropy in neuronal processes, or NA value, for one inferior field on a postnatal day (P)6 control (C) mid-coronal slice and the NA value for one inferior field on a P6 ethanol (E) mid-coronal slice were compared. Additionally, these values were compared with FA values of the same area measured via DTI. A. Original maximum intensity projections of 3D confocal images of DiOlistically stained neurons. B. Binary representations of the maximum intensity images. C. Line segments calculated from 3D binary images, and used to determine the distribution of neuronal processes. D. A close-up of groups of neurons in each image presented to further demonstrate the more complex arborization in the C versus E group. E. Schematic illustration provided for reference to cerebral cortex location. F. DTI FA maps corresponding to the slices from which the fields in Panel A were taken. Yellow squares outline the specific areas corresponding to the fields in Panel A. Scale bars in Panel A and Panel F are 200  $\mu\text{m}$  and 2 mm, respectively. NA values and FA values are pictured in Panels A and F, respectively.

**Figure 1.**



**Figure 2.**



**Figure 3.**

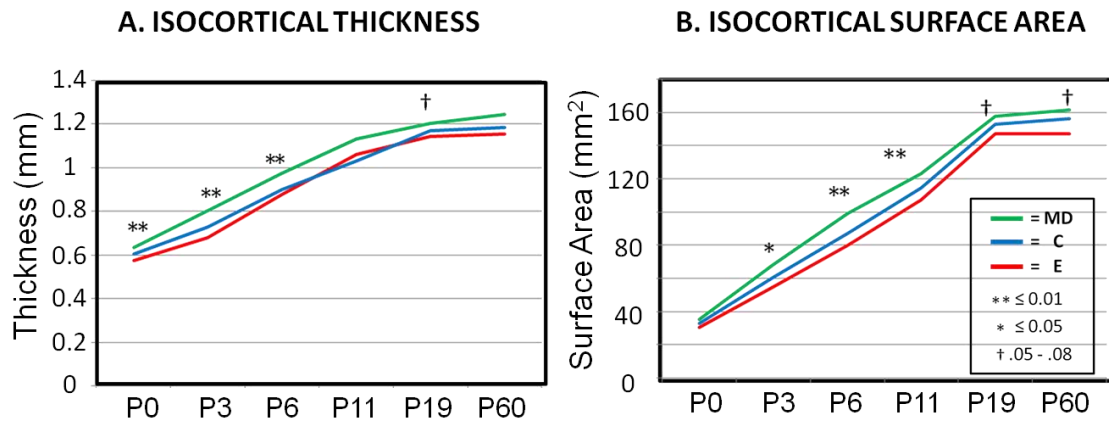


**Figure 4.**

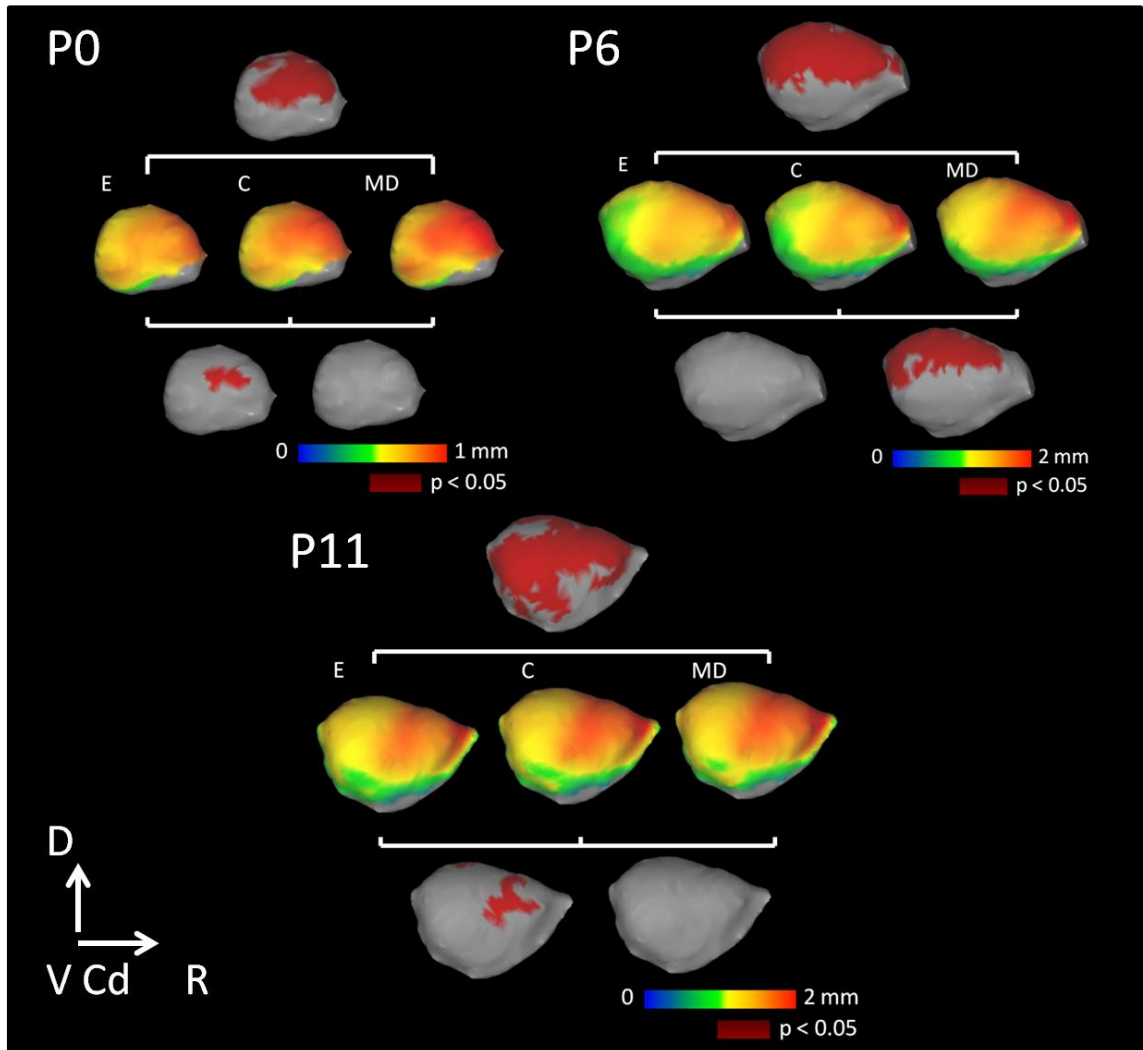


**Figure 5.**

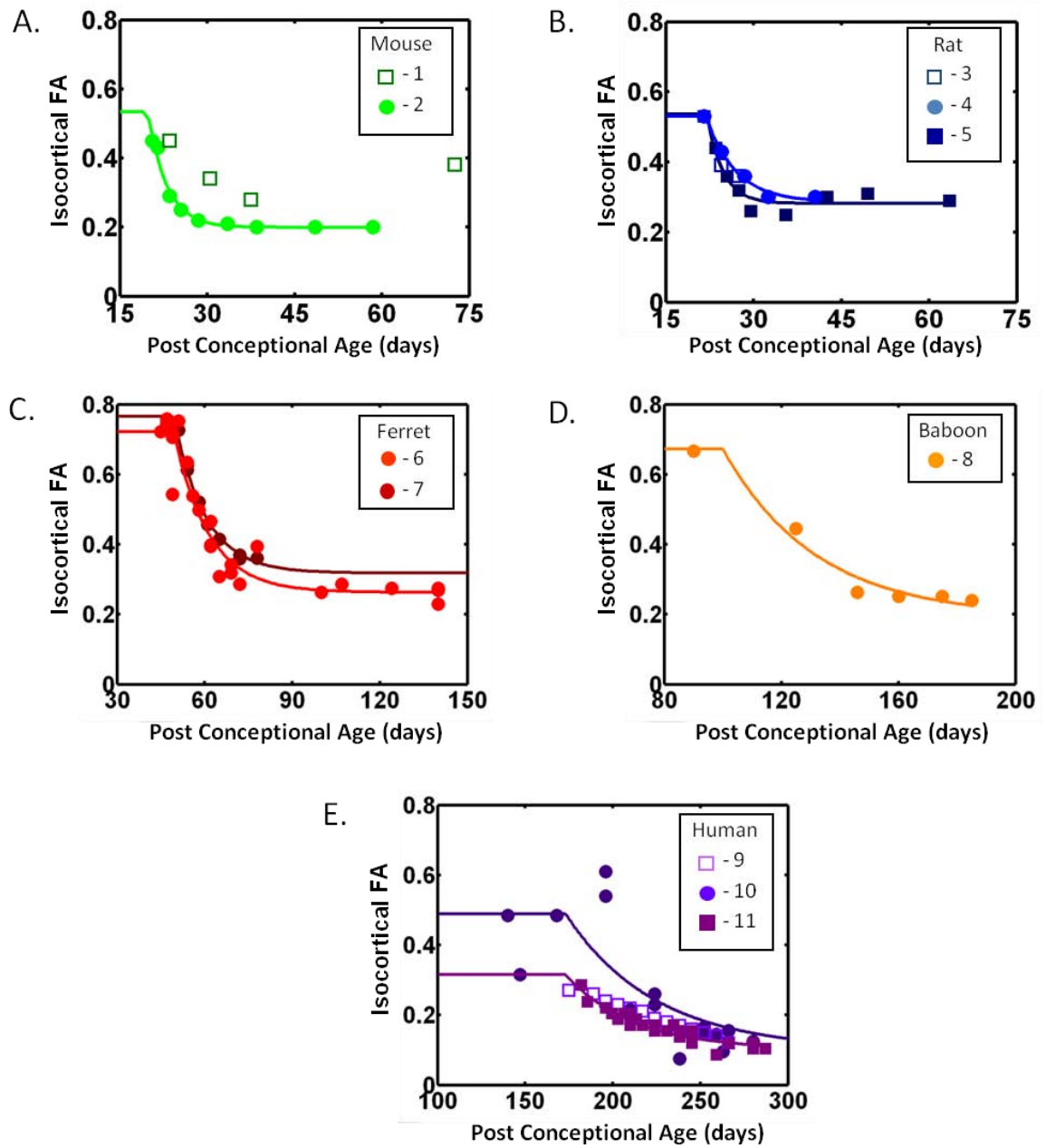


**Figure 6.**

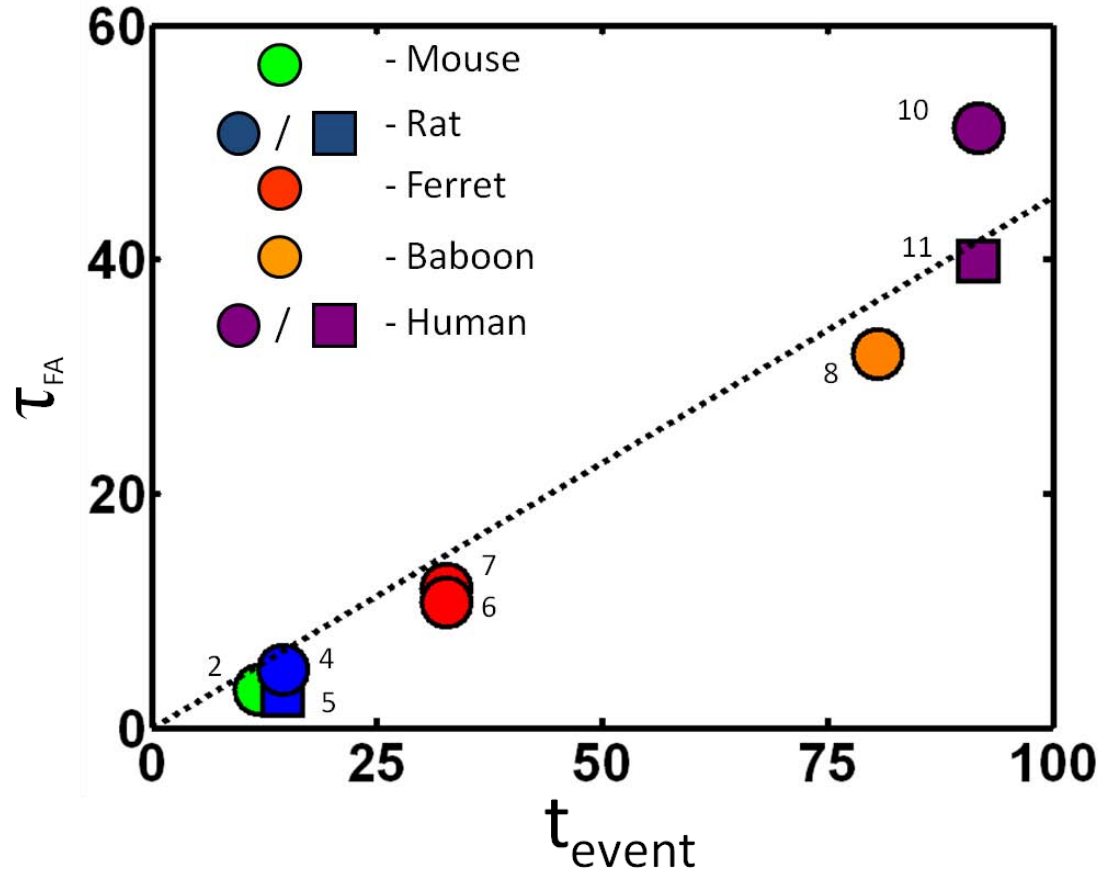


**Figure 7.**

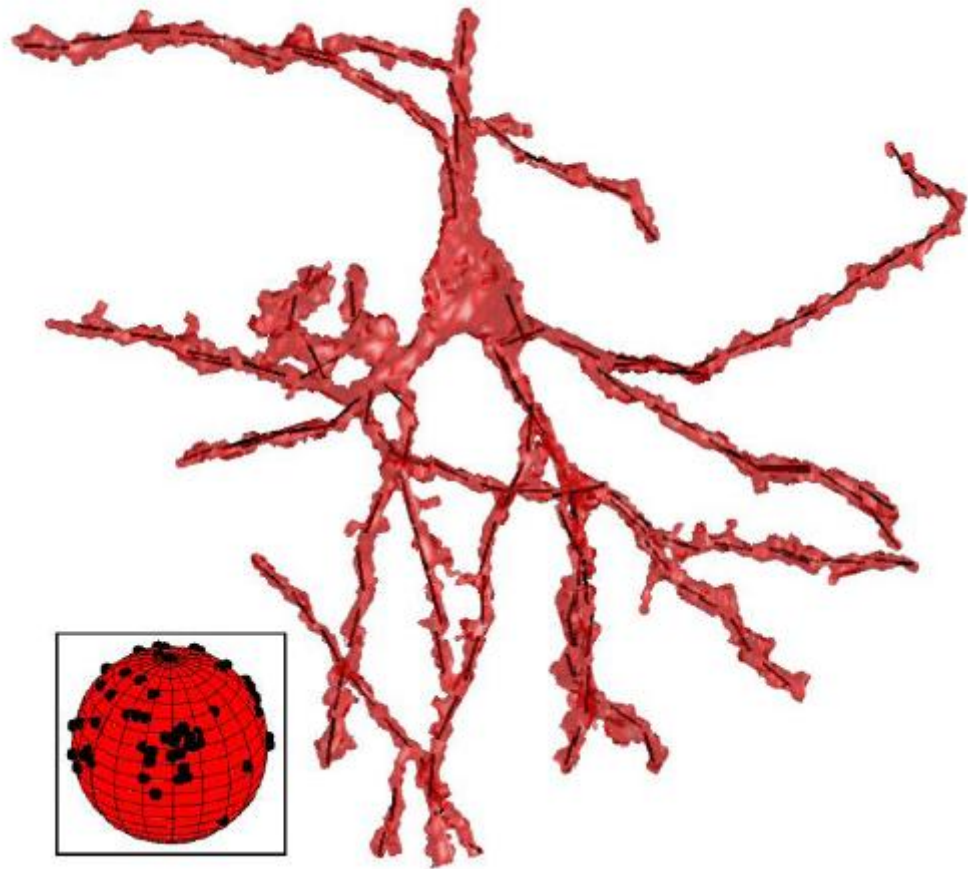


**Figure 8.**

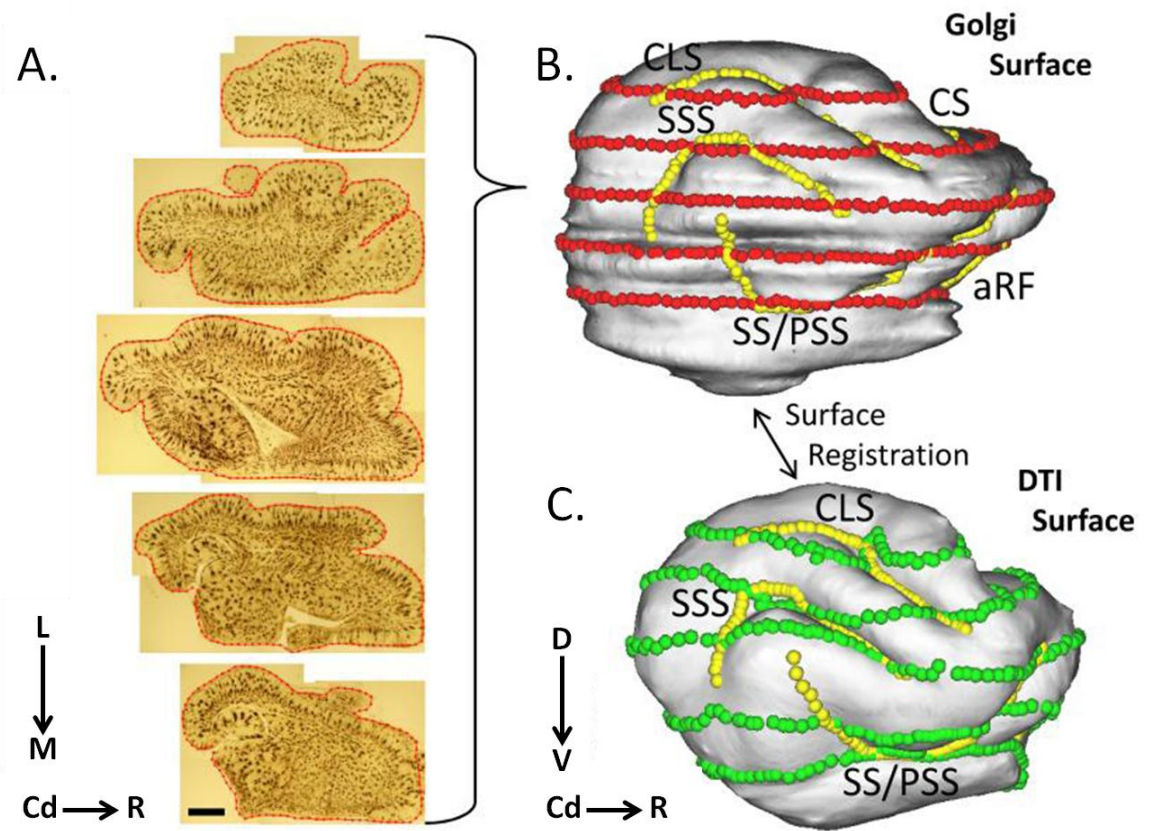


**Figure 9.**

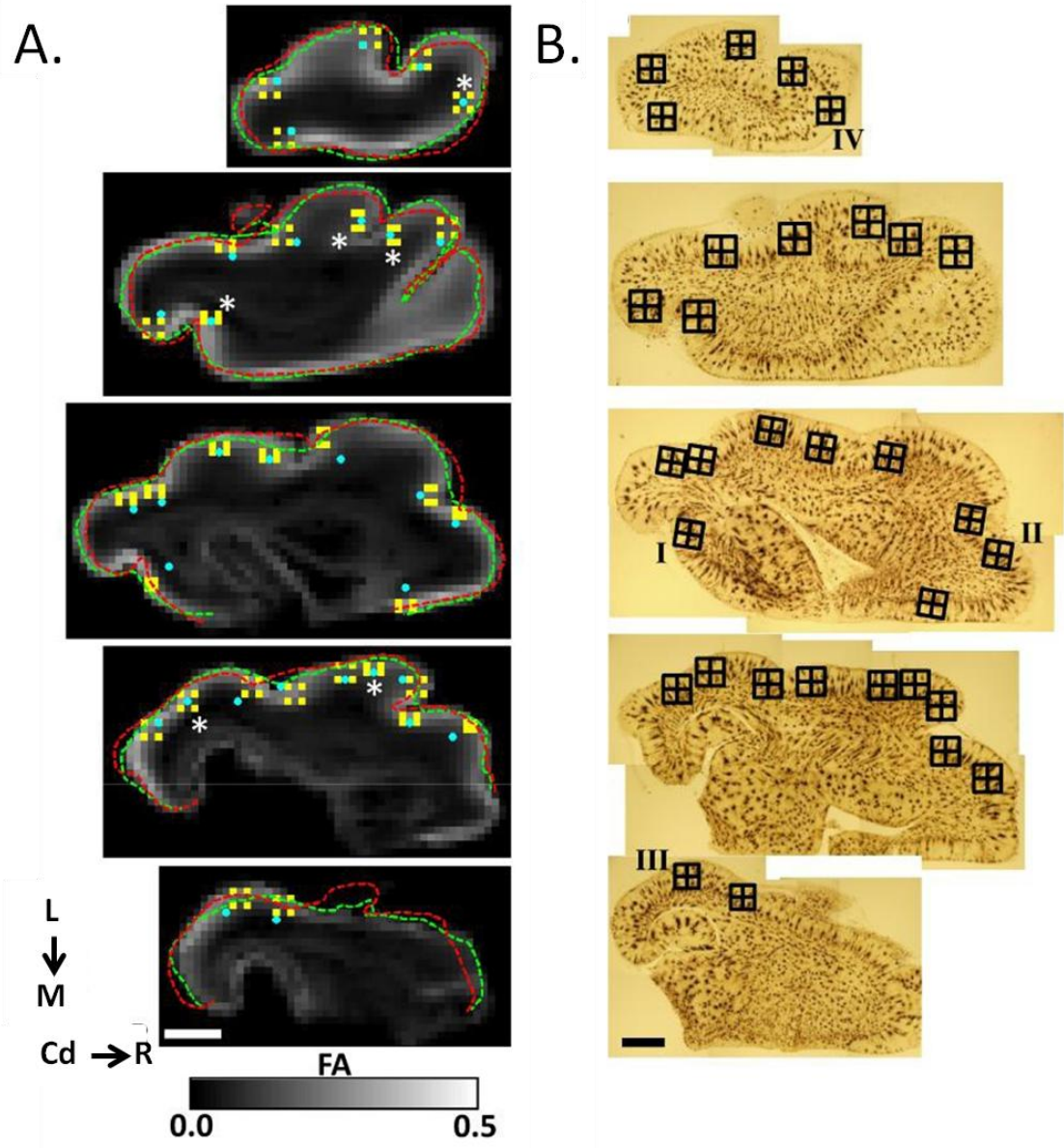


**Figure 10.**

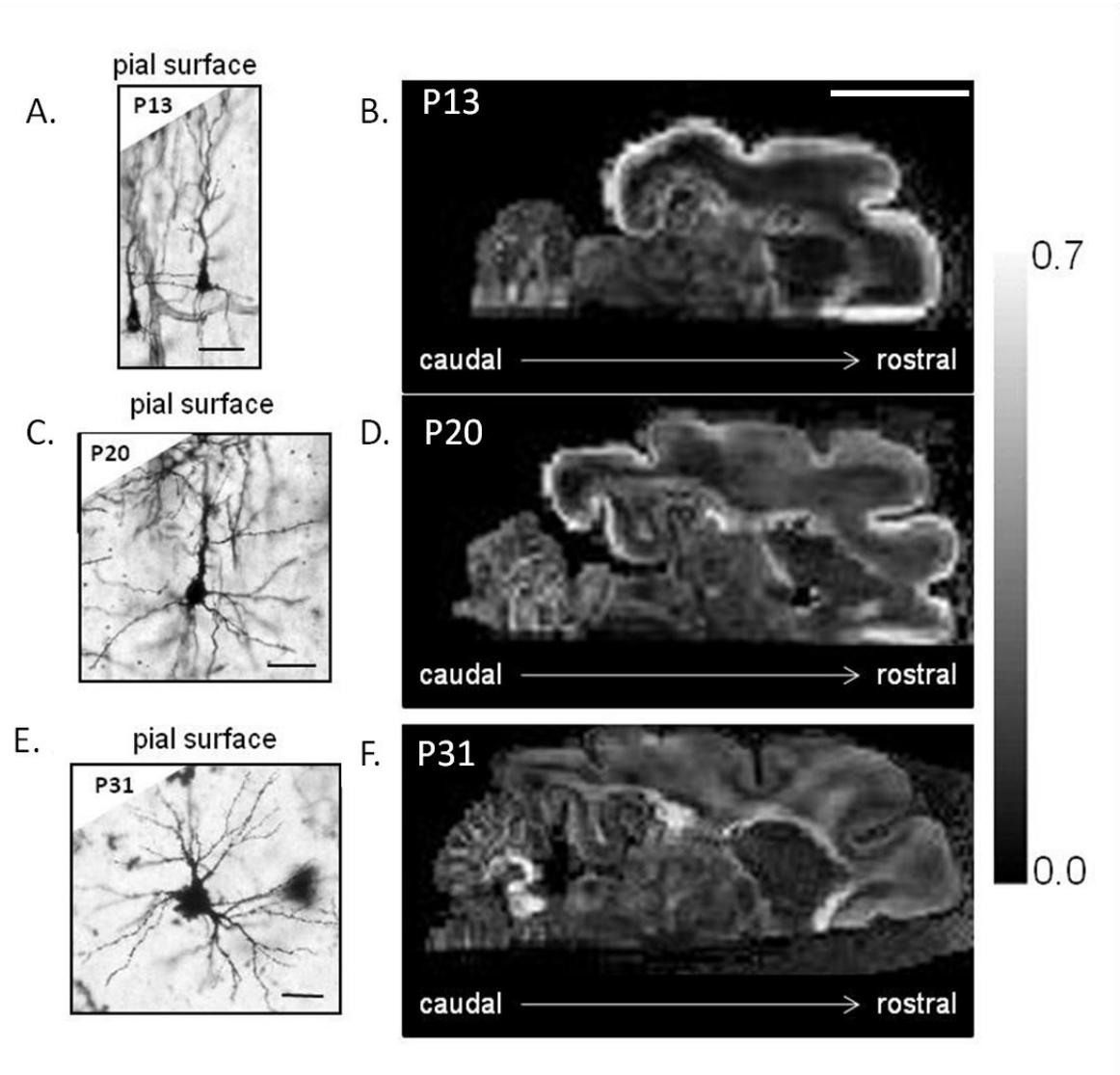
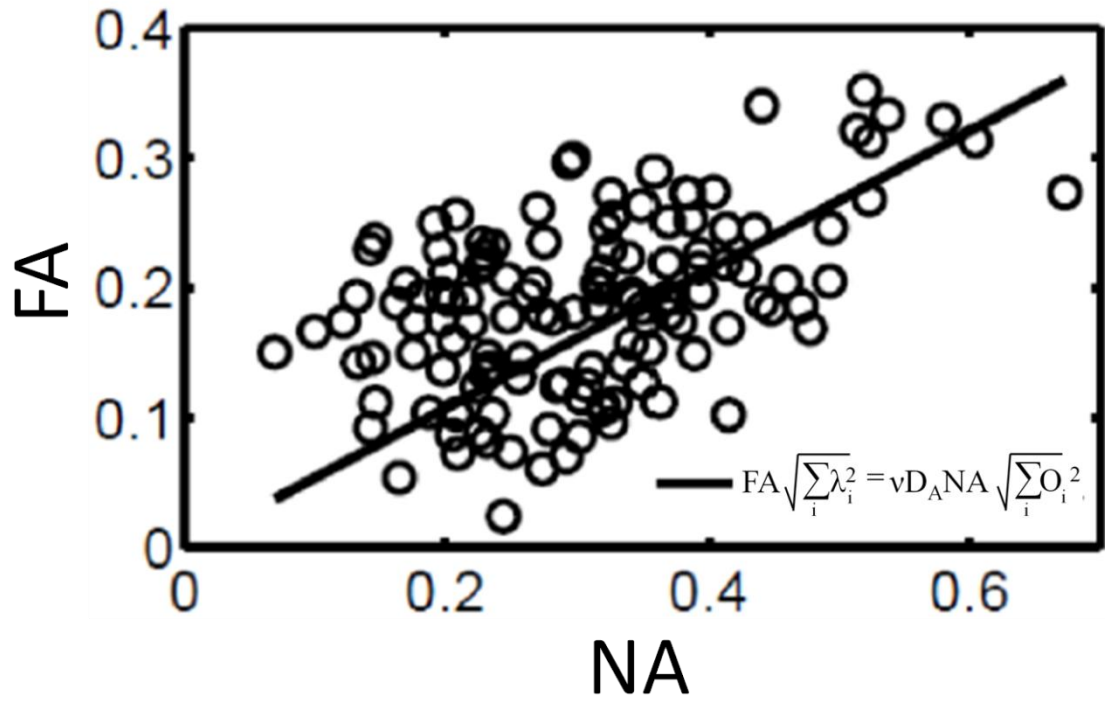
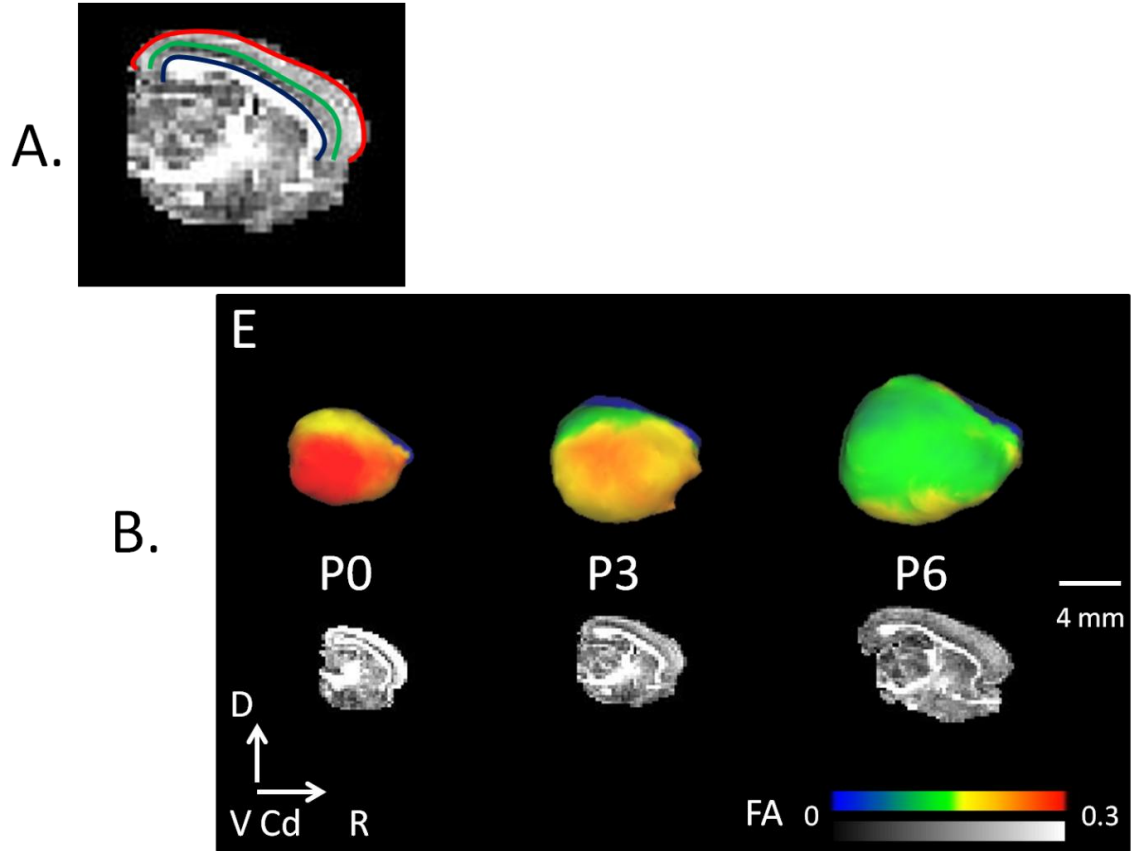


Figure 11.



**Figure 12.**



**Figure 13.**

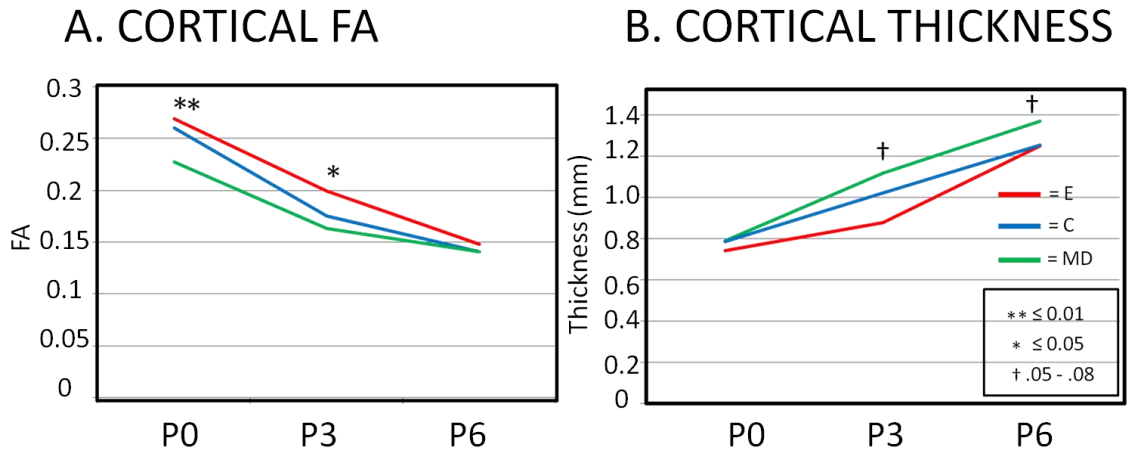


**Figure 14.**

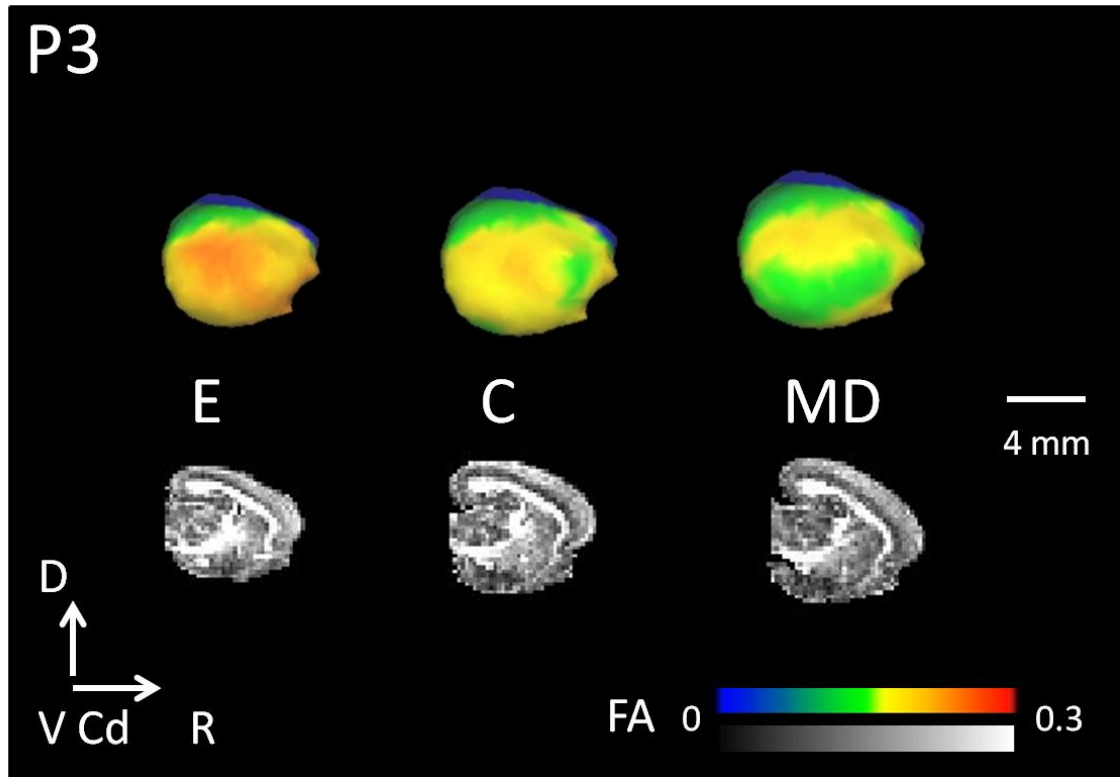


**Figure 15.**

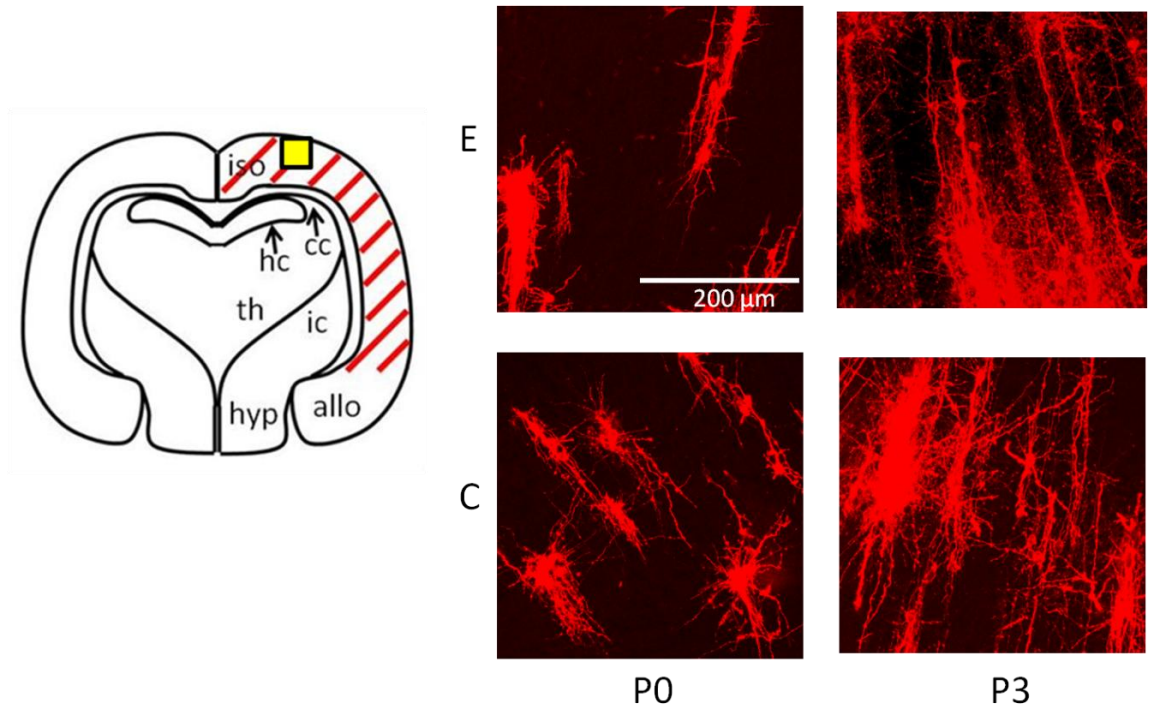


**Figure 16.**

